

# **Selective ethylene removal in industrial fruit conservation chambers**

Hugo Miguel Lourenço Lopes

Thesis to obtain the Master of Science Degree in

## **Chemical Engineering**

Supervisors:

Professor Doctor Maria Filipa Gomes Ribeiro

Professor Doctor Ana Cristina Ferreira de Oliveira Rodrigues

### **Examination Committee**

Chairperson: Professor Doctor Pedro Miguel Gil de Castro

Supervisor: Professor Doctor Maria Filipa Gomes Ribeiro

Members of the Committee: Professor Doctor Angela Martins Nunes

**June 2023**

## Declaration

I declare that this document is an original work of my own authorship and that it fulfils all the requirements of the Code of Conduct and Good Practices of the Universidade de Lisboa.

## Acknowledgments

The present research was carried out as part of the Nano4Fresh Project – Nanomaterials for an environmentally friendly and sustainable handling of perishable products, (PRIMA/0016/2019), which seeks to increase the shelf-life of perishable items by minimizing post-harvest and chemical treatments during transportation and storage, as well as food losses and wastes. This is accomplished through the development of new adsorbent nanomaterials with versatile properties that outperform conventional ripening control technologies.

## Abstract

Silver and copper-based ZSM-5 zeolites were developed to enable effective ethylene adsorption and regulation of ethylene concentration in industrial fruit storage chambers. Metal-loaded zeolite samples were subjected to breakthrough adsorption studies performed under dry and wet conditions (similar to industrial storage chambers). Shaped zeolite samples were subjected to breakthrough adsorption and adsorption-desorption tests in wet conditions. The latter experiments were conducted under "real-world" conditions in a pilot-scale adsorption system implemented in the Rocha-Center's test storage chambers.

The abundance of dispersed stabilized cations ( $\text{Ag}^+$ ,  $\text{Cu}^+$ ) capable of interacting with ethylene through  $\pi$ -complexations is directly correlated with ethylene adsorption efficiency. Lower adsorption capabilities were found for Cu-based zeolites due to the stabilization of species ( $\text{Cu}^{2+}$ ) incapable of interacting with ethylene through chemisorption ( $\pi$ -complexations). In summary, increasing the silver loading improved ethylene adsorption by increasing the number of active  $\pi$ -complexation species ( $\text{Ag}^+$ ). Water addition, on the other hand, resulted in a large drop in adsorption capabilities (about 75%), owing to the competing adsorption of water and ethylene. The hydrophobic nature of zeolite samples with greater Si/Al ratios minimized this influence.

Shaping had a significant adsorption influence, which was attributable to a reduction of active zeolite area for  $\text{Ag}^+$  stabilization. The outcome is related to a decrease in microporosity caused by binder aggregation on the zeolite pores. Because of the proven decreased loss in microporosity, an increase in zeolite percentage resulted in improved adsorption capabilities. The regeneration characteristics of adsorbents were proven under low-temperature desorption treatment, with adsorbents recovering the majority of their performance from cycle to cycle.

The experiments in the pilot scale system highlighted the efficient selective adsorption of ethylene under real-world conditions (16.3% drop in ethylene concentration after 8 hours with 3.5 g of silver extrudates) and regenerative properties of the prepared samples, as well as their mechanical properties.

**Keywords-** adsorption, ethylene, shaping, silver, zeolites, ZSM-5,  $\pi$ -complexation.

## Resumo

Zeólitos ZSM-5 à base de prata e cobre foram desenvolvidos com o intuito de promover a adsorção eficaz de etileno e a regulação da concentração do mesmo em câmaras industriais de armazenamento de fruta. As amostras de zeólito carregadas com metal foram submetidas a estudos de adsorção de rutura realizados em condições secas e húmidas (semelhantes às câmaras de armazenamento industrial). Após *shaping* das melhores amostras, os extrudidos foram submetidas a testes de adsorção de rutura e de adsorção-dessorção em condições húmidas. Estes últimos testes foram realizados em condições "reais" num sistema de adsorção à escala piloto implementado nas câmaras de armazenamento de teste do Rocha-Center.

A abundância de catiões estabilizados dispersos ( $\text{Ag}^+$ ,  $\text{Cu}^+$ ) capazes de interagir com o etileno através de complexação- $\pi$  correlacionou-se diretamente com a eficiência de adsorção do etileno. Neste sentido, foram obtidas capacidades de adsorção mais baixas para os zeólitos à base de Cu devido à estabilização de espécies ( $\text{Cu}^{2+}$ ) incapazes de interagir com o etileno através de quimisorção (*complexação- $\pi$* ). Em resumo, o aumento da carga de prata melhorou a adsorção de etileno, aumentando o número de espécies ativas para complexação- $\pi$  ( $\text{Ag}^+$ ). A adição de água, por outro lado, resultou numa redução significativa da capacidade de adsorção (cerca de 75%), devido à adsorção competitiva de água e etileno. A natureza hidrofóbica das amostras de zeólito com maiores rácios Si/Al minimizou esta influência.

O processo de *shaping* teve uma influência significativa na adsorção, que foi atribuída à redução da área ativa do zeólito para a estabilização do  $\text{Ag}^+$ . O resultado está relacionado com uma diminuição da microporosidade causada pela agregação do *binder* nos poros do zeólito. Devido à comprovada diminuição da perda de microporosidade, um aumento da percentagem de zeólito resultou em melhores capacidades de adsorção. As características de regeneração dos adsorventes foram comprovadas num tratamento de dessorção a baixa temperatura, com os adsorventes a recuperarem a maior parte do seu desempenho de ciclo para ciclo.

As experiências no sistema à escala piloto destacaram a eficiente adsorção seletiva de etileno em condições reais (redução 16.3% na concentração de etileno após 8 horas com 3.5 g de extrudidos de prata) e as propriedades regenerativas das amostras preparadas, bem como as suas propriedades mecânicas.

**Palavras-chave**- adsorção, complexação- $\pi$ , etileno, prata, *shaping*, zeólitos, ZSM-5.

## Index

|   |             |
|---|-------------|
| <b>Acknowledgments</b> .....  | <b>iii</b>  |
| <b>Abstract</b> .....   | <b>iv</b>   |
| <b>Resumo</b> .....   | <b>v</b>    |
| <b>List of figures</b> .....  | <b>viii</b> |
| <b>List of tables</b> .....   | <b>x</b>    |
| <b>Glossary</b> .....   | <b>xi</b>   |
| <b>Introduction</b> .....   | <b>1</b>    |
| <b>1. State of the art</b> .....  | <b>2</b>    |
| <b>1.1 Overview of fruit and vegetable production within the EU economics</b> ..... | <b>2</b>    |
| 1.1.1 Production and occupied area .....  | 2           |
| 1.1.2 Trade market .....  | 3           |
| 1.1.3 Importance of Mediterranean region .....                                      | 4           |
| 1.1.4 Almería's case study.....   | 4           |
| 1.1.5 Agricultural production state in Portugal.....                                | 5           |
| 1.1.6 Economic context within EU .....  | 5           |
| 1.1.7 Rocha pear's relevance .....  | 6           |
| <b>1.2 Fruit physiology</b> .....   | <b>7</b>    |
| <b>1.3 Fruit conservation</b> .....   | <b>9</b>    |
| 1.3.1 Harvest .....   | 9           |
| 1.3.2 Post-Harvest controlled atmosphere storage .....                              | 9           |
| <b>1.4 Ethylene removal technologies</b> .....                                      | <b>14</b>   |
| 1.4.1 Inhibition through plant level regulation .....                               | 15          |
| 1.4.2 Ethylene removal through destructive oxidation .....                          | 16          |
| 1.4.3 Recuperative adsorption .....   | 22          |
| <b>1.5 Zeolite shaping</b> .....  | <b>26</b>   |
| <b>2 Experimental methodology</b> .....   | <b>29</b>   |
| <b>2.1 Adsorbents preparation</b> .....   | <b>29</b>   |
| 2.1.1 Materials.....  | 29          |

|   |           |
|---|-----------|
| 2.1.2 Preparation of zeolite samples.....                                   | 29        |
| 2.1.3 Preparation of extruded zeolite samples .....                         | 30        |
| <b>2.2 Adsorbent characterization.....</b>                                  | <b>31</b> |
| 2.2.1 Chemical analysis: ICP-OES.....                                       | 31        |
| 2.2.2 UV-Visible Reflectance Spectroscopy.....                              | 31        |
| 2.2.3 N <sub>2</sub> Sorption measurements .....                            | 32        |
| 2.2.4 Thermogravimetric Analysis (TGA).....                                 | 32        |
| 2.2.5 H <sub>2</sub> Temperature Programmed Reduction.....                  | 32        |
| <b>2.3 Breakthrough curve adsorption experiments.....</b>                   | <b>32</b> |
| 2.3.1 Experimental setup .....  | 32        |
| 2.3.2 Breakthrough curves interpretation under experimental condition ..... | 34        |
| 2.3.3 Calculation of ethylene adsorption capacity.....                      | 35        |
| <b>2.4 Adsorption-desorption experiments under real conditions .....</b>    | <b>36</b> |
| 2.4.1 Pilot scale experimental setup .....                                  | 36        |
| <b>3 Results and discussion .....</b>                                       | <b>39</b> |
| <b>3.1 Ag-based zeolite powders.....</b>                                    | <b>39</b> |
| 3.1.1 Adsorbents characterization .....                                     | 39        |
| 3.1.2 Adsorption breakthrough experiments under dry conditions.....         | 44        |
| 3.1.3 Adsorption breakthrough experiments under wet conditions .....        | 47        |
| <b>3.2 Cu-based zeolite powders.....</b>                                    | <b>51</b> |
| 3.2.1 Adsorbents characterization .....                                     | 51        |
| 3.2.2 Adsorption breakthrough experiments under wet conditions .....        | 54        |
| <b>3.3 Ag-based extrudates.....</b>   | <b>55</b> |
| 3.3.1 Adsorbents characterization .....                                     | 56        |
| 3.3.2 Adsorption breakthrough experiments under wet conditions .....        | 60        |
| 3.3.3 Adsorption-desorption cycles experiments under wet conditions.....    | 62        |
| 3.3.4 Adsorption-desorption cycles experiments under real conditions.....   | 65        |
| <b>Conclusion and future perspectives.....</b>                              | <b>71</b> |
| <b>References .....</b>   | <b>73</b> |

## List of figures

|   |    |
|---|----|
| Figure 1- Area of fruit and vegetable by main producing EU Member State, 2017 (source Eurostat [2]) .....                         | 2  |
| Figure 2- Fruit and vegetable production value by main producing Member State, 2017 (source Eurostat [2]) ...                     | 2  |
| Figure 3- Extra EU-28 trade of fruits by main groups, 2017 (source Eurostat [2]) .....  | 3  |
| Figure 4- Extra EU-28 trade of vegetables by main groups, 2017 (source Eurostat [2]).....   | 3  |
| Figure 5- Mediterranean biogeographical region (yellow) (adapted from [3]) .....  | 4  |
| Figure 6- EU's pears production (adapted from[19]) .....  | 6  |
| Figure 7- Rocha pear.....   | 7  |
| Figure 8- Relative rate of respiration, ethylene production, and growth profiles in fruits (adapted from [30]) ....               | 8  |
| Figure 9- Scheme of a controlled atmosphere (CA) room (adapted from [44]) .....   | 10 |
| Figure 10- Scheme of pressure swing adsorber (PSA) N <sub>2</sub> generator (adapted from [43]).....                              | 11 |
| Figure 11- CO <sub>2</sub> scrubbers (SCS LTD).....   | 12 |
| Figure 12- Dynamic controlled atmosphere concept (adapted from [58]).....   | 14 |
| Figure 13- Methods of ethylene removal and control (adapted from [36]) .....  | 15 |
| Figure 14- Schematic representation of 1-MCP treatment impact (adapted from [59]) .....   | 16 |
| Figure 15- Corona (left) and light (right) discharge ozone generators (adapted from [79]) .....                                   | 19 |
| Figure 16- UV lamp for ethylene removal .....   | 22 |
| Figure 17- ZSM-5 zeolite (MFI structure) and pentasil SBU .....   | 23 |
| Figure 18- Schematic of $\pi$ -complexation interaction (adapted from[114]).....  | 24 |
| Figure 19- Zeolite shaping process .....  | 28 |
| Figure 20 Schematic of the experimental set-up for adsorption experiments under wet conditions .....                              | 34 |
| Figure 21 Breakthrough curves obtained under dry and wet conditions (adapted from [147]) .....                                    | 35 |
| Figure 22- Schematic of the adsorption system installed in the Rocha-Center's test chambers .....                                 | 36 |
| Figure 23- Rocha-Center's adsorption-desorption pilot scale set-ups.....  | 37 |
| Figure 24- Adsorption-desorption profiles.....  | 38 |
| Figure 25-TGA mass and heat flow profiles versus temperature for the HM04 sample .....  | 39 |
| Figure 26- UV-Vis DRS spectra of Ag-based zeolites .....  | 41 |
| Figure 27- H <sub>2</sub> TPR profile of Ag-based zeolites .....  | 42 |
| Figure 28- Relationship between total Ag amount and Ag <sup>+</sup> amount calculated from the H <sub>2</sub> -TPR measurements   | 43 |
| Figure 29- Breakthrough curves for Ag-based zeolites (Si/Al=15) under dry conditions.....   | 44 |
| Figure 30- Breakthrough curves for Ag-based zeolites (Si/Al=40) under dry conditions.....   | 45 |
| Figure 31- Ethylene adsorption capacity for Ag-based zeolites tested under dry conditions .....                                   | 46 |
| Figure 32- Ethylene adsorption capacity as a function of Ag <sup>+</sup> content for Ag-based zeolites under dry conditions ..... | 47 |



|   |    |
|---|----|
| Figure 33- Breakthrough curves for Ag-based zeolites (Si/Al=15) under wet conditions .....  | 48 |
| Figure 34- Breakthrough curves for Ag-based zeolites (Si/Al=40) under wet conditions.....   | 48 |
| Figure 35- Comparison of ethylene adsorption capacity for Ag-based zeolites under wet and dry conditions ...                      | 50 |
| Figure 36- Ethylene adsorption capacity in function of Ag <sup>+</sup> content for Ag-based zeolites under wet conditions .....   | 51 |
| Figure 37- UV-Vis DRS spectra of Cu-based zeolites .....  | 52 |
| Figure 38- H <sub>2</sub> TPR profile of Cu-based zeolites .....  | 53 |
| Figure 39- Breakthrough curves for Cu-based zeolites (Si/Al=15) under wet conditions.....   | 54 |
| Figure 40- UV-Vis DRS spectra of Ag-based extrudates .....  | 57 |
| Figure 41- UV-Vis DRS spectra of Ag-based $\gamma$ -Al <sub>2</sub> O <sub>3</sub> extrudates.....                                | 58 |
| Figure 42- H <sub>2</sub> TPR profile of silver supported in $\gamma$ -Al <sub>2</sub> O <sub>3</sub> extrudates .....            | 59 |
| Figure 43- H <sub>2</sub> TPR profile of silver extrudates .....  | 60 |
| Figure 44- Breakthrough curves for silver-based extrudates (Si/Al=40) under wet conditions .....                                  | 61 |
| Figure 45- Breakthrough curves for the adsorption-desorption cycles for 1.5Ag(40) extrudates under wet conditions .....           | 63 |
| Figure 46- Summary of ethylene capacities for 1.5Ag(40) extrudates adsorption-desorption cycles tested under dry conditions ..... | 63 |
| Figure 47- Breakthrough curves for the adsorption-desorption cycles for 3Ag(60) extrudates under wet conditions .....             | 64 |
| Figure 48- Summary of ethylene capacities for 3Ag(60) extrudates adsorption-desorption cycles tested under dry conditions .....   | 64 |
| Figure 49- Ethylene concentration profile during the adsorption-desorption cycles with 3%Ag(40) on 27/10/2022.....                | 66 |
| Figure 50- Ethylene concentration profile during the adsorption-desorption cycles with 3%Ag(40) on 03/11/2022.....                | 67 |
| Figure 51- Ethylene concentration profile during the adsorption-desorption cycles with 3%Ag(60) on 22/11/2022.....                | 68 |
| Figure 52- Ethylene profile concentration during the adsorption-desorption cycles with 3%Ag(60) on 19/01/2023 and 20/01/2023..... | 69 |

## List of tables

|   |    |
|---|----|
| Table 1- Temperature impact on ethylene production rate for apple[36] .....   | 10 |
| Table 2 -Ag-based ZSM-5 powders characteristics .....   | 29 |
| Table 3- Cu-based ZSM-5 powders characteristics (Cu content quantified ICP-OES).....  | 30 |
| Table 4- Ag-based ZSM-5 extrudates characteristics .....  | 31 |
| Table 5- Ag-based ZSM-5 powders characteristics and preparations.....   | 40 |
| Table 6- H <sub>2</sub> -TPR results for the Ag-based zeolites .....  | 43 |
| Table 7- Summary of ethylene adsorption capacity values and break-point time for Ag-based zeolites under dry conditions .....                                     | 45 |
| Table 8- Summary of ethylene capacity values and break-point time for Ag-based zeolites under wet conditions .....  | 49 |
| Table 9- Cu-based ZSM-5 powders characteristics and preparations.....   | 51 |
| Table 10- H <sub>2</sub> -TPR results for the Cu-based zeolites .....   | 54 |
| Table 11- Summary of ethylene capacity values and break-point time for Cu-based zeolites under wet conditions .....   | 55 |
| Table 12- N <sub>2</sub> sorption results and microporosity loss by extrudates with different zeolite loads.....  | 56 |
| Table 13- Summary of ethylene capacity values and break-point time for Ag-based extrudates under wet conditions .....   | 61 |
| Table 14- Summary of conditions verified during the adsorption-desorption cycle experiments performed in Rocha-Center .....                                       | 65 |
| Table 15- Summary of ethylene adsorption capacity in each cycle and the overall reduction of ethylene concentration (3%Ag(40) on 27/10/2022) .....                | 66 |
| Table 16- Summary of ethylene adsorption capacity in each cycle and the overall reduction of ethylene concentration (3%Ag(40) on 03/11/2022) .....                | 67 |
| Table 17-Summary of ethylene adsorption capacity in each cycle and the overall reduction of ethylene concentration (3%Ag(60) on 22/11/2022) .....                 | 68 |
| Table 18- Summary of ethylene adsorption capacity in each cycle and the overall reduction of ethylene concentration (3%Ag(60) on 19/01/2023 and 20/01/2023) ..... | 69 |

## Glossary

|           |  |
|-----------|--|
| ACC       | 1-Aminocyclopropane-1-Carboxylate                        |
| ACP       | Anaerobic Compensation Point                             |
| ATP       | Adenosine Triphosphate                                   |
| C         | Outlet Ethylene Concentration                            |
| $C_0$     | Inlet Ethylene Concentration                             |
| CA        | Controlled Atmosphere                                    |
| DFT       | Density Functional Theory                                |
| DRS       | Diffuse Reflectance Spectroscopy                         |
| EU        | European Union   |
| FID       | Flame Ionization Detector                                |
| GAC       | Granular Activated Carbon                                |
| GC        | Gas Chromatography                                       |
| GMO       | Genetically Modified Organisms                           |
| HFM       | Hollow Fibre Membrane                                    |
| ICP-OES   | Inductively Coupled Plasma Optical Emission Spectroscopy |
| K         | Absorption Reflectance                                   |
| LO        | Low Oxygen   |
| M         | Molarity   |
| 1-MCP     | 1-Methylcyclopropene                                     |
| MOF       | Metal-Organic Frameworks                                 |
| PCO       | Photocatalytic Oxidation                                 |
| PDO       | Protected Designation of Origin                          |
| PGI       | Protected Geographic Indication                          |
| PSA       | Pressure-Swing Adsorbers                                 |
| PZC       | Point of Zero Charge                                     |
| q         | Ethylene Capacity  |
| $q_{ads}$ | Ethylene Capacity per mass of adsorbent                  |
| Qv        | Volumetric Flow Rate                                     |
| R         | Diffuse Reflectance                                      |
| RCA       | Rapid controlled atmosphere                              |
| RH        | Relative humidity  |
| ROS       | Reactive organic species                                 |
| RT        | Room temperature   |
| S         | Scattering Reflectance                                   |
| SBU       | Secondary Building Units                                 |

|           |                                  |
|-----------|----------------------------------|
| $t_{bp}$  | Breakpoint Time                  |
| TCD       | Thermal Conductivity Detector    |
| TGA       | Thermogravimetric Analysis       |
| TPR       | Temperature Programmed Reduction |
| $t_s$     | Saturation Time                  |
| ULO       | Ultralow Oxygen                  |
| $V_{mic}$ | Microporous Volume               |
| VOC       | Volatile Organic Compounds       |
| ZSM-5     | Zeolite Socony Mobil-5           |

## Introduction

Fresh fruit and vegetable production plays a crucial role in the EU's socioeconomic landscape, accounting for 13.9% of total agricultural output value with a devoted area of 5.6 million hectares. The economic and political nature of the European Union encourages the trade market for fresh products among its members (36.8 billion fresh items transported among EU countries), although the market balance is shifting toward the importation of fresh goods. The fruit and vegetable market is heavily reliant on the maturation process, either before or after harvest, because fruit and vegetables continue to execute the majority of metabolic processes after being picked up. Thus, regulating these processes is critical to meeting market demands without incurring significant losses.

The majority of the losses are caused by water loss, microbial activity, and the generation of ethylene during storage. Ethylene is a phytohormone generated by fresh foods that is responsible for ripening and senescence. Ripening is an important stage in the development of fruits because it develops the desired market characteristics (colour, taste, scent, and texture). Ethylene, while being responsible for the ripening process, has an important role in the fresh goods production landscape. Ethylene production is related to metabolic reactions, thus low temperatures and controlled gas compositions are important to mitigate this hormone production. These conditions limit ethylene generation, although the static nature of the storage chambers may lead to an eventual build-up of this hormone. The effect is magnified for climacteric fruits, which are known to emit more ethylene during ripening. As a result, ethylene removal technologies offer a way to extend the shelf life of fresh foods while meeting market demands without incurring major economic losses.

The fundamental goal of this work is to produce novel adsorbents based on metals supported on zeolite with the purpose of selective ethylene adsorption. To investigate the role of water in the adsorption processes, the ethylene adsorption performance of synthesized silver and copper metals supported in zeolites with varying characteristics (Si/Al, compensating cation) and metal loadings was studied in dry and wet conditions. The best performing metal supported zeolites were shaped through mixing-extrusion, and their performance under wet conditions was compared to the powder samples, as well as the influence of varied zeolite percentages and metal loadings. Furthermore, wet adsorption-desorption cycle studies were performed to investigate the regeneration capacities and their influence on adsorption performance. In addition, wet adsorption-desorption cycle studies were performed to determine the regeneration capacities and their influence on adsorption performance. Ultimately, the shaped samples were submitted to real (or close to real) conditions adsorption-desorption cycles in a pilot scale adsorption system installed in Rocha-Center's test storage chambers (filled with Rocha Pear fruits) to evaluate the performance capabilities under practical storage conditions. UV-Vis Diffuse Reflectance Spectroscopy, H<sub>2</sub> Temperature Programmed Reduction, Thermogravimetric analysis, and N<sub>2</sub> sorption measurements were used to characterize the synthesized materials.

# 1. State of the art

## 1.1 Overview of fruit and vegetable production within the EU economics

### 1.1.1 Production and occupied area

To comprehend the extent to which fruit and vegetable conservation affects society, it is essential to understand the economic influence that this production has within the EU's member states. Fruit and vegetable production plays a major part in the economic landscape of the EU, accounting for 13.9% of the overall value of the EU's agricultural production in 2017 (€57.5 billion, with fresh veggies generating €34.5 billion and fruits contributing €22.9 billion). Overall, fresh goods production is dispersed across the EU on 2.3 million farms, with a total area of 3.4 million hectares dedicated to fruits and 2.2 million hectares dedicated to fresh vegetables. In terms of crops, the most valued fresh goods are apples and tomatoes, which account for €3.8 billion and €7.3 billion, respectively (which corresponds, respectively, to 16.5% and 21.1% of the value of the fruit production in the EU).[1], [2]

As seen in Figure 1, Spain and Italy emerge as leaders in total area dedicated to fruit (57.6%) and fresh vegetable production (35.1%). This geographic investment is closely related to the overall value generated, where, as shown in Figure 2, both nations are leaders as well (fresh vegetable 40.2%, and fruits 47%).[1], [2]

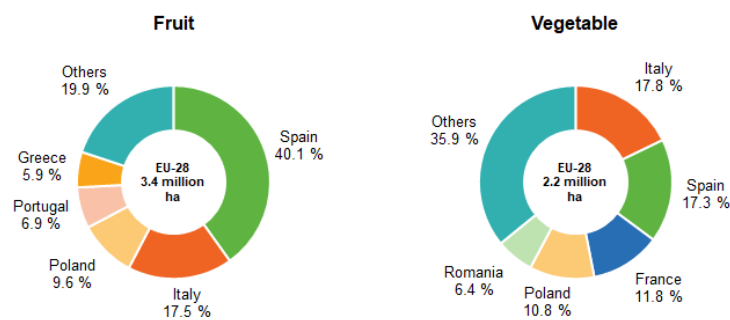


Figure 1- Area of fruit and vegetable by main producing EU Member State, 2017 (source Eurostat [2])

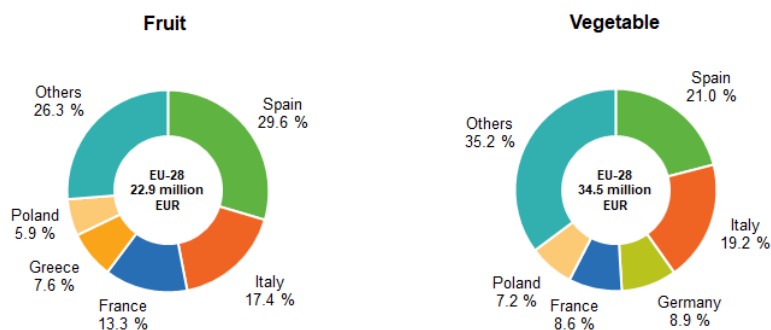


Figure 2- Fruit and vegetable production value by main producing Member State, 2017 (source Eurostat [2])

### 1.1.2 Trade market

Regarding the fresh products market, the EU is a net importer (Figure 3 and Figure 4), owing mostly to imports of nuts and bananas (20% of total value of fruit imports in 2017) from countries such as the United States (11.9%), South Africa (8.9%), and Turkey (8.7%). In terms of value of exports, the EU member states' trade flow of fresh goods is significantly larger within the EU, with €36.8 billion shipped to EU members and just €4.6 billion in sales to non-EU countries. In the EU, three nations account for two-thirds of intra-EU export values: Spain (33.3%), The Netherlands (26.8%), and Italy (10.9%). [1], [2]

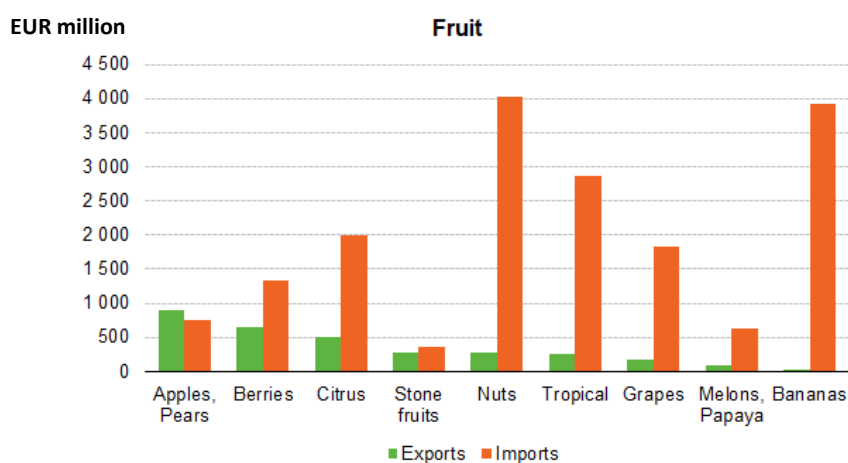


Figure 3- Extra EU-28 trade of fruits by main groups, 2017 (source Eurostat [2])

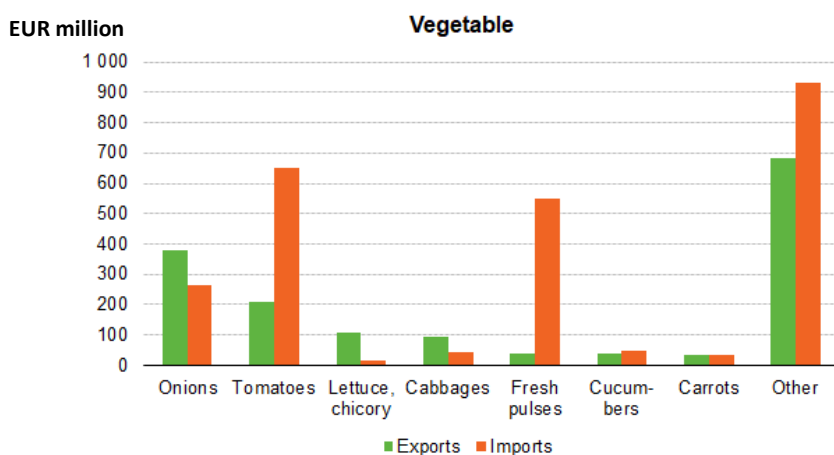


Figure 4- Extra EU-28 trade of vegetables by main groups, 2017 (source Eurostat [2])

### 1.1.3 Importance of Mediterranean region

Despite being dispersed throughout many EU member states, the sector is particularly relevant in some regions, most notably the Mediterranean region (Figure 5) and some eastern European countries. The Mediterranean region comprises seven nations (Cyprus, France, Greece, Italy, Malta, Portugal and Spain) and the Mediterranean Sea. The climate is particularly distinctive, with hot, dry summers and humid, cool winters. Not only that, but the hilly topography also contributes to the region's biodiversity. Because of these favourable conditions, Mediterranean countries within the EU are responsible for the largest share of fresh vegetables and fruits produced in the EU. Across the areas within this region, beyond the inherent economic importance, the development of specialized production systems is deeply connected with the social and environmental impacts as well as derivative agri-food sectors.[3]

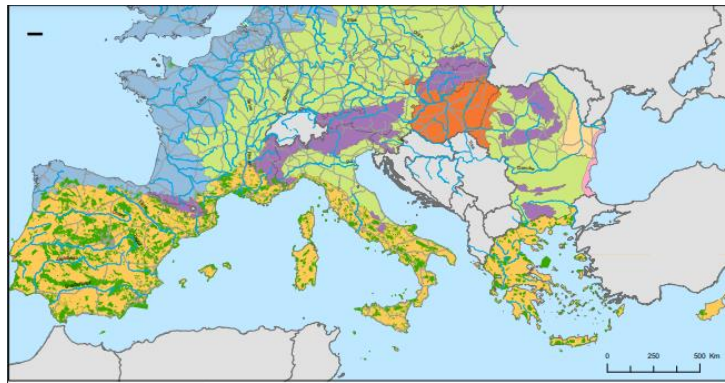


Figure 5- Mediterranean biogeographical region (yellow) (adapted from [3])

### 1.1.4 Almería's case study

The intensive agriculture in Almería's greenhouse complexes, for example, exemplifies this link quite clearly. In the 1960s, the Spanish government allocated parcels of land to a young population in hopes of developing the economy and providing jobs, resulting in migration from all over the country. This plan resulted in the construction of the world's largest greenhouse area (320 km<sup>2</sup>), accounting for 38% of total horticultural production on Spanish territory.[4] The operation's substantial impact is felt in numerous sectors, much beyond the economic one, from the 110 thousand employments (ranging from farm employees, marketing companies, auxiliary companies, etc.) created to the environmental burden on natural resources and ecosystems.[5] The primary environmental risks stem from the substantial reliance on aquifer water (80% of the water utilized in Almería's agriculture).[6] The pace of utilization exceeds the rate of natural refilling, resulting in deteriorated depleted aquifers.[6] Another worrisome component of the intense process is the plastic trash generated by agricultural practices. Because of the tons of plastic waste created, the area is



frequently referred to as the "plastic sea" (33500 tonnes).[7], [8] The inadequate waste management, aided by an increase in nitrate concentrations from fertilizer runoff, has had a negative impact on local aquatic biosystems.[9], [10][11]

Notwithstanding the serious consequences of this type of production, considerable work has been made toward achieving a more efficient circular operation. This is supported by research that shows that Spanish greenhouses use 22 times less energy than Dutch greenhouses by harnessing light and heat. Almería's farms are dependent on technological innovation and changes in methods to ensure their sustainability.[12] To lessen the impact on natural resources and ecosystems, rainwater collection from rooftops, automated irrigation-optimized systems, and reliance on insects as biological pest management are being introduced.[13], [14] In accordance with the development of sustainable progress, the white greenhouse tops give a reflective medium to the solar radiation, leading to a decrease of 0.8 °C temperature (compared to the regional trend), partially lessening the greenhouse effect and indirectly offsetting the greenhouses' carbon footprint by up to 45%.[11], [15]

#### 1.1.5 Agricultural production state in Portugal

In Portugal, the agricultural sector is ruled by small farms (70% of farms have fewer than 5 hectares), which are managed by an elderly population with low educational levels. As a result, manufacturing efficiency is poorer when compared to European competitors. Portugal, for example, produces 1400 euros per hectare on average, significantly less than the euro area with 2400 euros. Nonetheless, there has been a shift in the agricultural sector, with the emergence of larger agricultural farms (above 50 hectares, accounting for 4% of all farms) and a higher degree of specialized trained personnel in the field (47% of producers in 2018 compared to 16% in 2013). Additionally, there is a consolidation of the worldwide market, whether via efforts to penetrate new markets such as China, Japan and India, or the growing tendency of contractual partnerships with international companies. All these variables directly lead to greater production efficiency and profit. Fruit and derivative product exports, which account for half of the agricultural commodity exports, are critical to the sector's success.[16]

#### 1.1.6 Economic context within EU

Portugal has a large area dedicated to fresh goods production, mostly in the fruit sector, with a 6.9% portion of the EU market.[2] This translates to a total volume generated of 1.2 million tonnes, placing the country eight in the EU ranking. Three crops dominate the fruit sector: oranges (350 thousand tonnes), apples (341 thousand tonnes) and pears (183 thousand tonnes).[17] Most Portuguese fruits are produced in accordance with European quality standards labels, PDO (Protected Designation of Origin) and PGI (Protected Geographic Indication). This certification is given to products that come from a certain location, have

inherent/special qualities that ensure high quality standards and respect production traditions related to a specific territory of origin.[18]

1.1.7 Rocha pear's relevance

Portugal ranks fifth (Figure 6) in Europe in terms of pear production (6% of EU's output)[19], with a dedicated area of 13000 hectares producing around 190 thousand tonnes of European pear (*Pyrus communis*).[20] Nonetheless, in terms of market share, China leads, accounting for 71% of worldwide output, with Europe accounting for 13%.[21] In terms of cultivars, the Rocha Pear dominates the national market, accounting for 97% of all pears produced in the country.[22] Despite the considerable demand for pears in the domestic market (6.2 kg per inhabitant), the bulk of Rocha pears (60% of total output) is exported, with sales totalling 90 million in 2019.[23] Portugal primarily exports to Brazil, Morocco, the United Kingdom, Germany, France, Spain and to a smaller extent to the United States and Canada, as well as Poland.[24], [25]

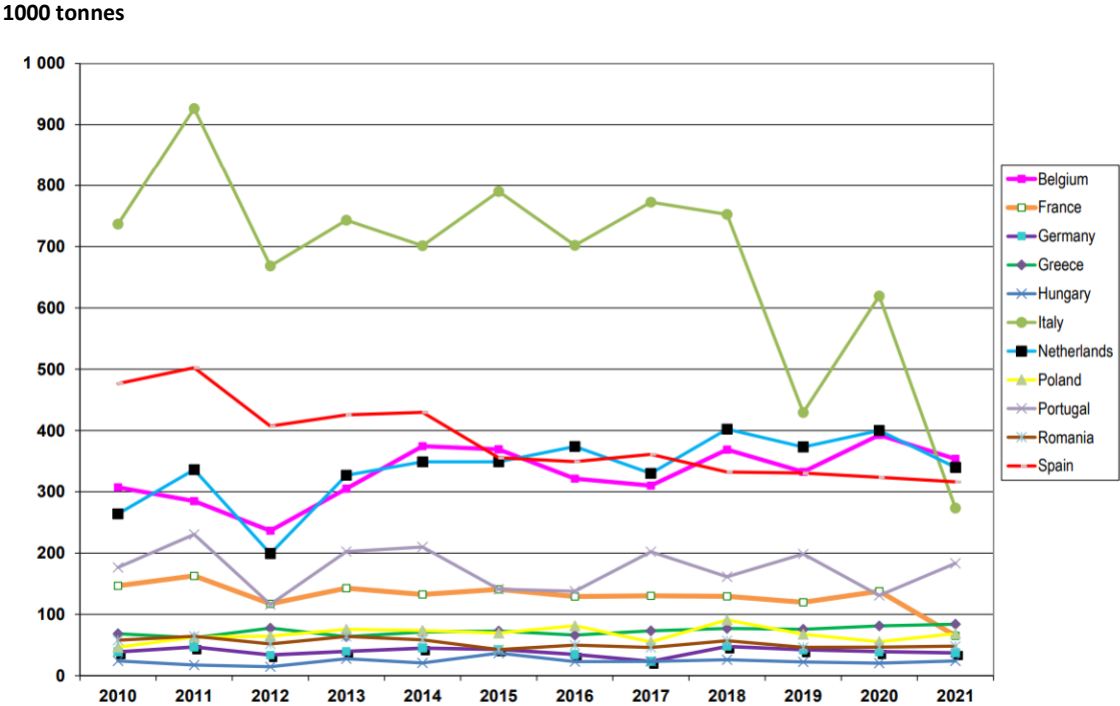


Figure 6- EU's pears production (adapted from[19])

Rocha pear (Figure 7) has a rich history in Portuguese culture, dating back to the nineteenth century, and was granted PDO status in 2003. This cultivar is grown in 29 municipalities in the west-region, more specifically in Torres Vedras, Bombarral, Cadaval and Caldas da Rainha, where the edaphoclimatic conditions are favourable for its development. Apart from its great nutritional value, this species' remarkable conservation capacity and resistance to transportation are key features for both internal and external markets.[26]



*Figure 7- Rocha pear*

The economic value of fruits is dictated by their quality, which is influenced by a variety of factors ranging from production and harvesting to storage conditions. Many of the desired features emerge throughout the ripening phase. This process is characterized by colour changes, chlorophyll degradation and pulp softening, altered sugar metabolisms and volatile production. Since ethylene, a phytohormone, is responsible for the ripening and senescence of fresh goods, its production must be closely monitored throughout.[27]

## 1.2 Fruit physiology

The physiologic development of the fruit must be analysed to better understand the mechanism by which ethylene affects the fruit. Fruit can be termed "alive" after harvest since it continues to complete most of the metabolic reactions (aerobic respiration with oxygen, anaerobic without) and maintains the physiologic function. Nevertheless, because the fruit is no longer attached to the plant, the losses associated with its metabolism are not compensated for by the flow of resources provided by the plant (water, photosynthates and minerals). In the absence of these resources, the fruit must rely on its own reserves as well as the ambient moisture content, which is influenced by temperature and air relative humidity.[28], [29]

Growth, maturation and senescence are the three major phases of physiological development (Figure 8). Cell division is involved in the initial stage, which is followed by cell growth. The second stage is maturation, which includes the late phases of growth up to ripening. The fruits are picked at their physiologic maturation stage, but continue to develop until they achieve horticultural maturity, which corresponds to the full development of consumer-interesting characteristics that might vary depending on the market. Ripening occurs in the final stages of maturation and coincides with physiologic, chemical, biochemical and sensory changes that lead to the development of desirable consumer characteristics. Ripening is an essential step

during the maturation stage that leads to senescence, in which synthetic activities are replaced by degenerative catalytic processes, eventually leading to aging and tissue death. [29]

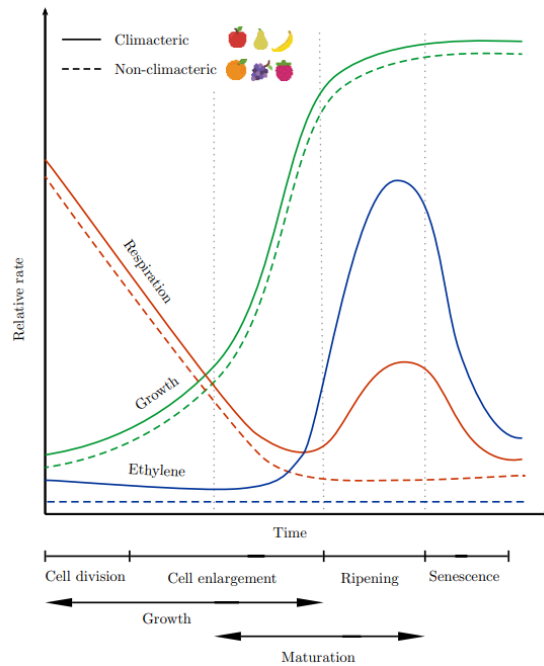


Figure 8- Relative rate of respiration, ethylene production, and growth profiles in fruits (adapted from [30])

Fruits exhibit diverse behaviour throughout ripening, as demonstrated in Figure 8. From a physiological standpoint, fruits can be divided in climacteric and non-climacteric. In the case of climacteric fruits, an increase in respiration rate and increased ethylene production is observed during the onset of ripening, promoting the ripening process after harvest. This is true for apples, pears and all other climacteric fruits such as bananas, kiwis, avocados, tomatoes, peaches, plums, mangos... Non-climacteric fruits, on the other hand, do not show an increase in ethylene production or respiration rate. Fruits such as oranges, grapes, cherries, lemons and strawberries must be harvested in a mature stage because of the process described above.[29], [31]

Researchers identified two ethylene production systems occurring throughout fruit growth. One is autoinhibitory (system 1) and is active during growth and stress responses, while the other is autocatalytic (system 2) and is active during ripening and senescence. In contrast to system 1, a rise in ethylene concentration results in increased ethylene production in system 2. Because of the absence of system 2, non-climacteric ripening behaviour differs from climacteric ripening behaviour.[29], [31]

Hormonal activity is essential for plant regulation and development. Ethylene, in collaboration with other hormones, operates in the processes by binding to certain receptors. After complex formation, the ethylene receptor turns off, kicking off the ripening process. Working on this interaction, either by changing the

number of receptors or by modifying the binding process, is one strategy to influence ethylene production. The composition of oxygen and carbon dioxide in the atmosphere involving the fruits is extremely important in this latter approach because the former increases and the latter decreases the affinity of the ethylene receptor.[31]

## 1.3 Fruit conservation

### 1.3.1 Harvest

Fruit physiologic stage at harvest is a predominant factor in determining the storage approach. Maturation tests (physio-chemical and organoleptic) are conducted prior to and during harvest to determine the maturity stage and optimal harvest time. Nonetheless, unique market requirements for fruit characteristics should be considered. These traits are closely connected to the maturity state during harvest.[32]

Pears collected later are more prone to internal browning, reduced firmness and shorter storage period, but they develop more flavour and colour. On the other hand, pears collected earlier are more vulnerable to surface scald and are less capable of developing flavour, however their storage time is substantially enhanced. To maintain the quality during long-term storage and the development of certain market characteristics, storage techniques must be selected in accordance with the maturity state at harvest. Rocha pear is typically harvested around 133 days after full bloom.[33] However, climatological factors may influence this timing. Pears and most fruits are pre-cold treated after harvest to immediately slow down the metabolic rate before being kept in a refrigeration chamber (between 0 and 1 °C) with proper storage technology.[32], [33]

### 1.3.2 Post-Harvest controlled atmosphere storage

Post-harvest fruit quality is deeply associated with water loss, microbial activity and ethylene production. Controlled gas composition and refrigeration are the principles for controlled atmosphere (CA) storage methods, which ensure quality under longer periods of conservation (7 to 8 months). Rocha pears exposed to this conservation technique retain their colour, firmness and sweatiness after leaving the CA chambers and can complete the normal physiological maturation.[34]

The most critical factor in fruit preservation is temperature.[35] Fruit metabolism is strongly temperature sensitive, with lower temperatures resulting in a slower metabolic rate.[36] This is seen in Table 1, where temperature increase affects metabolic activities such as ethylene synthesis. Another effect of rising temperatures is the increase in transpiration rates and consequent water loss.[37] Higher temperatures not only supply energy that increases water evaporation [38], but also increases peel permeability promoting water diffusion.[39]

Table 1- Temperature impact on ethylene production rate for apple[36]

| Temperature (°C)  | 0    | 5    | 10   | 20     |
|---|------|------|------|--------|
| Rate of ethylene production ( $\mu\text{L kg}^{-1} \text{h}^{-1}$ ) | 1-10 | 2-20 | 5-40 | 20-125 |

Another important factor to consider is relative humidity (RH). Lower RH causes more moisture diffusion from fruit to air.[40] Additionally, water loss may lead to accelerated decay development, physiological disturbances and uneven fruit ripening.[36] The water content of the surroundings should match the water content of the fruit to minimize water loss through transpiration.[35]

Apart from temperature and relative humidity, physiologic condition and mechanical injury are major contributors to water loss.[41]

These parameters should be managed and established based on fruit-specific criteria. Rocha pear is a climacteric fruit that is mostly composed of water (80-89%)[42], therefore controlling water loss and ethylene production is critical to sustaining quality during storage. Because this control relies on the regulation of parameters such as temperature and RH, lower temperatures (between -0.5 and 0.5 °C) and high RH (95%) are advised for these crop storage (these values consider storage under a normal atmosphere, as well as controlled atmospheres).[33]

Some of the differences between CA methods include the gas composition values (mostly O<sub>2</sub> and CO<sub>2</sub>) and how they are regulated and set. Control and regulation of oxygen and carbon dioxide (Figure 9) are at the core of CA room operation.[43]

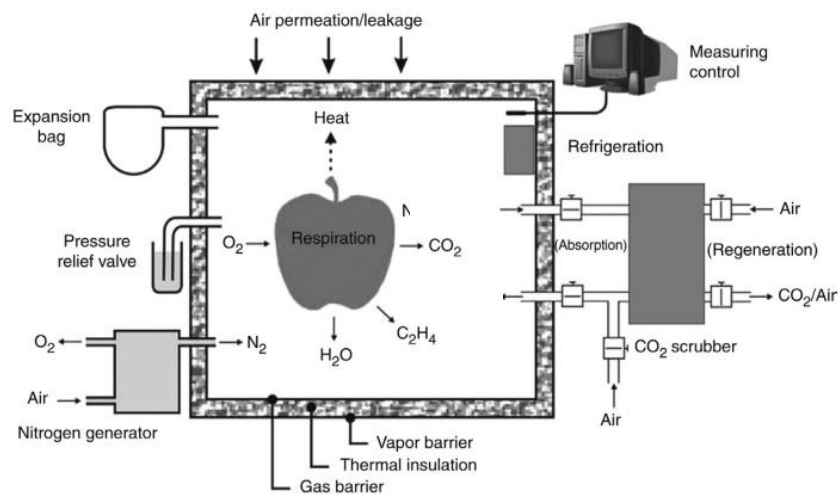


Figure 9- Scheme of a controlled atmosphere (CA) room (adapted from [44])

Oxygen removal has been applied from the beginning of CA. Currently, the most common method for rapidly lowering  $O_2$  levels (3-5 kPa) is to discharge  $N_2$  into the environment of the CA storage room, followed by natural fruit respiration to assure lower levels (method used in the early stages of CA).[45] Rapid CA technique, which is based on fast  $O_2$  reduction (purging  $N_2$  in 1 or 2 days), reduces fruit susceptibility to ethylene. However, there are certain limitations to this procedure since some cultivars suffer from problems like as cavities and interior browning (Conference pears and Fuji apples) upon exposure to low oxygen levels.[46] To address this issue, delaying the establishment of CA conditions and gradually adapting to lower  $O_2$  concentrations result in fruits that are more resistant to browning diseases.[47] Fruits subjected to this technique have higher concentrations of energy source organic molecules such as adenosine triphosphate (ATP) that prevent physiological disorders.[43]

An on-site  $N_2$  generator separates  $N_2$  and  $O_2$  from atmospheric air to generate  $N_2$  gas. Notwithstanding the necessity for on-site storage, the low cost of installation of  $N_2$  generators and their cost-effectiveness give a less costly alternative to the pricey liquid  $N_2$ . [48] As the name indicates, pressure-swing adsorbers (PSA) rely on adsorption technology and are the most often utilized, however  $N_2$  generators based on hollow fiber membrane (HFM) technologies are also used. Stream gases, such as  $O_2$  and  $CO_2$ , are removed from the compressed incoming stream by two beds of carbon molecular sieve that allow nitrogen to flow through in PSA  $N_2$  generators (Figure 10). Following that, the molecular sieve material is vacuum regenerated, releasing the adsorbed gases.[43], [45]

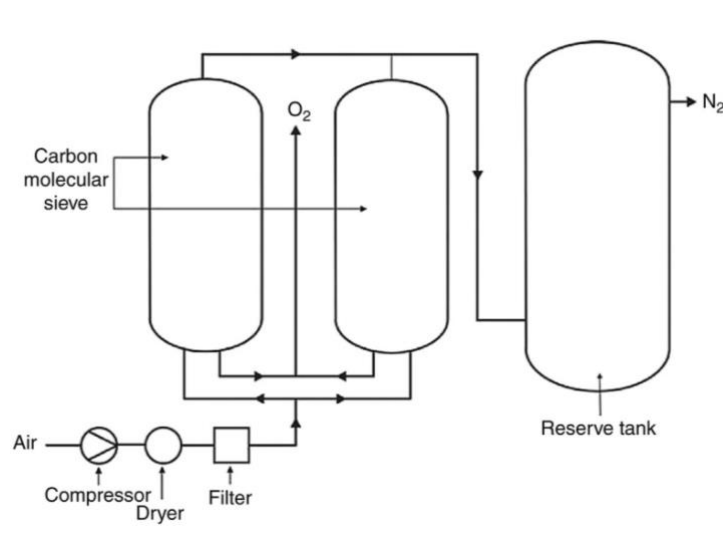


Figure 10- Scheme of pressure swing adsorber (PSA)  $N_2$  generator (adapted from [43])

As previously stated, N<sub>2</sub> generators can be utilized to remove and manage CO<sub>2</sub>, however specialised CO<sub>2</sub> scrubbers are preferred due to their efficiency.[49] Scrubbers are classified into two types: passive scrubbers, which use chemicals that react with CO<sub>2</sub>, and active scrubbers, which use renewable technologies.[50] Despite the emphasis on CO<sub>2</sub> removal, investigations show that various CO<sub>2</sub> removal technologies result in varying volatile profiles inside the chambers. This is a factor that may have an impact on how various ethylene removal technologies perform. [51]

In active scrubbing, the air from the storage chamber is recirculated via the CO<sub>2</sub> adsorbing material in this scrubber, which is made up of two cylindrical beds or a chamber filled with activated charcoal, that switches between adsorption and regeneration to ensure continuous CO<sub>2</sub> removal (Figure 11). The saturated charcoal is then recharged by flowing air from the storage chamber (held in a breath bag). Air from within the chamber is utilized to prevent outside O<sub>2</sub> from impacting ultralow oxygen (ULO) storage technologies.[49]

To a lesser extent, passive scrubbing can be used alone or in conjunction with active scrubbing (in high CO<sub>2</sub> sensitive crops). In this procedure, a bag or pallet is placed inside the room and filled with calcium hydroxide (hydrated lime), which interacts irreversibly with CO<sub>2</sub> to form calcium carbonate (limestone), water and heat.[50] The primary drawbacks of this technology are the wasted space and the inefficient CO<sub>2</sub> distribution due to insufficient interaction between lime and CO<sub>2</sub> in the bags.[52] Yet, studies show that for operations up to 100 tonnes, this technology is well suited for CO<sub>2</sub> removal while being less expensive than active scrubbing.[53]



Figure 11- CO<sub>2</sub> scrubbers (SCS LTD)

Despite many similarities, CA approaches differ in terms of complexity. The most basic method, controlled ventilation, regulates ripening by increasing CO<sub>2</sub> (5-10 kPa) through natural fruit respiration in an



airtight chamber. Ventilation with outside air controls the surplus CO<sub>2</sub>. Oxygen levels are not directly controlled and range from 10-16 kPa, with studies indicating that they have an insufficient effect on respiration rate.[54] Because of the high CO<sub>2</sub> concentration, this approach is a good low-cost option for storing fruits with greater CO<sub>2</sub> tolerance levels. This CO<sub>2</sub> concentration, however, can cause internal and external physiologic disorders such as superficial scald and interior browning in fruits with lower tolerance limits to CO<sub>2</sub> (Rocha Pears, for example).[50] This method also provides a cheap way to remove ethylene.

Conventional CA rooms were developed to more precisely and effectively monitor and control gas composition (O<sub>2</sub> and CO<sub>2</sub>) and temperature. In that sense, more accurate temperature ( $\pm 0.5$  °C) and gas composition sensors (O<sub>2</sub> and CO<sub>2</sub>,  $\pm 0.5$  kPa) were utilized, with scrubbers eliminating excess CO<sub>2</sub> from the storage environment. These changes resulted in lower concentrations of CO<sub>2</sub> (2-3 kPa) and O<sub>2</sub> (2-3 kPa) impossible to obtain through ventilation.[55]

According to research on fruit on O<sub>2</sub> concentration thresholds (anaerobic compensation point), lower concentrations of O<sub>2</sub> can be imposed without triggering anaerobic respirations, which contributes to minimizing the respiration rate and ethylene biosynthesis since oxygen is required for the final step in the ethylene production pathway (1-Aminocyclopropane-1-Carboxylate, ACC to ethylene).[29], [43] However, the low O<sub>2</sub> concentrations results in the production of toxic by-products such as alcohols and aldehydes.[50] Based on this discovery, CA rooms currently rely on Low Oxygen (LO) (1.5-2 kPa) and Ultra Low Oxygen (ULO) (0.8-1.2 kPa) storage to reduce ethylene biosynthesis respiration. To maintain low O<sub>2</sub> levels, rapid CA (RCA) techniques are utilized, and gas composition is thoroughly controlled every 4-6 hours and adjusted every 30 min.[55] Prior to ULO CA storage, fruits, in some cases, are kept in anaerobic conditions (100% N<sub>2</sub> or 0.5 kPa O<sub>2</sub>) for a short length of time (7 days). This pre-storage treatment (initial low oxygen stress) has been demonstrated to be beneficial in inhibiting fruit diseases (superficial scald), resulting in longer storage life and fresher and firmer fruits.[56]

Fruit storage is a complex problem since different conditions impact cultivars differently. Certain parameters, on the other hand, are transversal and might be utilized to monitor ripening. Ethanol synthesis and chlorophyll degradation, for example, occur under stress metabolic reactions on fruit kept at low oxygen conditions. Yet, ethylene production is the best physiological sign of ripening. Dynamic CA storage (DCS) occurs near the anaerobic compensation point (ACP) by lowering O<sub>2</sub> levels within the chamber to the lowest allowed by certain cultivars while avoiding the development of anaerobic metabolism (Figure 12). This threshold is maintained by continuous monitoring of parameters via ethanol and ethylene sensors, as well as chlorophyll fluorescence stress (HarvestWatch™ measurement technology).[57] Data is then analyzed in a control system, and the composition of the atmosphere is altered accordingly. DCS systems are at the forefront of CA technology, being used in more than 200 storage rooms with lower energy consumption when compared to ULO systems.[43], [50]

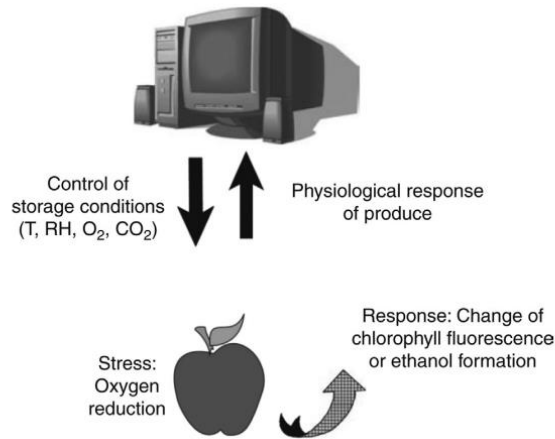


Figure 12- Dynamic controlled atmosphere concept (adapted from [58])

Despite promising findings in increasing the shelf life of fruits stored under CA, this technology has a long way to go before becoming a viable option for agricultural storage for the majority of crops. Economically, the high investment cost in CA storage chambers (cold equipment, humidity control, temperature and ventilation), trained personnel and safety risks make this storage financially unviable in most cases, with most commercially available CA storage rooms being used to store apples and pears. Yet, the biggest disadvantage is a serious absence of knowledge on how different storage conditions affect different fruits. Since physiological responses differ between fruit cultivars, significant comparative studies are still required before implementing these technologies.

#### 1.4 Ethylene removal technologies

Controlled atmosphere methods retard ripening by reducing respiration rates and ethylene production. However, despite the use of ULO chambers, the static nature of these atmospheric systems eventually leads to ethylene build-up. Even in low concentrations (< 0.01 ppm), this hormone stimulates ripening and increases the risk of physiological disorders and microbe development. According to statistical studies, if no additional ethylene treatment is performed on CA storage, up to 80% of the product may be lost.[36]

Several strategies were developed to protect postharvest commodities from the effects of ethylene. These strategies are classified into two categories: plant level actions and environment level actions. Ethylene build-up can be managed using inhibition or removal technologies in this manner. The technology used would be determined by a variety of factors, including removal efficiency, prices, safety, commodity specification, storage area, and so on. This chapter will explore these technologies in order to have a better understanding of the existing and future landscape of ethylene control and removal.

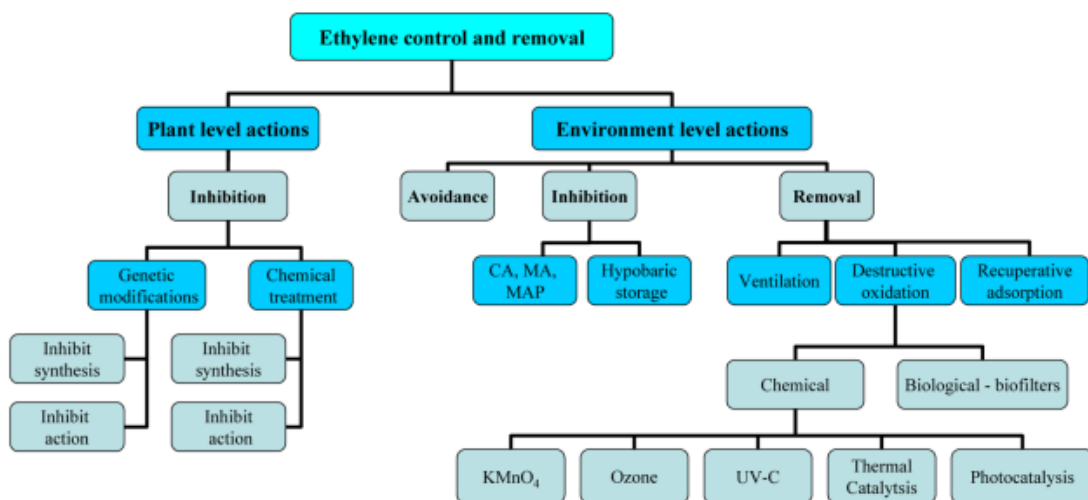


Figure 13- Methods of ethylene removal and control (adapted from [36])

#### 1.4.1 Inhibition through plant level regulation

Ethylene control through plant-level regulation can be accomplished in two ways: ethylene synthesis inhibition and ethylene action inhibition. The second option is far more appealing since it protects crops from both endogenous and exogenous ethylene by preventing ethylene effects at the receptor level.[59] These techniques can be achieved through a variety of methods, including genetic modification and the use of chemical inhibitor compounds. Although the function of genetic modification is plagued by known issues that extend far beyond general concerns about genetically modified organisms (GMOs).[36] In the case of transgenic ethylene synthesis, research indicates that this change has a negative influence on fruit flavour, colour, and nutritional value.[60] When it comes to ethylene action inhibition, Brummel *et al.*[60] cites a lack of understanding of genetic modification effects on ethylene perception and response, as well as interferences with ethylene signalling, as the key barriers to commercial viability.

The most frequently utilized commercial chemical inhibitory substance is methylcyclopropene (1-MCP). 1-MCP is a nontoxic olefine that may efficiently prevent the interaction between fruits and ethylene at low concentrations, hence extending the fresh-keeping period of climacteric fruits.[61] This is accomplished by binding tightly 1-MCP to the ethylene receptor, keeping it inactive and blocking ethylene binding.[36] 1-MCP is a planar molecule that, due to its greater compound energy and double-bond tension, may successfully compete with ethylene for the binding site (Figure 14).[59] The effectiveness of this treatment is predicated on the exposure time and concentration of 1-MCP utilized, as well as the fruit's ability to recover from the blockage and allow normal ripening to proceed. In most cases, fruits treated with 1-MCP are unable to recover from the blockage, thereby stopping maturation processes (evergreen state).[62]

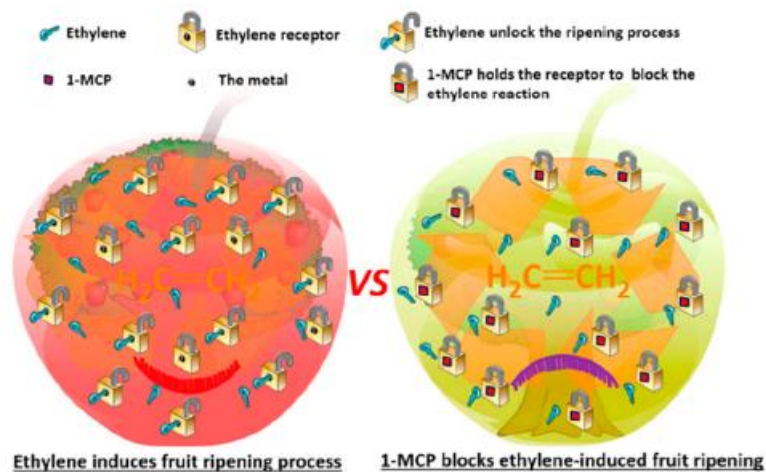


Figure 14- Schematic representation of 1-MCP treatment impact (adapted from [59])

The influence of 1-MCP on fruit goes beyond ethylene inhibition. Studies using 1-MCP-treated Rocha pears have shown the ability to prevent physiological problems such as superficial scald and internal browning. Moreover, research using papayas treated with these chemicals found that the treatment did not prevent sugar build-up. [50], [63]

However, the usage of 1-MCP is limited due to its high cost and difficulties in maintaining the right concentration in order to obtain fruit with adequate taste and quality.[64] Also, more studies are needed to understand the influence of this treatment on various fruits at various physiological stages and the potential long term health impact provoked by the ingestion of fruit treated with these chemical compounds.

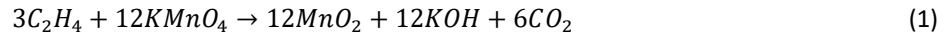
#### 1.4.2 Ethylene removal through destructive oxidation

Another method of reducing ethylene effects is to remove (clean) this molecule from the storage environment. This is accomplished by the application of destructive technologies based on oxidation processes. These approaches, unlike inhibitory technologies, rely on external scrubbing systems, so there is no direct contact with the fruit.

##### 1.4.2.1 Potassium permanganate

Oxidation scrubber is a technology that relies on continuous irreversible oxidation reactions to decompose ethylene. This can be achieved by recirculating air from the storage chamber via the oxidation-filled external scrubber.[36]

Potassium permanganate reacts stoichiometrically with ethylene according to the following overall reaction:



Aside from ethylene removal, the carbon dioxide produced by this reaction helps to prevent ethylene endogenous synthesis, however, as already stated, its uncontrolled increase could promote fruit disorders.

Since diffusion and natural convection are driving forces behind the efficacy of this technology, small particles with a high specific surface area exposed to the atmosphere are required to remove trace ethylene.[65] To enhance this property, potassium permanganate is immobilized on porous inert materials with high surface areas such as zeolites, alumina (Al<sub>2</sub>O<sub>3</sub>) gel, silica (SiO<sub>2</sub>) gel, clays, activated carbon and so on.[66] In certain circumstances, the adsorption qualities of the support may improve the process by forming an adsorption-oxidation system in which ethylene is adsorbed by the support and oxidized by the potassium permanganate.[67] Permanganate carriers vary in pore size, pore volume, and bulk density, with these parameters influencing ethylene oxidation efficiency. Several commercial potassium permanganate-based ethylene scrubbers available nowadays, are made of activated alumina as KMnO<sub>4</sub>'s support, due to their physical and mechanical properties.[65] Alumina has many interesting properties, including high adsorption capacity and thermal stability, as well as being non-toxic and inexpensive.[68] According to Kavanagh and Wade 's[69] research on ethylene carrier substances, reduced bulk density and increased capacity to absorb permanganate resulted in greater capacity to decrease ethylene.

Although potassium permanganate is rapidly consumed at room temperature, it must be refilled frequently over extended conservation periods. The correlation is exemplified by Blanpied *et al.*'s[70] studies on Empire apples. In 200-tonne storage, removal efficiency reduces to 25% after 12 days due to permanganate consumption and detrimental water absorption.[70] This interaction with water is exemplified in Wills and Warton's line of studies, where a 50% loss in efficiency was observed when RH increased from 70% to 90%.[36] These authors' studies concluded that the loss in efficiency with time relates to the difficulty of ethylene diffusion since untreated potassium permanganate remained in the bed. It is proposed that a use-skin (oxidation of the surface layer) formed, conditioning ethylene diffusion.[36] To overcome diffusion issues, a nanomaterial solution with improved water resistance characteristics should be considered for the long-term preservation of a large number of fruits.

According to Wills and Wator's study, efficiency is directly connected to the amount of potassium permanganate, with 60 g of potassium permanganate capable of offsetting 90% of the 10 μL Kg<sup>-1</sup> h<sup>-1</sup> of ethylene created by 1 Kg of produce (90% RH and 20 °C). Hence, this material appears to be appropriate for smaller

packages with lower ethylene production rates. However, when greater production rates are examined, its feasibility is called into question, as bigger amounts of reactant are required, resulting in by-product buildup.[71]

Nowadays, the most prevalent commercial application is in small sachets that are included directly in the package. This form of modified environment packaging is gathering study attention in the field of fruit conservation. Silva *et al.*[72] indicated that KMnO<sub>4</sub> sachets may effectively prolong fruit in a pre-climacteric (for 25 days) without interfering with natural ripening after the sachet was removed. In the same scope, Dobrucka *et al.*[73] found that 1-2 g of potassium permanganate supported on zeolites might inhibit pathogen development related to ethylene rise. This correlation is supported by Kader *et al.*'s[74] work on fungi growth in oranges, where an increase in C<sub>2</sub>H<sub>4</sub> made the fruit more susceptible to pathogens by inhibiting the formation of antifungal compounds.

Aside from the non-reversible character of this method, another notable drawback is the production of a significant amount of by-products such as KOH. Despite their economic worth as organic fertilizer, their usage is contingent on the additional treatment of the spent product.[36]

#### 1.4.2.2 Ozone

Ozone oxidant/disinfectant properties are well documented. Its use in the storage environment provides tangible benefits in terms of postharvest disease prevention by inhibiting microorganisms, spore production delay, sanitation and ethylene elimination via the following oxidation equation[75]:



Ozone is generated easily using light or corona discharge generators (Figure 15).[36] Crisosto *et al.*[76] examined the latter option (OxtomCav generator) as a method of removing ethylene from a refrigerated storage container (0 °C for 24 hours at 3.8 ppm of ethylene). The rate of ozone formation was proportional to the rate of ethylene reduction, and it performed similarly to the potassium permanganate filter. Following that, the oxygen and ozone concentrations were 0.2 ppm and 3.9 ppm, respectively. Notwithstanding the intriguing results, certain precautions regarding ozone exposure should be taken. The European Union's Air Quality Directive establishes stringent requirements in order to reduce health and pollution consequences. The daily maximum 8 hours mean ozone concentration threshold suggested is 0.06 ppm.[77] While adopting this method for fruit preservation, ozone toxicity is a crucial factor to consider since certain quantities of ozone can cause irreparable damage to human and plant cells. As a result, its regulation and monitoring are critical to ensuring human safety and preventing fruit damage.[36]

Alternative designs are being considered to address these issues, such as day-night cycles of ozone generation to reduce worker exposure and recirculation of storage air through specific ozone chambers (Bio-turbo by Miatec, USA).[78] Yet, because there is no direct contact with the fruit in the latter case, the anti-fungal capabilities of ozone are absent.

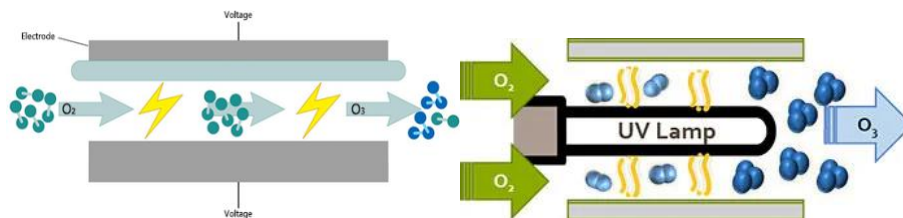


Figure 15- Corona (left) and light (right) discharge ozone generators (adapted from [79])

#### 1.4.2.3 Bio-filtration

Biofiltration, as the name implies, is a technology that resorts to biological filters to remove ethylene from horticultural storage waste gas.[80] This technology is still in an early stage of development due to complex, physical, chemical and biological phenomena.[81] Therefore, no commercially available application is used either in storage/transport conditions, and only a few academic studies were published.[36]

This technology's efficiency is closely connected to microbial activity at low storage temperatures.[36] Elsgaard's research confirmed this relationship, with efficiency declining from 99% at 20 °C to 83% at 2 °C (inlet flow 73 mL/min with 2 ppm ethylene) and sub-stoichiometric CO<sub>2</sub> generation confirmed below 5 °C, implying by-product build-up in the biofilter.[82]

In addition to microorganism selection, filter media properties influence efficiency. The efficacy of soil biofilters is hampered by their small surface area, low permeability and limited adsorption capacity.[83] Nevertheless, peat and compost biofilters have limitations, most notably the requirement for replacement medium and large installation areas.[84] Some alternative mediums, like granular activated carbon (GAC), were studied to overcome these problems. Kim's research with GAC concluded that an increase in efficiency is expected during effluent treatment since microbial enzymes induced by the micro-organisms resulted in the growth of specific ethylene-degrading organisms. In the same research, 34 g C<sub>2</sub>H<sub>4</sub> m<sup>-3</sup> day<sup>-1</sup> was eliminated from an inlet stream composed of 331 ppm of ethylene with 100 % efficiency reached after a few days and maintained for 20 days.[85]

The key advantage of this technology is the minimal amount of energy required, as well as the low investment and maintenance costs. Nevertheless, in addition to the difficulties of eliminating lower biodegradability chemicals such as ethylene, the large amount of area required and the slow nature of the process limit the feasibility of this technique in horticultural storage facilities.[36], [86]

#### 1.4.2.4 Catalytic oxidation

Catalytic oxidation is an ethylene removal process that depends on ethylene catalytic combustion at high temperatures.[36] This destructive method provides constant and irreversible ethylene elimination (as do all oxidation technologies) via the oxidation process described below:



Catalytic oxidation is a heterogeneous process in which reactant adsorption on the catalyst surface changes the reaction route and activation energy.

Scrubbing systems for ethylene removal that employ a catalytic oxidation method are already commercially available (Swingtherm by Fruit Control Equipments srl), particularly in large-volume storage rooms.[86] The recirculation of ethylene-rich gas from storage rooms via the scrubbing tower filled with catalyst is the foundation of this process. A ceramic heat exchanger is used to heat the incoming gas and then reinject the air at a temperature closer to that of the storage chamber after the treatment.[36]

The fundamental benefit of this system is its ease of installation and operation, as well as its high conversion efficiency (90-98%). Several studies revealed that decreased ethylene concentrations resulted in a considerable drop in efficiency; nevertheless, the key caveat is the heat load provided to the refrigeration system, even when efficient heat exchangers are utilized.[36]

Current research is being conducted to develop catalysts that efficiently decompose ethylene without the need of high temperatures. Therefore, operational expenses are reduced, reusability is increased, toxicity is reduced and overall conditions for fruit preservation are improved.[59]

Noble metals and transition metal oxides are the active components often utilized on catalysts for the oxidation of volatile organic compounds (VOCs) in low-temperature catalytic oxidation processes. Because this process is based on ethylene adsorption on the catalyst surface, support features like pore structure, surface chemistry and morphology play a crucial role in the process by acting as an interface between ethylene and the active sites.[59] Lately, studies have focused on active metal sites made up of gold nanoparticles, platinum, silver, copper and cobalt. Xue *et al.*[87] study on Au/CO<sub>3</sub>O<sub>4</sub> nanorods demonstrated significant activity at low temperatures (0 °C) and efficient ethylene conversion (93.7%). Au nanoparticles increased oxidation by promoting oxygen species adsorption and dissociation.[59] Yang *et al.*[88] achieved 100% conversion of 100 ppm of ethylene at 25 °C with a silver-based catalyst. This is strongly related to Ag<sup>+</sup> species, through strong  $\pi$ -complexation bonds with ethylene.[89]

#### 1.4.2.5 Photocatalytic oxidation

Photocatalysis is an emerging environmental-friendly technology for the low-temperature catalysis of ethylene. It refers to the photocatalytic oxidation of ethylene into water and carbon dioxide.[90] The photon-activated catalyst is often a semiconductor that has been irradiated by suitable wavelength radiation. Due to



the small energy difference between the valance band and the conduction one (band gap)[91] in these materials, appropriate radiation (with energy larger than the band gap) can excite electrons from the valance band to the conduction one, resulting in holes in the valance band. When paired with surface adsorbed water and oxygen molecules, the electron-hole pairs formed are highly charged and capable of initiating reduction and oxidation reactions. [86] These reactions (described by equations 4,5,6) are triggered by reactive oxygen species (ROS) such as hydroxyl and superoxide radicals. Titanium oxide-based semiconductors are the most used catalysts owing to TiO<sub>2</sub>'s high stability, low costs, biological and chemical inertness and high ultraviolet adsorption. [86]



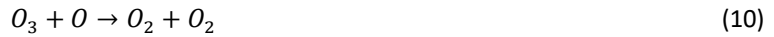
The primary disadvantages of this method are the necessity for UV light stimulation in photocatalysts with larger band gaps and the decline in photocatalytic activity owing to hole-electron pair recombination, which eventually leads to catalyst deactivation.[92] To compensate for this problem, according to Kumar *et al.*[93] and Lin *et al.*'s[94] studies on ethylene photocatalytic oxidation (PCO), TiO<sub>2</sub> doped with non-metals (such as nitrogen and carbon) exhibits an increase in activity under visible light. Additionally, Young *et al.*'s[95] work utilized noble metals (such as platinum or rhodium) in addition to TiO<sub>2</sub> that avoid electron-hole recombination by acting as "electron sinks". Furthermore, Yamazaki *et al.*'s[96] studies suggested that water and ethylene compete for the same adsorption sites, thus RH atmospheres have a negative impact on the ethylene photooxidation rate.

Despite the presence of commercial equipment based on this method (for example, Absorger's ECOscrub and KES Science & Technology, Inc's AiroCide®), research publications on their efficiency and effectiveness in increasing fruit shelf life are scarce.[86] The majority of the published papers discuss photocatalysis inclusion in food packaging. Research on nanofibers containing TiO<sub>2</sub> revealed strong photocatalytic activity, resulting in decreased ethylene concentrations in fruits stored with these materials (cherry tomatoes, banana).[97]

#### 1.4.2.6 VUV photolysis of ethylene

Another method for ethylene degradation is VUV photolysis. UV-C lamps (Figure 16) emit radiation in the wavelength range (184-254 nm) where ethylene is degraded (184 nm).[67] Additionally, Scoot *et al.*'s [98]study has demonstrated that, in addition to removing ethylene, these lamps may assist in eliminating microorganisms, which is a key factor in fruit storage. Because its removal process is directly tied to atomic oxygen created by oxygen exposure to UV radiation, ethylene degradation is an indirect reaction to UV

radiation.[67] Jozwiak *et al.*[99] created the model below (equations 7-12) to represent the ethylene elimination pathway:



As demonstrated by Jowiak's model, ozone and a slew of by-products are created, thus treatment is required. Apart from this issue, Lawton's[100] research found that the total effectiveness of this oxidation approach in low ethylene concentration (0.086 ppm) on CA fruit preservation is unusually poor (7%). Furthermore, the process is oxygen limited, and because CA uses low oxygen concentrations, this results in poor VUV photolysis performance. On the bright side, this scrubber system consumes less energy, leading to a lower heat load on the refrigeration system. [36]

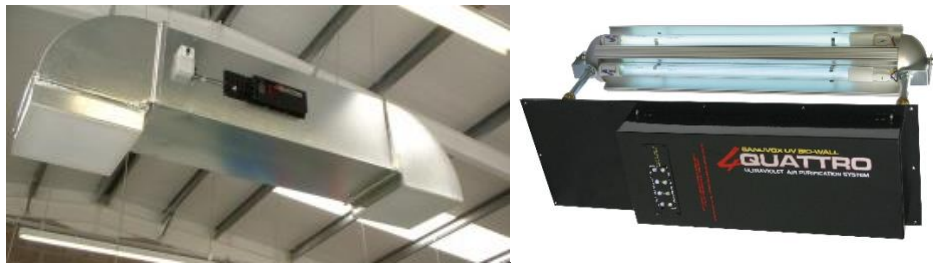


Figure 16- UV lamp for ethylene removal

### 1.4.3 Recuperative adsorption

By relying on reversible selective adsorption of ethylene, recuperative methods provide an alternative to destructive oxidation methods. Lower temperatures are required for fruit storage chambers, which can improve exothermic processes like adsorption. This relationship was verified by Hernández *et al.*'s[101] investigation, where potassium-base zeolites were used in the adsorption of ethylene and ethane, with an increase of the adsorption temperature resulting in a lower amount of ethylene adsorbed. Depending on the kind of interaction between the adsorbate and adsorbent surface, adsorption can be either physical (physisorption) or chemical (chemisorption).[102] Physisorption includes weaker intermolecular interactions known as Van der Waals forces (enthalpy lower than 50 kJ/mol), which comprise London dispersion forces and dipole-dipole (permanent or induced) forces. Chemisorption is based on stronger interactions (enthalpy higher than 50 kJ/mol) between molecules whenever the electronic structure of the adsorbent/adsorbate changes and a chemical bond is formed.[103] The nature of these interactions helps the regeneration capacity of

zeolites, as bound molecules may be easily removed by increasing the temperature and decreasing the pressure.

Adsorbents should have a high adsorption capacity with fast diffusivity, as well as a high hydrophobic nature, ease of regeneration, low cost, shape ability, and thermal and hydrothermal durability. Multiple adsorbent materials of various natures have been studied in the literature, including inorganic (activated carbons, zeolites, etc.), organic (polymers) and inorganic-organic hybrids (MOFs).[104] Despite the research into several materials, only zeolite-based adsorbents are commercially employed for preventing fruit ripening. This commercial product, named It's Fresh![105], employs palladium-impregnated zeolite sheets. The lack of variety in adsorbents is due to critical faults in the materials investigated. The rationale for activated carbons is built on the flammability of these materials, which makes regeneration problematic.[104] Metal-organic frameworks (MOFs) have gathered interest in recent years. Although the primary drawbacks are significant efficiency difficulties at higher RH conditions and difficult scale-up due to expensive synthesis procedures.

Zeolites are crystalline inorganic microporous materials made of tetrahedrally-connected framework structures formed by corner-sharing of aluminate ( $\text{AlO}_4$ ) and silicate ( $\text{SiO}_4$ ) tetrahedra.[106] Zeolites can be either natural or synthetic, however, the latter gives greater control over characteristics. The primary building units are aluminate and silicate tetrahedra, however, the way these tetrahedra units are ordered and connected across the network can vary, resulting in secondary building units (SBUs) which form pores and channels.[102] Pores of varying sizes (ranging from 0.03 nm to 0.75 nm) provide molecular sieving properties, which are valuable for the selective adsorption of molecules with varying kinetic diameters. Furthermore, the porous nature of the structures results in high surface areas, which are critical for improving adsorption.[102]

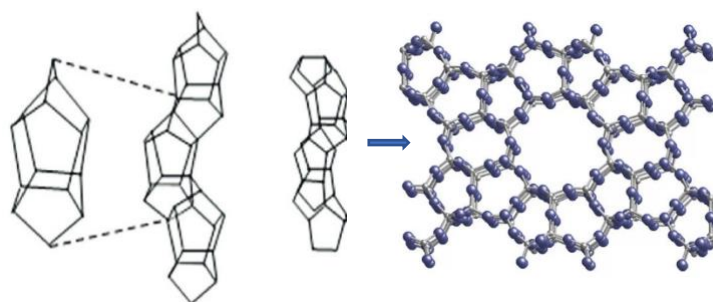


Figure 17- ZSM-5 zeolite (MFI structure) and pentasil SBU

The Si/Al ratio is also important in determining zeolite polarity. Higher Al levels promote interactions with polar molecules such as water, resulting in more hydrophilic zeolites. Because fruit storage is generally associated with a high RH, hydrophobic zeolites perform better in adsorbing non-polar molecules such as ethylene rather than polar molecules such as water.[107] This relationship was studied and corroborated in

Calleja *et al.*'s[108] study on ethylene adsorption of ethylene on ZSM-5 zeolite in a multicomponent environment (ethylene, propane and carbon dioxide). Furthermore, they reveal that lower Si/Al zeolites have a greater attraction for polar molecules due to increased heterogeneity and a larger electrostatic field.

The total negative charge obtained by  $[\text{AlO}_4]^{-1}$  must be balanced by compensating cations (organic or inorganic) positioned inside the pores and cavities giving rise to ion exchange properties.[109] In these processes, high silica zeolites have an affinity for cations with low charge density (large and monovalent), while cations with high charge density have an attraction for low silica zeolites.[110] The nature of the compensating cation has a significant role in improving selective ethylene adsorption. Erdogan *et al.*[111] investigated the ethylene adsorption isotherms between zeolites with various compensating cations (Na, Ca, K, and P) and determined that elements with higher electronegativity give stronger adsorption sites. Noble metals, such as palladium, platinum and silver, and transition metal ions like nickel and copper appear to have a high affinity towards ethylene, because of the chemisorption of this molecule through a mechanism called  $\pi$ -complexation (Figure 18), which expands on the physisorption of ethylene through electrostatic interaction between CH and O of the zeolite frameworks.[112], [113]  $\pi$  electrons cloud and higher quadrupole moment present on ethylene favour the formation of  $\pi$ -complexation with these metal species. There is an interaction between the metals' outer s and d orbitals and the ethylene  $\pi$  bond. The overlap of the electron cloud with the metal's unoccupied outermost s-orbital results in the formation of a  $\sigma$  bond. There is also a back donation from the metal's d-orbital and the unoccupied  $\pi^*$  anti-bonding orbitals of the ethylene molecule. This interaction is enhanced by zeolites exchanged by larger cations; however, larger cations can block the CH-O adsorption sites, thus reducing ethylene adsorption.[114]

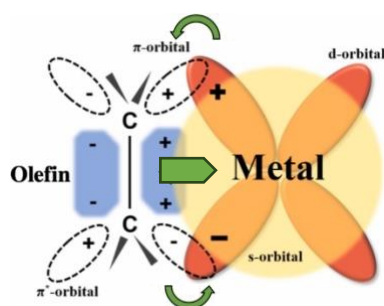


Figure 18- Schematic of  $\pi$ -complexation interaction (adapted from[114])

The significance of these interactions on multicomponent ethylene adsorption on metal-based zeolites has been extended to various fundamental studies as well as commercial products (It's Fresh). Johnson Matthey Technology Research-Center investigated this subject [115], resulting in a patent for palladium supported on ZSM-5 zeolites. In addition, Pd-promoted zeolite efficiency was compared to  $\text{KMnO}_4$  supported on alumina (5% wt. of  $\text{KMnO}_4$ ), with the zeolite-based adsorbent showing a greater ethylene adsorption

capacity. Despite the recorded promising results obtained with Pd-based zeolites, their usage on a broader scale is limited by the high cost of this noble metal (46517 € per kg[116]). Various alternative studies employing zeolite loaded with other metals, but with similar characteristics have been undertaken in this field of study. In this regard, silver has emerged as a more cost-effective alternative to palladium (742 € per kg).[117] This is demonstrated by the large number of research on silver-based zeolites indicating their potential for ethylene adsorption.

Further research on silver-based zeolites revealed that an increase in silver content is not directly linked to an increase in ethylene adsorptions because the chemical state and position of silver on the matrix impact the process. Monzón *et al.*'s[118] study indicated that the presence of metallic silver (Ag(0)) has no effect on ethylene adsorption because the absence of empty orbitals prevents  $\pi$ -interaction with ethylene. Its presence on the zeolite structure also causes pore obstruction, preventing ethylene from accessing active sites. Larisha *et al.*'s[119] research confirmed the lack of metallic silver contributions and concluded that the better ability to form complexes, and therefore higher adsorption capacity, is explained by the strong stability of highly dispersed Ag<sup>+</sup> species on zeolites. However, Monzón *et al.*[118] showed that the aggregation of Ag ions (Ag<sub>n</sub><sup>δ+</sup>) reduces the number of active sites for ethylene  $\pi$ -interaction. Furthermore, the size of the agglomeration reduces active surface and increases pore obstruction. Horvatis *et al.*'s[120] DFT calculation revealed that ethylene can be adsorbed on Ag<sub>2</sub>O particles. According to Lee *et al.*'s[121] findings, higher Ag ionic exchange on zeolites results in reduced dispersion of Ag particles, resulting in the formation of Ag<sub>2</sub>O particles. These oxides also undergo  $\pi$ -complexation with ethylene; however, the interactions are noticeably weaker than those of Ag<sup>+</sup> due to the Ag atom's electron shortage. According to Min *et al.*'s[122] findings, lesser framework Al in zeolites corresponds to more stable Ag<sup>+</sup> ions, implying that this is due to greater repulsive interactions between higher intrazeolitic Ag<sup>+</sup> concentrations. Mok *et al.*'s[123] studied several zeolite structures (ZSM-5, 13 X and USY) loaded with Ag and palladium-base zeolites and concluded that the latter demonstrated better ethylene adsorption ability, especially under wet conditions.

Another metal that has gathered attention is copper (Cu). The similarities with silver and even lower price (8.25 € per Kg [124]) make it an interesting alternative. There is a severe lack of research on Cu-based zeolites. However comparative adsorption work from Abdi *et al.*'s[125], with Ag and Cu-based zeolites led them to conclude that Cu presents a competitive adsorption performance and should be considered as an alternative to expensive metals.

Most of the research focuses on ethylene adsorption in dry conditions. However, because fruit storage requires high RH, the competitive nature of ethylene and water for adsorption sites is of greater importance in the field of fruit quality preservations. Despite the presence of several chemicals in the air of fruit storage rooms, water is by far the most prevalent. Because of the negative charges, water has a great attraction for zeolites. Interactions with compensation cations, on the other hand, should not be overlooked, especially in cations with greater polarization, which results in stronger interactions with water.

Lee *et al.*'s[121] studies on ethylene/toluene adsorption on Ag-ZSM-5 zeolites (wet conditions, 5% concentrations) showed that ethylene and water compete for adsorption sites, resulting in a reduction in adsorption capacity (from 121 mol/g to 94 mol/g). DFT's study suggests that water competes with ethylene for  $\text{Ag}^+$  and  $\text{Ag}_2\text{O}$  sites, but only water covers Brönsted acid sites.

Despite the obvious benefits of zeolites, there has been little study conducted under conditions close to those found in CA storage rooms. Zeolites' viability is dependent on the development of more selective and hydrophobic zeolite-based adsorbents. However, the easy properties tuning of synthetic zeolites, together with the exclusive properties afforded by the inclusion of transition metals, demonstrate the technology's promise.

There are already several commercial products available that use ethylene removal processes, such as sheets, pads and filtration equipment. When utilized in fresh produce packages or large storage rooms, these products have various degrees of ethylene removal efficiency. As a result, the selection of a suitable ethylene removal method is dependent on many parameters, including the fruit's ethylene sensitivity, storage space and amount of fruit. However, there is currently a scarcity of relevant scientific data investigating the influence of various ethylene removal technologies on fruit quality under actual storage conditions. This, along with the lack of cost analysis makes comparisons between these techniques difficult. Despite the hurdles, recuperative adsorption presents itself as a promising technology, with clear economical and performance advantages. The advantages rise from the highly tunability of the zeolite characteristics and the role as a support for highly ethylene selective species. Furthermore, the recuperative nature of the adsorption process offers a way to maximize adsorption capacities, leading to a cheaper more sustainable way to control ethylene concentration.

## 1.5 Zeolite shaping

As previously indicated, commercial zeolites are usually employed in fruit packing as zeolite sheets. However, zeolite-based technologies have inherent properties that allow them to be used on larger scales. The scale-up process is a crucial step in implementing a technology on an industrial scale. The majority of the ethylene adsorption investigations documented in the literature include trials using powder adsorbents. Zeolite powders are shaped into pellets or extrudates to improve physical, chemical, or mechanical properties.[126]

An ideal shaped adsorbent should be able to reproduce powder performance, guarantee mechanical strength and chemical/thermal stability, be easy to recover and prevent excessive pressure drops. Furthermore, the manufacturing process must be repeatable, and the formed adsorbent must be both safe and cost-effective.[127], [128] In practice, the shaping process is somewhat delicate due to the extra layer of complexity provided by the shaped materials that evidence different properties (composition, porosity, structure) than the raw powders.[126]

The most frequent method of zeolite shaping is mixing-extrusion. Shaped zeolites have low mechanical strength, hence shaping with a binder (usually alumina or silica) is necessary to improve this property.[129]

Mechanical strength is a critical concern in industrial settings since shaped zeolite deterioration may have a negative impact on performance and equipment integrity. Furthermore, extra safety problems should be considered in the realm of fresh products storage since the fines might potentially interact and harm the stored crops.[130] The mixing-extrusion process begins with the mixing of the binder precursor and is followed by two phases of kneading. In the first stage, an acid (peptizing agent) is added to the mixture to separate the particles of the binder precursor by reducing the pH of the produced paste below the binder precursor's zero charge point (PZC). Following that, a neutralizing technique is used to raise the pH of the mixture over the PZC, resulting in an increase in viscosity.[129] Additional lubricants and plasticizers can be used to minimize the risk of structural damage during mechanical processing.[126] Perego *et al.*'s[131] study demonstrated the relevance of methyl cellulose as a plasticizer in extrusion operations. The paste is extruded once its proper rheological qualities have been obtained. The amount of water added during kneading is critical for producing a paste with appropriate consistency for extrusion.[129] The form and size of the extrudate (which is critical for mitigating diffusion problems) are dictated by the shape and size of the extrusion die. Finally, the extrudates are dried to evaporate the water and thermally treated (calcined) to confer mechanical strength and textural properties.[130] This stability is achieved by significant interparticle contact and chemical bonding modifications.[132] Organic additives (such as methyl cellulose) are eliminated throughout those steps, generating pores within the structure.[130]

Binder addition may be correlated with significant changes in zeolite characteristics such as acidity and structure. Martin *et al.*[133] investigated the interaction of HZSM-5 and boehmite and concluded that the introduction of the binder (boehmite) partly neutralized the Brønsted acid sites and promoted the development of weak and strong Lewis' acid sites. However, certain occurrences of increased acidity have been described in the literature, indicating that the behaviour is very dependent on the zeolite type.[134] Extrudates containing bentonite and other zeolites, for example, exhibited varying acidity behaviour. While BEA zeolite exhibited more acidic sites, the ZSM-5 and MOR zeolites lost some of their Brønsted acidity.[135]

Another well-known effect of shaping is a loss of performance due to increased diffusion path and micropore (binder-blinding) obstruction, which might restrict active site accessibility.[136], [137] Sun *et al.*[138] investigated the influence of the binder on the adsorption of n-paraffins on 5A molecular sieves using binderless (less than 10 wt.% binder[130]) techniques. Experiments demonstrated that binderless pellets had better adsorption capabilities, although they had lower mechanical strength. To overcome mass-transfer limitations studies have focused on the insertion of an auxiliary network of meso/macropores to build hierarchical zeolites.[126], [130]

The selective adsorption of ethylene is strongly reliant on the metals, that can be loaded directly in the powder or after extrusion. Nevertheless, the shaping process poses (Figure 19) additional hurdles in terms of metal dispersion control in the final materials. The loading of the active metal onto non-zeolite phases, as well as the migration of metal species from the zeolite, may change metal functions and metal dispersion,

ultimately leading to unanticipated adsorption behaviours. The nature of the selective deposition is yet unknown; however, the selective load appears to be dependent on the synthesis process and the zeolite-binder interaction strength.[126]

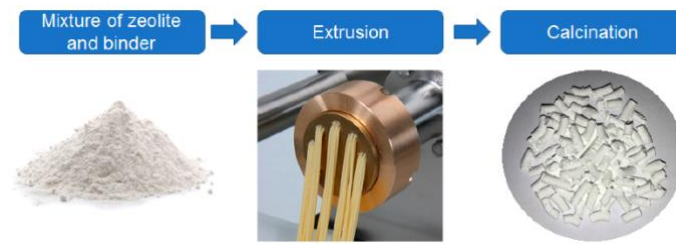


Figure 19- Zeolite shaping process



## 2 Experimental methodology

### 2.1 Adsorbents preparation

#### 2.1.1 Materials

NH<sub>4</sub>ZSM-5 CBV8014 from Zeolyst (Si/Al=40), NH<sub>4</sub>ZSM-5, CBV 3024E Zeolyst (Si/Al=15), sodium nitrate (NaOH, > 98 wt.%) from Sigma-Aldrich, silver nitrate (AgNO<sub>3</sub>, > 99 wt.%) from ThermoScientific, cupric acetate monohydrate (Cu(CH<sub>3</sub>COO)<sub>2</sub>.H<sub>2</sub>O) from Fluka, PURAL SB (Al<sub>2</sub>O<sub>3</sub>, 70.3 %) from Condea, *Methocel* from DuPont, nitric acid (10 mol/L) from Merck and ammonium hydroxide (NH<sub>4</sub>OH, 25% NH<sub>3</sub>) were used as received.

#### 2.1.2 Preparation of zeolite samples

The powder Ag-based ZSM-5 zeolites, depicted in Table 2, used in the experiments were prepared by Ferreira, a PhD student from the Nano4Fresh project.[139]

Table 2 -Ag-based ZSM-5 powders characteristics

| Sample reference | Si/Al | Compensation Cation | Ag content (% wt.)* |
|------------------|-------|---------------------|---------------------|
| RF026MFI         | 15    | H <sup>+</sup>      | 0.69                |
| RF017MFI         | 15    | H <sup>+</sup>      | 3.1                 |
| RF015MFI         | 15    | H <sup>+</sup>      | 4.6                 |
| RF022MFI         | 15    | Na <sup>+</sup>     | 4.3                 |
| RF024MFI         | 15    | Na <sup>+</sup>     | 6.1                 |
| RF027MFI         | 40    | H <sup>+</sup>      | 0.52                |
| RF019MFI         | 40    | H <sup>+</sup>      | 1.9                 |
| RF016MFI         | 40    | H <sup>+</sup>      | 2.8                 |
| RF023MFI         | 40    | Na <sup>+</sup>     | 3.2                 |
| RF025MFI         | 40    | Na <sup>+</sup>     | 3.9                 |

\*Ag content quantified by ICP-OES

Two Cu-based zeolites were prepared by ionic exchange. Two different ZSM-5 zeolite parents either ammonium (protonic form after calcination) and sodium form, were used. Since the commercial zeolites available are ammonium-based, the sodium form should be prepared. This synthesis consisted of three one-hour ionic exchanges that were performed to ensure 100% exchange. Each step consisted of exchanging 15 g of NH<sub>4</sub>ZSM-5 with 276 mL of a 1 M NaNO<sub>3</sub> solution under constant vigorous stirring at room temperature (RT). Between each exchange, the zeolite was recovered by vacuum filtration (ME 1 c vacuum pump from Vacuubrand). After the final exchange, the zeolite was washed with deionized water multiple times before being dried overnight at 80 °C in an oven. Both the Cu-zeolites (Table 3) were prepared by exchanging 8 g of

the respective parent zeolite form with 605 mL of a 0.03 M  $\text{Cu}(\text{CH}_3\text{COO})_2 \cdot \text{H}_2\text{O}$  solution under constant vigorous stirring (J.P. SELECTA AGITAMATIC-N) at room temperature during 8 hours. Then the zeolites were recovered by vacuum filtration and dried overnight at 80 °C in an oven. Finally, the powders were subjected to a calcination treatment: 2 °C/min heating ramps, plateaux at 200 °C (for 1 hour) and 500 °C (for 6 hours) under a dry air stream (4 L/h/g).

Table 3- Cu-based ZSM-5 powders characteristics (Cu content quantified ICP-OES)

| Sample name | Si/Al | Compensation Cation | Cu content (% wt.)* | $\text{Cu}(\text{CH}_3\text{COO})_2$ Ionic Exchanges performed |
|-------------|-------|---------------------|---------------------|--|
| HM04MFI     | 15    | $\text{Na}^+$       | 2.33                | 1 (0.03 M)   |
| HM05MFI     | 15    | $\text{H}^+$        | 1.84                | 1 (0.03 M)   |

\*Cu content quantified by ICP-OES

### 2.1.3 Preparation of extruded zeolite samples

The zeolite extrudates were prepared by mixing-extrusion method, according to Mendes's[140] procedure with some minor changes. The ZSM-5 (Si/Al=40) zeolite was mixed with the pseudo-boehmite and *Methocel* powders. Two mixtures were prepared by varying the zeolite proportion (40%/60% zeolite to dry content and 1% *Methocel*). Firstly, 10 g of the powders were mixed with 5.8 mL of a  $\text{HNO}_3$  solution (3.6 wt.%) and 5.4 mL of water was added through the kneading process. After kneading for 15 minutes, 5.9 mL of a  $\text{NH}_4\text{OH}$  solution (1.4 wt.%) was added to the mixture. The kneading of the paste proceeded for about 15 minutes and 5.6 mL of water was added through the process. Cylindrical extrudes were finally obtained by extrusion through a syringe. The alteration made to the documented procedure where the addition of more water (double the amount) to facilitate the extrusion with a syringe. After extrusion, the extrudates were dried at 80 °C overnight in the oven and calcined at 500 °C with a heating rate of 10 °C/min. Calcination was performed on a muffle (Nabertherm). After the heat treatment at 500 °C, the pseudo-boehmite (PURAL SB) transforms into  $\gamma\text{-Al}_2\text{O}_3$ . [141] After the calcination, the silver-based extrudates (Table 4) were prepared through ionic exchange by adding the appropriate amount of silver precursor solution (silver nitrate on 100 mL) to the extrudates. The process was carried out in a rotary evaporator (BUCHI) with a bath temperature of 40 °C under a vacuum, programmed to evaporate the water, leaving silver deposited in the extrudates. Finally, the silver-loaded extrudates were subjected to another calcination process, under the same conditions as the first one.

Table 4- Ag-based ZSM-5 extrudates characteristics

| Sample name | Si/Al | Compensation Cation | Ag content (% wt.) | Zeolite content (% wt.) |
|-------------|-------|---------------------|--------------------|-------------------------|
| HMEI9       | 40    | H <sup>+</sup>      | 3                  | 40                      |
| HMEI10      | 40    | H <sup>+</sup>      | 1.5                | 40                      |
| HMEI16      | ---   | ---                 | 3                  | 0                       |
| HMEI18      | 40    | H <sup>+</sup>      | 3                  | 60                      |

## 2.2 Adsorbent characterization

### 2.2.1 Chemical analysis: ICP-OES

Chemical studies were performed on powder zeolites samples to determine the amount of Ag and Cu after the ion exchange. The procedure was carried out at the IST Analysis Laboratory (LAIST). The chemical analysis was performed using Inductively Coupled Plasma Optical Emission Spectroscopy (ICP-OES), which involves using plasma to excite the atoms/ions and measuring the amount of light and specific wavelengths as the atoms/ions return to lower energy levels. The amount of light emitted is proportional to the number of atoms or ions that make the transitions, and the wavelength of light emitted is characteristic of the atom that emits. [142]

### 2.2.2 UV-Visible Reflectance Spectroscopy

Ultraviolet-Visible Diffuse Reflectance Spectroscopy (UV-Vis DRS) was utilized to characterize Ag and Cu species (in various chemical states) present on powder samples of zeolites and extrudates (extrudates were ground into powder before characterizations). Raw zeolite was used as a baseline. According to Kubelka Munk's theory, the function  $F(R)$  is proportional to the concentration  $c$  of the absorbing species. The Kubelka Munk function, as represented by equation 13, depicts an infinite-thickness layer where both light adsorption and scattering phenomena can occur and is comparable to the transmittance absorbance transformation. The reflectance  $R$  is defined as the ratio of incoming light intensity  $I$  to reflected part  $J$ .  $K$  and  $S$  are the K-M adsorption and scattering coefficients, respectively. [143]

$$F(R) = \frac{K}{S} = \frac{(1 - R)^2}{2R} \approx c \quad (13)$$

The characterization was carried out at RT on a Varian Cary 5000 with wavelengths ranging from 200 to 800 nm and a Praying Mantis (integration sphere) attachment for DRS measurements.

### 2.2.3 N<sub>2</sub> Sorption measurements

N<sub>2</sub> sorption was used to determine the textural properties (most notably the micropore volume). The instruments utilized were a Quantachrom Autosorb IQ and a Micromeritics ASAP 2010 analyzer. Prior to analysis, the samples were outgassed under vacuum for 1 hour at 90 °C and for 5 hours at 350 °C with a temperature ramp of 5 °C/min. The measurements were conducted at the boiling point of liquid nitrogen (-196 °C). This analysis is based on measurements of the volume of nitrogen physisorbed while changing pressure in equilibrium conditions. The ASiQwin program used the t-plot approach to calculate the micropores volume.

### 2.2.4 Thermogravimetric Analysis (TGA)

Water loss was determined and quantified using thermogravimetric tests on adsorbents (powder and extruded forms). Before TGA analysis, the samples were saturated in a desiccator with a saturated calcium carbonate solution. The analysis was carried out in a Seteram SETSYS Evolution 16 with an airflow of 30 mL/min from RT to 800 °C. The sample was subjected to two temperature cycles, the second of which was subtracted to the first eliminate Archimedes' effect on apparent mass loss and heat flow signals.

$$\text{Weight loss (wt. \%)} = \frac{\Delta m}{m_i} \quad (14)$$

### 2.2.5 H<sub>2</sub> Temperature Programmed Reduction

H<sub>2</sub> TPR was performed to assess the reducibility profile metals (silver and copper), and hence quantify the various reducible species present on the zeolites. Micromeritics AutoChem II was used to record the H<sub>2</sub> consumption profiles. Peaks at increasing temperatures imply more difficulty in the reducibility of the respective metal. In this analysis, a stream of reducing hydrogen gas (30 cm<sup>3</sup>/min of 5% H<sub>2</sub> in Ar) was fed into a temperature-controlled reactor (200 mg sample, zeolites were ground beforehand) while the temperature was raised (900 °C at 10 °C/min) to reduce the reducible species in the samples. A TCD (thermal conductivity detector) sensor was used to monitor the variation of H<sub>2</sub> concentration in the gas stream. Prior to analysis, samples were pre-treated with an Argon (Air for extrudates) stream (50 mL/min) and temperature ramped at 10 °C/min from RT to 250 °C (for roughly 25 min).

## 2.3 Breakthrough curve adsorption experiments

### 2.3.1 Experimental setup

The adsorption process was carried out in a U-shaped fixed bed flow reactor loaded with the adsorbent, immersed in a thermostatic bath (Grant LTD 6) to maintain the temperature (1°C). The feed consisted of a gas flow mixture of ethylene and nitrogen (50 mL/min, 50 ppm of ethylene) controlled by

Bronkhorst® gas flow controller. There are 2 three-way valves to alternate between the bypass and the reactor. If the test is conducted under wet conditions, the nitrogen gas is saturated by flowing through a bubble humidifier (filled with de-ionized water) contributing to an RH of 80%. This set is bypassed on the dry condition's experiments. During the adsorption process the reactor gas effluent is analysed in a gas chromatograph (Shimadzu GC-2010 Plus) with a flame ionization detector (FID) with an air and H<sub>2</sub> flame and N<sub>2</sub> carrier. This detector works by combusting organic substances (only ethylene for example), producing gas-phase charged ions that are collected by the detector electrode resulting in a current. This current is then converted to an electrical signal (mV) that is proportional to the number of molecules ionized.[144], [145] The signals are then analysed through the LabSolutions software during the experiments. Effluent samples were injected each minute and analyses were performed with the intent to follow the adsorption process. The areas of the ethylene peaks were measured with the LabSolutions software. Beforehand a calibration curve was obtained by changing the feed concentrations and collecting the area of the peaks associated (after stabilization).

The reactor was filled with a mixture of 100 mg zeolite and 200 mg SiC stabilized between two quartz wool beds for all powder experiments. The aggregate size of powders was adjusted to achieve a more uniform reactor bed, hence preventing diffusional problems. Prior to each test, the powder was pelletized with a pressure of 1.5 tons for 30 s, in order to avoid zeolite structure damage. Then, the pellet was crushed and sieved with a particle size between 250-125 µm. In the extrudates testing, 300 mg of extrudates were supported by quartz wool beneath.

Prior to each test, the samples were pre-treated *in situ* to remove water and contaminants that had been adsorbed from the saturated samples. This was accomplished by heating the reactor to 250 °C in a ThermoLab oven controlled by a thermocouple (with a heating ramp of 10 °C/min and a 25-minute plateau at 250 °C) with N<sub>2</sub> flow (50 mL/min) for powders and air flow (50 mL/min) for extrudates.

The pre-treatment between each cycle for the adsorption-desorption cycling studies (Figure 20) was performed by raising the thermostatic bath temperature to 60 °C under air flow (50 mL/min), resulting in the desorption of ethylene and water adsorbed during the adsorption tests. The GC apparatus monitored the ethylene desorption, and the procedure terminated when no ethylene signals were observed. After each desorption process the reactor (with adsorbent samples) was covered with aluminium foil to prevent light-induced reduction of ionic silver species.[146]

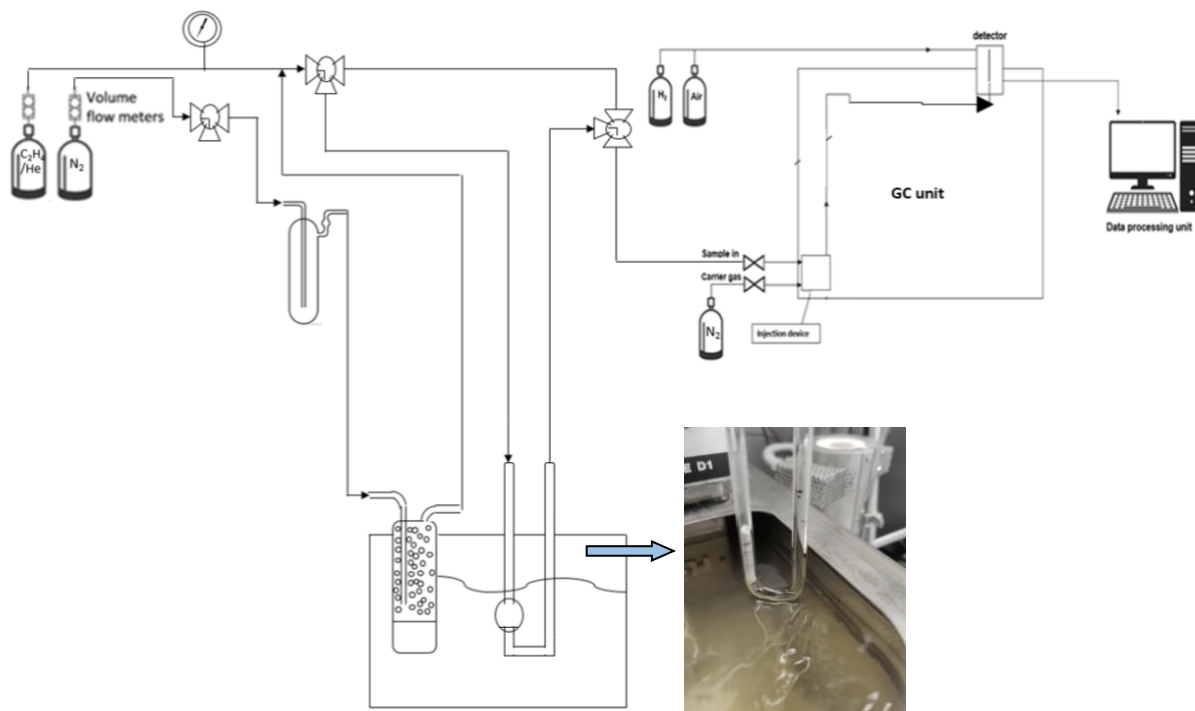


Figure 20 Schematic of the experimental set-up for adsorption experiments under wet conditions

### 2.3.2 Breakthrough curves interpretation under experimental condition

Breakthrough curves followed the dynamic ethylene adsorption process. These curves can be plotted into graphs that represent the adsorbate concentration (relative to the feed concentration  $C/C_0$ ) in the effluent stream as a function of time  $t$ . As shown in Figure 21, during the initial phase, the ethylene concentration in the reactor effluent stream is zero, corresponding to ethylene adsorption on the adsorbent. After the first phase, the ethylene concentration starts rising ( $t=t_{bp}$ - breakpoint time) until the adsorbent is fully saturated and the effluent concentration matches the feed concentration ( $C/C_0=1$ ,  $t=t_s$  saturation time). Overshoot ( $C/C_0$ ) phenomenon can be noticed in wet condition studies because water can replace ethylene previously adsorbed onto the adsorbent, causing ethylene to desorb, leading to an increase in ethylene concentration at the system outlet (above the  $C/C_0=1$  line).

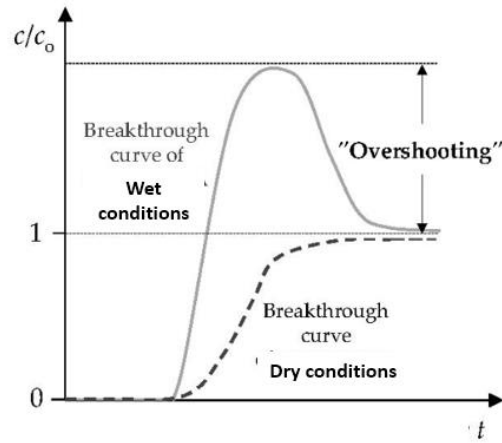


Figure 21 Breakthrough curves obtained under dry and wet conditions (adapted from [147])

In an ideal case, these curves would be symmetrical/flatter, with the area above the curve (below  $C/C_0$ ) proportional to the quantity of ethylene adsorbed. In real experiments, the asymmetrical shape of the curve might reveal important information about mass-transfer processes, particularly diffusional difficulties (either external or internal). Because the mass-transfer rate is proportional to the difference between  $t_s$  and  $t_{bp}$ , this value will be smaller at larger mass-transfer rates (lower diffusion problems), resulting in steeper curves (approaching the ideal case). [148]

### 2.3.3 Calculation of ethylene adsorption capacity

Prior to any calculation, the dead volume time is removed. In the experimental setup used the time estimated for the feed to reach the adsorbent was 1.5 minutes.

The total capacity ( $q$  mL<sub>(ethylene)</sub>) can be given by equation 15, where  $C_0$  is the feed ethylene concentration (ppm),  $S_1$  is the total area under the curve at each time interval,  $Q_v$  is the total flow (mL min).

$$q = \left( \sum_n (t_n - t_{n-1}) \times C_0 - S_1 \right) \times 10^{-6} \times Q_v \quad (15)$$

The  $S_1$  area was estimated by the Trapezium rule, described by the following equation:

$$S_1 = (t_n - t_{n-1}) \times (C_n + C_{n-1}) \times \frac{1}{2} \quad (16)$$

Finally, the total capacity value in  $\mu$ mL of ethylene per gram of adsorbent is given by:

$$q_{ads} = \frac{q}{22,4} \times 10^6 / \text{adsorbent dry mass} \quad (17)$$

## 2.4 Adsorption-desorption experiments under real conditions

### 2.4.1 Pilot scale experimental setup

The silver-based zeolite extrudates samples were evaluated under real conditions in the Rocha-Center's test chambers. Citicell sensors were used to monitor gas concentrations ( $O_2$ ,  $N_2$  and  $C_2H_4$ ) every hour. The injection of  $N_2$  (made by  $N_2$  generators) controls the oxygen concentration, while the potassium hydroxide scrubber controls the carbon dioxide levels. The concentrations of  $O_2$  and  $CO_2$  gases in the chamber used for these tests are not actively regulated, that is, no precise concentration is specified. However, some control is done since the  $O_2$  and  $CO_2$  gas concentrations are kept below certain thresholds. Each chamber holds 90-120 kg of pears (6 boxes of pears) and has a total volume of 592 L (74 cm-80cm-1m).

The fundamental principle behind the pilot scale adsorption system (Figure 22 and Figure 23) is to remove ethylene by recirculating air from the chamber through an active adsorbent (silver-based extrudates) encased in a cartridge. A pump (flow rate 6,8 L/min) is utilized to recycle the gas in the chamber. The incoming gas is then passed through the cartridge (surrounded by aluminium foil), which holds about 3.5 g of extrudates. Following adsorption, the gas is returned to the chamber, where small particles (resulting from extrudates degradation) are caught by a filter (RoHS-compliant ZFC).

The ethylene level is measured before and after the cartridge using two sensors (C-10 by Membrapor) connected to a microcontroller. The ethylene concentration data (inlet and outflow) is collected and analysed using the MembraSens 4.0 software.

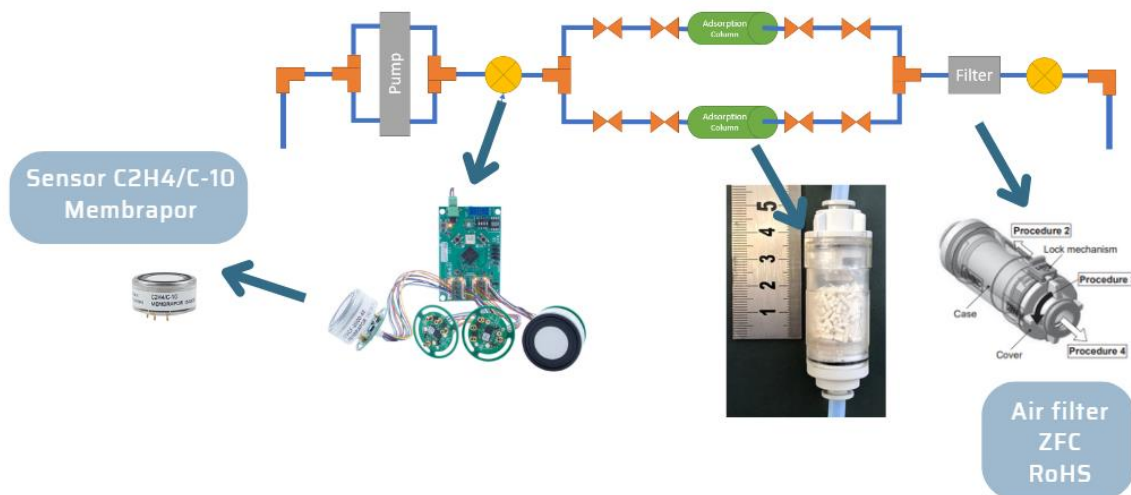
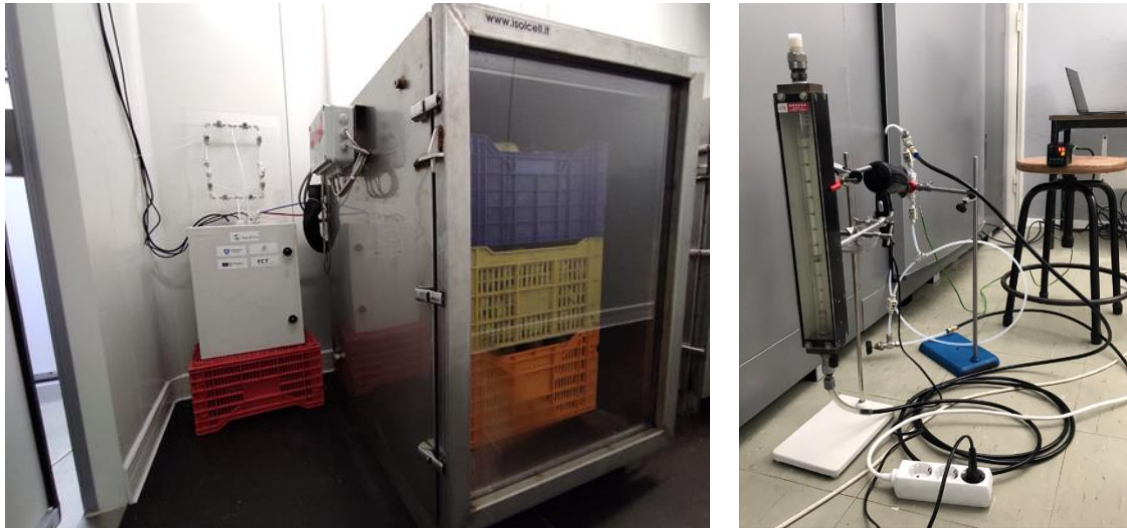


Figure 22- Schematic of the adsorption system installed in the Rocha-Center's test chambers

The adsorption-desorption method was quite similar to the lab scale experiments. The adsorption procedure lasted 1 hour (30 minutes in certain experiments). Following each adsorption, the silver-based extrudates samples were thermally treated at 60 °C with an air stream (flow rate 30 L/min) for 30 minutes. The



samples were also thermally treated (using the same desorption process) prior to the initial adsorption to eliminate any adsorbed compounds.



*Figure 23- Rocha-Center's adsorption-desorption pilot scale set-ups*

The adsorption process is characterized by differing concentration profiles in the inlet (sensor before the extrudates' cartridge) and outlet signals (sensor after the extrudates' cartridge), as shown in Figure 24. The inlet sensor indicates the ethylene concentration inside the chamber, whilst the other sensor indicates the concentration immediately after the cartridge. The outlet profile is distinguished by a gradual increase in concentration caused by adsorbed ethylene. The inlet signals are distinguished by a gradual decrease in ethylene concentration until the active material is completely saturated. The oscillating behaviour in the outlet signal is caused by the ventilation system.

The adsorbed ethylene was calculated by integrating the region delimited by the input and outflow signals (Origin software). To calculate the area associated with the sensor delay response, a blank test (cartridge without active material) was performed. This value was removed for each cycle to calculate the quantity of ethylene adsorbed more precisely.

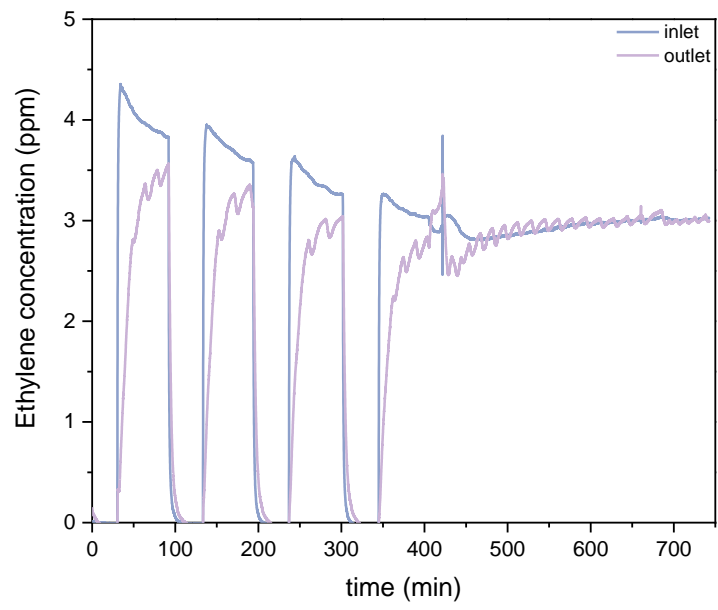


Figure 24- Adsorption-desorption profiles

## 3 Results and discussion

### 3.1 Ag-based zeolite powders

Although the ethylene adsorption capacity of Ag-based zeolites has been widely reported in the literature, there is a serious shortage of research done under conditions similar to those verified in industrial storage chambers. This chapter will concentrate on evaluating the effect of high RH on the ethylene adsorption performance.

#### 3.1.1 Adsorbents characterization

##### 3.1.1.1 TGA results

To guarantee the same load in each adsorption experiment, all samples were kept saturated in other samples. A TGA was used to measure the water loss after pre-treatment (Figure 25). The mass loss was employed to calculate the exact mass of dry zeolite during each experiment.

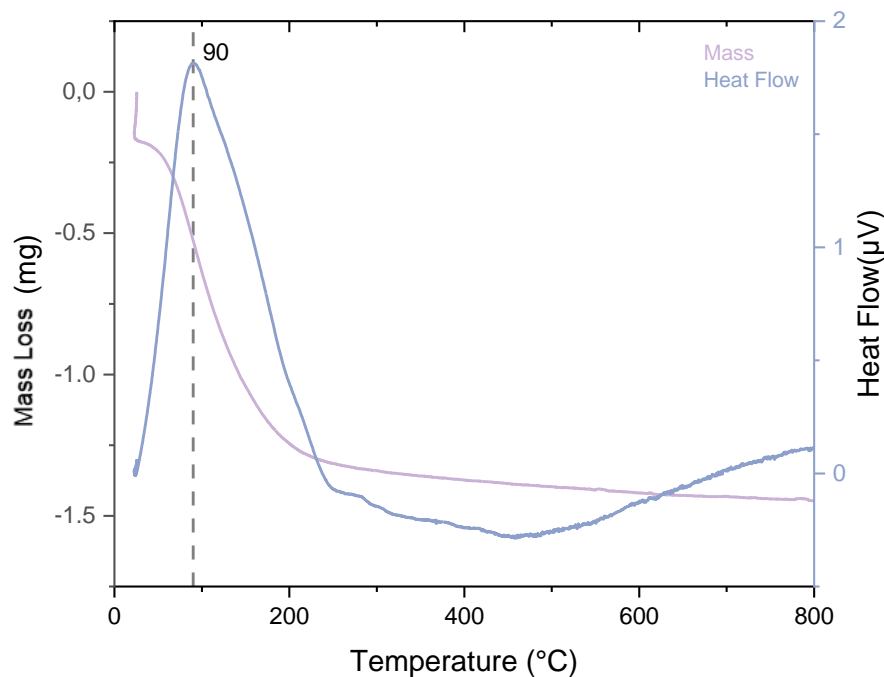


Figure 25-TGA mass and heat flow profiles versus temperature for the HM04 sample

A significant decrease in mass (8%), located at 90 °C, can easily be associated with the endothermic evaporation of adsorbed water. The further mass decrease at higher temperatures is attributed to the dehydroxylation of the zeolite framework.[149]

### 3.1.1.2 Chemical analyses results

The results from the ICP-OES chemical analysis are summarized in *Table 5*, as well as the information regarding the preparation method.

The theoretical maximum concentration of exchanged silver was estimated using the ZSM-5 chemical formula  $Cation_{x/n}Al_xSi_{(96-x)}O_{192}$ , which demonstrates the unit cell composition, where n indicates the metal cationic species' oxidation state.[150]

*Table 5- Ag-based ZSM-5 powders characteristics and preparations*

| Sample reference | Si/Al | Compensation cation | Ag content (wt.%)* | Theoretical max. Ag content (wt.%) | Exchange ratio (%) | Number of AgNO <sub>3</sub> ionic exchanges performed |
|------------------|-------|---------------------|--------------------|------------------------------------|--------------------|---|
| RF026MFI         | 15    | H <sup>+</sup>      | 0.69               | 11                                 | 6                  | 1 (0.003 M)   |
| RF017MFI         | 15    | H <sup>+</sup>      | 3.1                | 11                                 | 28                 | 1 (0.01 M)  |
| RF015MFI         | 15    | H <sup>+</sup>      | 4.6                | 11                                 | 42                 | 3 (0.01 M)  |
| RF022MFI         | 15    | Na <sup>+</sup>     | 4.3                | 10.97                              | 39                 | 1(0.01 M)   |
| RF024MFI         | 15    | Na <sup>+</sup>     | 6.1                | 10.97                              | 56                 | 3 (0.01 M)  |
| RF027MFI         | 40    | H <sup>+</sup>      | 0.52               | 4.4                                | 12                 | 1 (0.003 M)   |
| RF019MFI         | 40    | H <sup>+</sup>      | 1.9                | 4.4                                | 44                 | 1 (0.01 M)  |
| RF016MFI         | 40    | H <sup>+</sup>      | 2.8                | 4.4                                | 65                 | 3 (0.01 M)  |
| RF023MFI         | 40    | Na <sup>+</sup>     | 3.2                | 4.3                                | 74                 | 1 (0.01 M)  |
| RF025MFI         | 40    | Na <sup>+</sup>     | 3.9                | 4.3                                | 90                 | 3 (0.01 M)  |

\*(Ag content quantified by ICP-OES)

The chemical analysis results can be used to infer certain conclusions. Silver cations have a greater affinity than Na<sup>+</sup> and NH<sub>4</sub><sup>+</sup> because they are highly polarizable and hence interact strongly (electrostatically) with the negatively charged zeolite frameworks.[151] Higher Si/Al ratios on the zeolite framework resulted in lower silver loadings for the same ionic exchange procedure. This is because zeolites with a higher aluminium content (lower Si/Al) contain a higher concentration of charge-balancing framework cations (in this example, either H<sup>+</sup> or Na<sup>+</sup>), which assure neutrality by compensating for the negative charge produced by the Al atom in the framework. As a result, the silver cationic species (Ag<sup>+</sup>) will exchange with the compensating cations contained in the zeolite via ionic exchange. [151]

Because the difference in concentration between the zeolite particle surface and inside the zeolite material drives ionic exchange, more concentrated silver solutions result in higher Ag loads on zeolites, as illustrated in Table 5.[152]

For the same exchange procedure, zeolites prepared from Na-based parents had greater silver loading, indicating a preference for Ag exchange with Na<sup>+</sup> rather than NH<sub>4</sub><sup>+</sup>. This association is also supported by the findings of Bartolomeu *et al.*[153] research.

### 3.1.1.3 Optical properties

All the Ag-based samples' UV-Vis spectra reveal two main bands at 210 and 225 nm (Figure 26). According to literature reports[154], these bands with a wavelength in the range of 208-238 nm, might be attributed to the  $4d^{10} \rightarrow 4d^9 5s^1$  electronic transition of trigonally coordinated Ag<sup>+</sup> species.[155] The distribution of Ag<sup>+</sup> in different positions inside the cages might explain the two peak positions. The lack of bands at higher wavelengths suggests the absence of the Ag<sub>n</sub><sup>δ+</sup> cluster or metallic silver. When small Ag<sub>n</sub><sup>δ+</sup> clusters are present, bands in the range of 260-285 nm develop, according to studies.[156], [157] Broader bands over 350 nm should be predicted for the bigger Ag<sub>n</sub><sup>δ+</sup> cluster and metallic species.[158] No bands were observed from 420-700 nm, evidencing a absence (or low concentration) of Ag<sub>2</sub>O species.[159] Despite the scarcity of bands indicating the presence of some Ag<sub>n</sub><sup>δ+</sup> cluster and metallic species, their existence should not be dismissed. TPR studies were done to further quantify as well as investigate the oxidation state of the Ag species present in the samples.

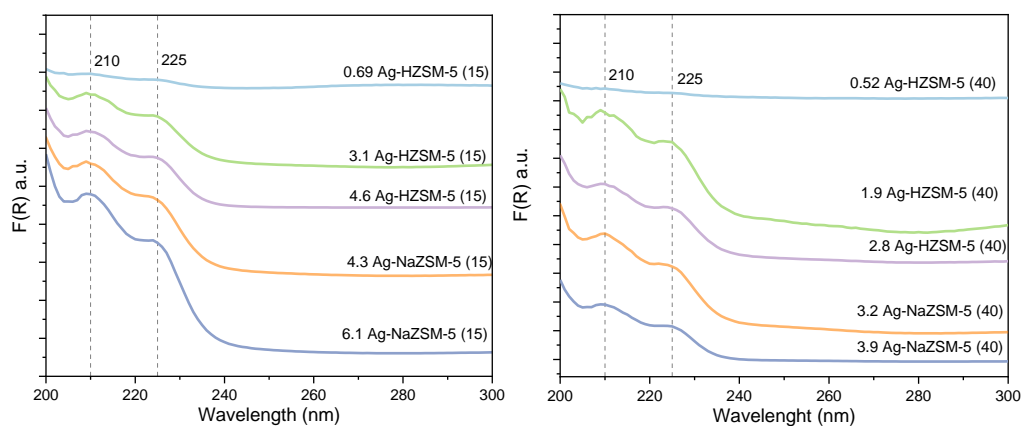


Figure 26- UV-Vis DRS spectra of Ag-based zeolites

### 3.1.1.4 H<sub>2</sub> Temperature Programmed Reduction

After being thermally treated the samples TPR analyses were performed. The profiles are depicted on Figure 27 and the quantitative results summarized in Table 6.

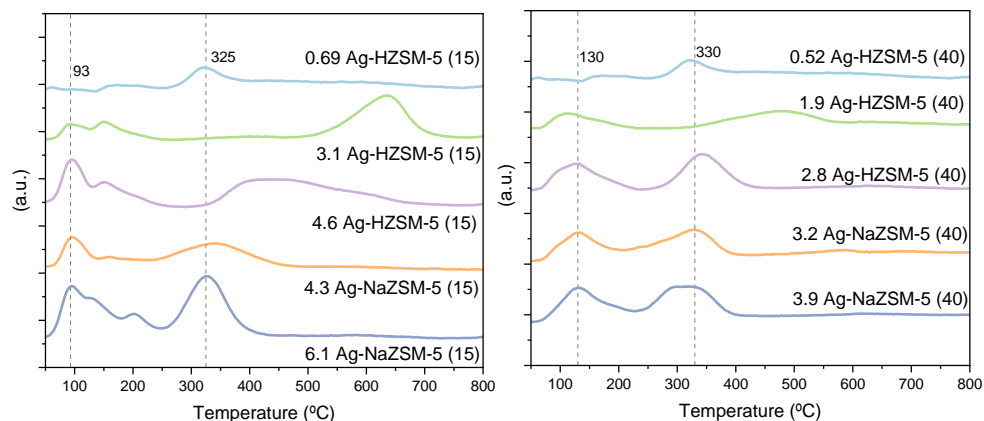


Figure 27- H<sub>2</sub> TPR profile of Ag-based zeolites

Figure 27 evidences two separate reduction bands in the H<sub>2</sub>-TPR profiles of the Ag-based samples, associated with the two-step reduction of Ag<sup>+</sup> species. The first is related to the reduction of Ag<sup>+</sup> to Ag<sub>n</sub><sup>δ+</sup> clusters while the second is connected with the reduction of Ag<sub>n</sub><sup>δ+</sup> cluster into metallic silver. The research conducted by Shibata *et al.*'s[160] supports these attributions. Furthermore, Shibata *et al.* explored the nature of the clusters formed on MFI structures, concluding that Ag<sub>4</sub><sup>2+</sup> clusters are the mostly likely species produced.

TPR profile investigations show that the conversion of Ag<sup>+</sup> to Ag<sub>n</sub><sup>δ+</sup> occurs at lower temperatures for zeolites with greater amount of framework Al, indicating poorer stability of the Ag<sup>+</sup> species. This is most likely due to the stronger repulsive interactions between higher intrazeolitic Ag<sup>+</sup> concentrations, as evidenced by Min *et al.*'s[122] research. Furthermore, the results show that Ag<sub>n</sub><sup>δ+</sup> cluster species are more stable when H<sup>+</sup> species (rather than Na<sup>+</sup>) are present. The band situated at higher temperatures for protonic-based zeolites, primarily on lower silica zeolites, indicates this. Bartolomeu *et al.*'s [153] studies support these findings, attributing reduction inhibition to the presence of protonic sites that affect the reduction process's equilibrium.

The current analyses make it difficult to precisely identify the Ag<sub>n</sub><sup>δ+</sup> cluster species present in the zeolite. As a result, for the sake of interpretation, these species were considered to be Ag<sub>4</sub><sup>2+</sup> clusters species (in accordance with the Shibata *et al.*'s study), and the results are presented in Table 6.



The total amount of Ag<sup>+</sup> species was estimated using equation 18, while the amount of H<sub>2</sub> was obtained by integrating the first peak.

Table 6- H<sub>2</sub>-TPR results for the Ag-based zeolites

| Sample              | Ag (μmol/g) | Ag <sup>+</sup> (μmol/g) | Ag <sup>+</sup> mol % |
|---------------------|-------------|--------------------------|-----------------------|
| 0.69 Ag-HZSM-5(15)  | 64          | 32                       | 50                    |
| 3.1 Ag-HZSM-5 (15)  | 287         | 183                      | 63                    |
| 4.6 Ag-HZSM-5 (15)  | 426         | 330                      | 77                    |
| 4.3 Ag-NaZSM-5 (15) | 399         | 218                      | 55                    |
| 6.1 Ag-NaZSM-5 (15) | 566         | 475                      | 84                    |
| 0.52 Ag-HZSM-5(40)  | 48          | 23                       | 46                    |
| 1.9 Ag-HZSM-5 (40)  | 176         | 138                      | 78                    |
| 2.8 Ag-HZSM-5 (40)  | 260         | 223                      | 86                    |
| 3.2 Ag-NaZSM-5 (40) | 297         | 221                      | 75                    |
| 3.9 Ag-NaZSM-5 (40) | 362         | 279                      | 77                    |

The relationship between the Ag<sup>+</sup> cations (calculated from TPR analysis) and the total silver loading (as determined by chemical studies) is in accordance with the UV-Vis analysis that evidence spectra profiles dominated by Ag<sup>+</sup> species. The overall low number of clusters (either metallic or charged) formed on the ZSM-5 zeolites is expected, since the phenome leading to their formation and growth is dependent on the size of the pores, thus medium pores (5.1 x 5.5 Å; 5.3 x 5.6 Å) of ZSM-5 limit the occurrence of these clusters.[151]

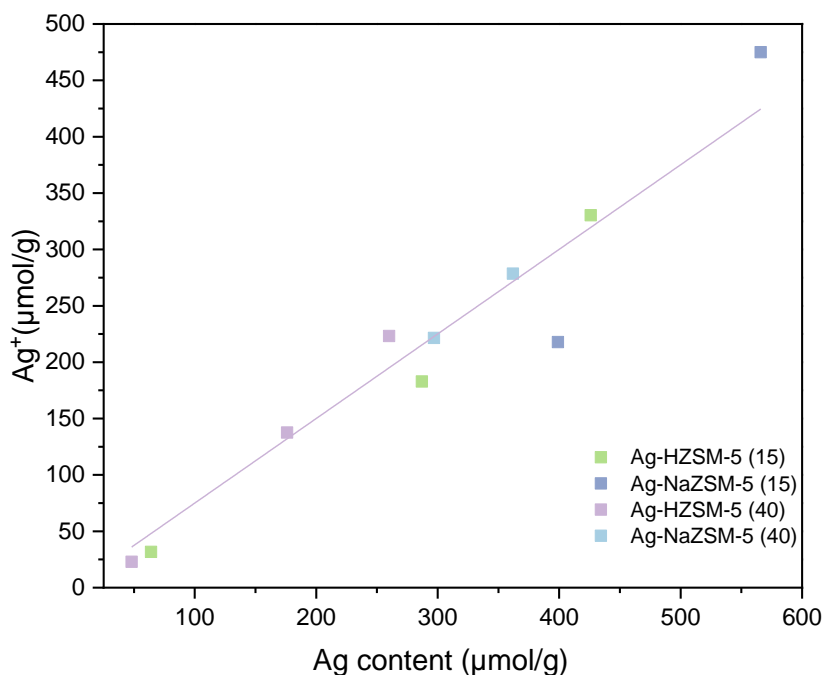


Figure 28- Relationship between total Ag amount and Ag<sup>+</sup> amount calculated from the H<sub>2</sub>-TPR measurements

In either case, a rise in silver load led to an increase in charged silver species. Despite the conclusion drawn from the stability of  $\text{Ag}^+$  species in different zeolite types (different Si/Al and compensation cation), through the Figure 28 the concentration of  $\text{Ag}^+$  species on the samples seems to be only correlated with the silver load. The proportion between Ag load and  $\text{Ag}^+$  species formed appears to be 0.6-0.8.

### 3.1.2 Adsorption breakthrough experiments under dry conditions

The breakthrough adsorption experiments performed under dry conditions (50 ppm  $\text{C}_2\text{H}_4$ , 1 °C, 50 mL/min) for the Ag-based zeolites are displayed in Figure 29 and Figure 30, and the respective adsorption capacities and breakthrough times are summarized in Table 7.

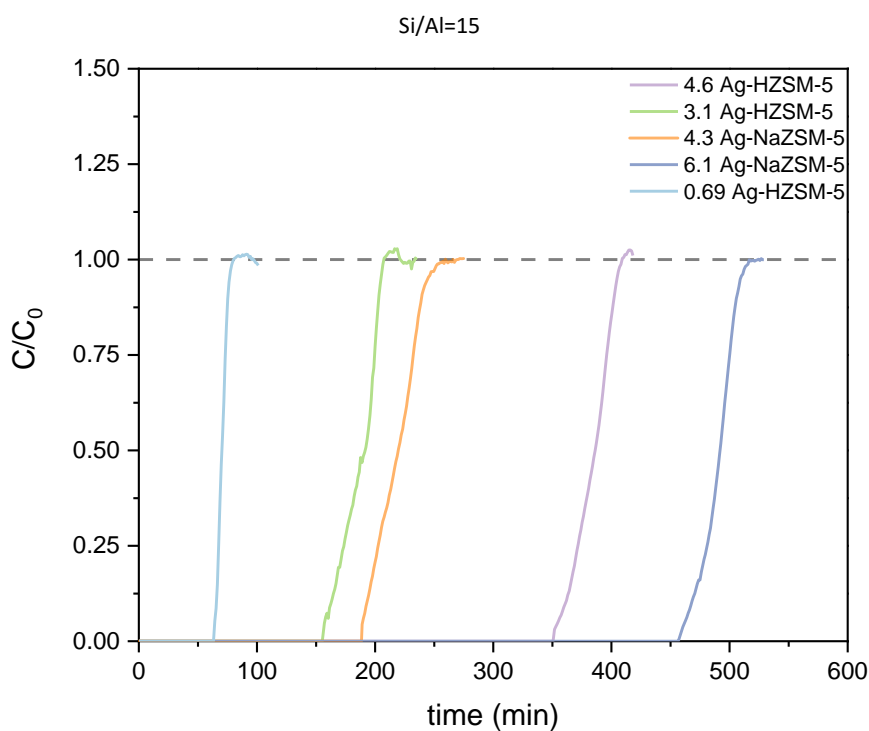


Figure 29- Breakthrough curves for Ag-based zeolites (Si/Al=15) under dry conditions



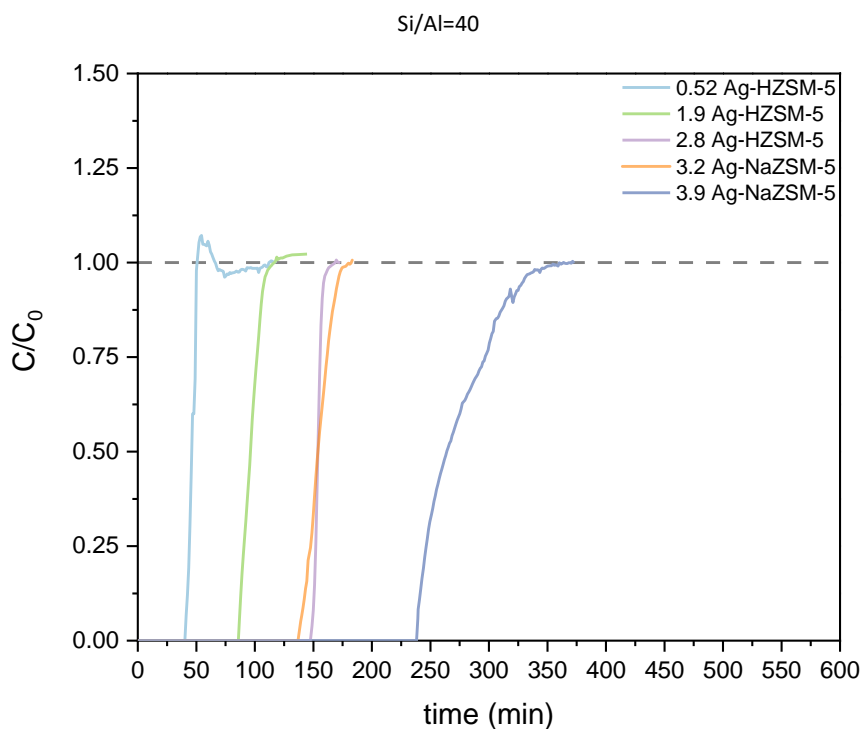


Figure 30- Breakthrough curves for Ag-based zeolites (Si/Al=40) under dry conditions

Table 7- Summary of ethylene adsorption capacity values and break-point time for Ag-based zeolites under dry conditions

| Sample              | $t_{bp}$ (min) | $q$ ( $\mu\text{mol/g}$ ) |
|---------------------|----------------|---------------------------|
| 0.69 Ag-HZSM-5(15)  | 64             | 91                        |
| 3.1 Ag-HZSM-5 (15)  | 155            | 205                       |
| 4.6 Ag-HZSM-5 (15)  | 351            | 451                       |
| 4.3 Ag-NaZSM-5 (15) | 189            | 239                       |
| 6.1 Ag-NaZSM-5 (15) | 461            | 517                       |
| 0.52 Ag-HZSM-5(40)  | 41             | 56                        |
| 1.9 Ag-HZSM-5 (40)  | 86             | 117                       |
| 2.8 Ag-HZSM-5 (40)  | 148            | 182                       |
| 3.2 Ag-NaZSM-5 (40) | 139            | 160                       |
| 3.9 Ag-NaZSM-5 (40) | 239            | 270                       |

Before analysing the adsorption capacity of the samples, some conclusions can be drawn by the shape of the breakthrough curves. In general, the behaviours the S-curves in all Ag-based zeolite samples are characterized by a sharp rise until the saturation plateau ( $C/C_0=1$ ) is reached. These suggest an adsorption process close to the ideal scenario, thus no significant diffusion limitations affect the adsorption process.

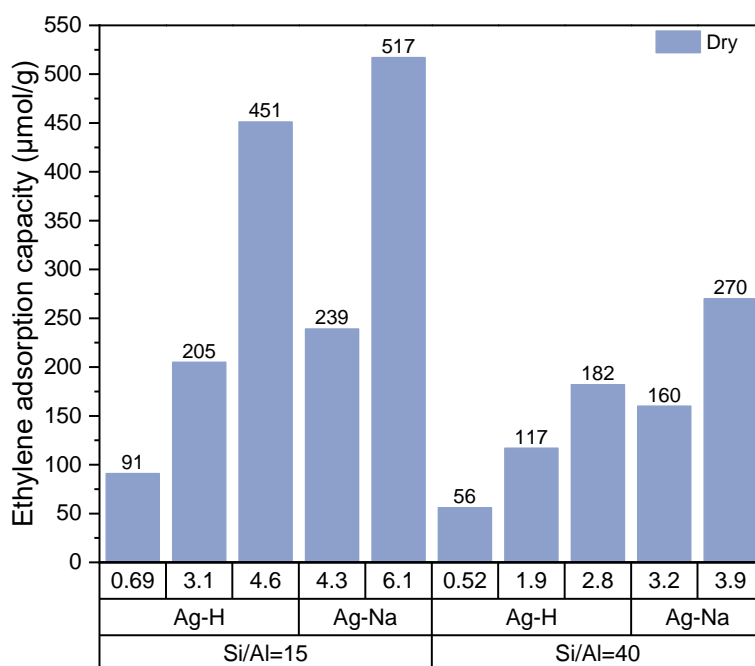


Figure 31- Ethylene adsorption capacity for Ag-based zeolites tested under dry conditions

As illustrated in Figure 31, an increase in ethylene adsorption capacity is associated with an increase in Ag content in the zeolite. Adsorption, as previously noted, is dependent on interactions between ethylene and the zeolite, which can be either physical or chemical. The latter one is based on stronger interactions through chemical bond formation, thus more selective and effective interactions are made between ethylene and adsorbent resulting in higher adsorption capacities. A chemisorption mechanism known as  $\pi$ -complexation can occur in the case of silver-based zeolites (as well as other transitional metals), although not all silver species can interact with ethylene in this way. According to Cisneros *et al.*[119] and Horvatits *et al.*[120] charged silver species, such as  $\text{Ag}^+$  and  $\text{Ag}_n^{\delta+}$  clusters, can establish  $\pi$ -interactions with ethylene. Monzón *et al.*[118], on the other hand, found that the silver cluster reduces the number of active sites for ethylene  $\pi$ -interaction and contributes to pore obstruction. Furthermore Horvatits *et al.*[120] determined that silver oxide can also undergo  $\pi$ -complexation with ethylene, however the interaction is less significant, due to the Ag atom's electron deficiency.[121] So, by far, the most significant species in ethylene adsorption are highly dispersed  $\text{Ag}^+$  ions. Figure 32 highlights this significance, since greater ethylene adsorption capacities were observed for samples with higher content of  $\text{Ag}^+$  species. The findings of Cisneros *et al.* [119] evidences the same impact with the increase of charged silver species content in zeolites.

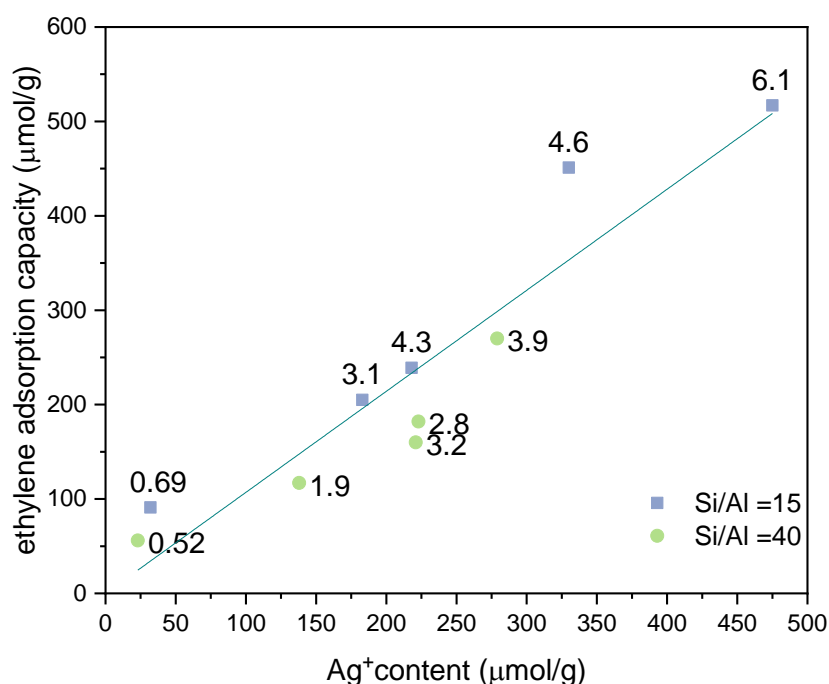


Figure 32- Ethylene adsorption capacity as a function of Ag<sup>+</sup> content for Ag-based zeolites under dry conditions

According to the trend line depicted in Figure 32, the relationship between the ethylene capacity and Ag<sup>+</sup> content appears to be roughly 1 to 1. As a result, each Ag<sup>+</sup> molecule can adsorb 1 molecule of ethylene. These findings are contradictory with Horvatis *et al.*'s [120] DFT's study, where 2 molecules of ethylene are adsorbed to the Ag<sup>+</sup> sites. However, the 1 to 1 ratio is in accordance with Kang *et al.*'s [161] experimental research. Finally, as the increase in capacity is noticeable for each increment in Ag<sup>+</sup> content (evidenced by the sharp trend line), Ag<sup>+</sup> is well dispersed and few silver oxides were formed, as concluded by the H<sub>2</sub>-TPR calculations. These results contrast with Lee *et al.* [121] findings that concluded that the incensement in silver loading results in reduced dispersion of Ag particles, eventually leading to formation of Ag<sub>2</sub>O.

### 3.1.3 Adsorption breakthrough experiments under wet conditions

To further understand how water affects adsorption performance and how different zeolite properties (Si/Al and compensating cation) affect these competitive interactions, dry and wet conditions results were compared. These wet conditions experiments provide a more accurate representation of the conditions to which the fruits are subjected in CA storage rooms.

The breakthrough adsorption experiments performed under wet conditions (50 ppm C<sub>2</sub>H<sub>4</sub>, 1 °C, 50 mL/min, RH 80%) for the Ag-based zeolites are displayed in Figure 33 and Figure 34, and the respective adsorption capacities and break-point times are summarized in Table 8.

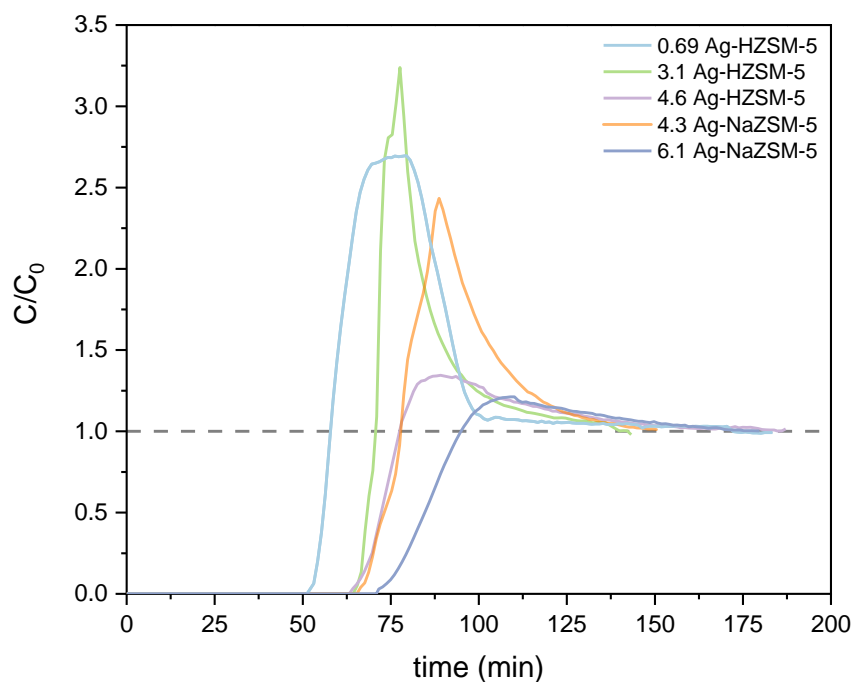


Figure 33- Breakthrough curves for Ag-based zeolites (Si/Al=15) under wet conditions

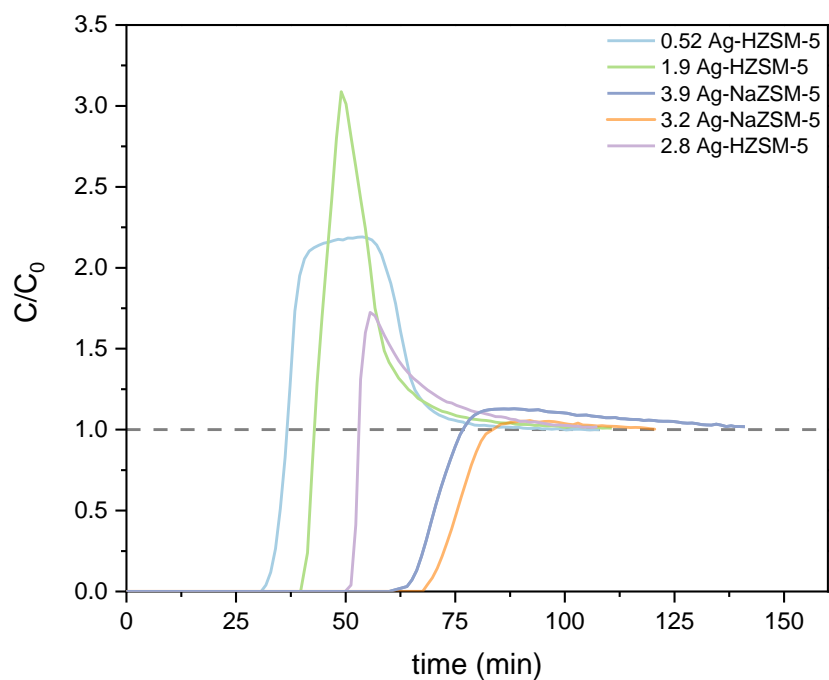


Figure 34- Breakthrough curves for Ag-based zeolites (Si/Al=40) under wet conditions

The adsorption breakthrough curves obtained from the experiments under wet conditions are characterized by a shift in the break-point to lower times and an overshoot phenomenon ( $C/C_0 \geq 1$ ). This behaviour is characteristic of a system where there is competition (between ethylene and water in this case) for the same adsorption sites.

Table 8- Summary of ethylene capacity values and break-point time for Ag-based zeolites under wet conditions

| Sample              | $t_{bp}$ (min) | q ( $\mu\text{mol/g}$ ) |
|---------------------|----------------|-------------------------|
| 0.69 Ag-HZSM-5(15)  | 53             | 8                       |
| 3.1 Ag-HZSM-5 (15)  | 66             | 49                      |
| 4.6 Ag-HZSM-5 (15)  | 64             | 79                      |
| 4.3 Ag-NaZSM-5 (15) | 67             | 58                      |
| 6.1 Ag-NaZSM-5 (15) | 72             | 105                     |
| 0.52Ag-HZSM-5(40)   | 32             | 7                       |
| 1.9AgHZSM-5 (40)    | 41             | 23                      |
| 2.8AgHZSM-5 (40)    | 42             | 57                      |
| 3.2Ag-NaZSM-5 (40)  | 69             | 97                      |
| 3.9Ag-NaZSM-5 (40)  | 64             | 87                      |

As shown in Figure 35, this competitive behaviour provoked by water additions led to a significant reduction (about 75%) in adsorption capacity in all samples. This drop in ethylene adsorption under wet conditions was also observed by Kang *et al.*'s[161] and Lee *et al.*'s[121] studies, although their experiments were performed under considerably lower RH and higher temperatures.

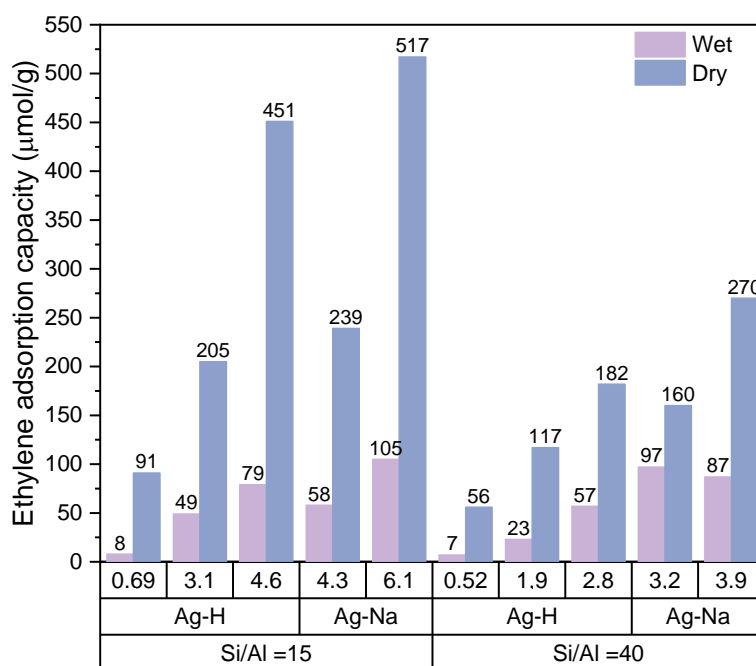


Figure 35- Comparison of ethylene adsorption capacity for Ag-based zeolites under wet and dry conditions

Figure 36 shows that, despite the wet circumstances, the linear rise in ethylene adsorption capacity with increasing Ag<sup>+</sup> species is still confirmed. However, the lower slope indicates competitive behavior between water and ethylene molecules. The C<sub>2</sub>H<sub>4</sub>/Ag<sup>+</sup> ratio decreased from 1 up to 0.23 (Si/Al=15) and 0.32 (Si/Al=40), which are in line with Kang *et al.*'s[161] results. Modifying the compensating cation had no discernible effect on the degree of interaction with water. However, increasing the Si/Al ratio improved the zeolite's hydrophobic characteristics (verified by the higher slope), resulting in improved adsorption performance. Chebbi *et al.*'s [151] also detected a rise in hydrophobicity for higher Si/Al ratios. The increase in Ag<sup>+</sup> species is accompanied by an increase in ethylene adsorption capability. According to Tahraoui *et al.*'s[109] work, an increase in highly polarizing species is related to an increase in water affinity via electrostatic interactions. However, as shown in Figure 36, an increase in silver load has no effect on water impact. This phenomenon may be explained by the fact that an increase in silver content resulted in a rise in Ag-charged species (mainly Ag<sup>+</sup>), which form stronger connections with ethylene via  $\pi$ -interactions, whereas water contact is associated with physical electrostatic adsorption on Ag sites. The results of Lee *et al.*'s[121] investigation also show that silver has a lower affinity for water.

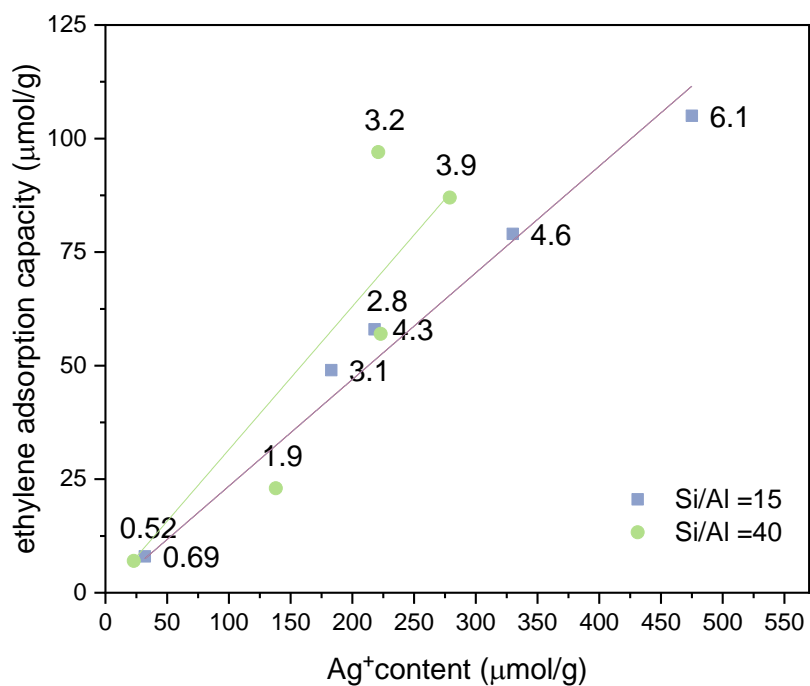


Figure 36- Ethylene adsorption capacity in function of Ag<sup>+</sup> content for Ag-based zeolites under wet conditions

### 3.2 Cu-based zeolite powders

To a lesser degree, Cu-based adsorbents have been investigated as an alternative to silver-based zeolites due to their similarities and cheaper cost. The viability of Cu-based zeolites as an alternative to silver adsorbents in wet conditions will be investigated in this section.

#### 3.2.1 Adsorbents characterization

##### 3.2.1.1 Chemical analyses results

The results from the ICP-OES chemical analysis are summarized in Table 9, as well as the information regarding the preparation process.

Table 9- Cu-based ZSM-5 powders characteristics and preparations

| Sample name | Si/Al | Compensation Cation | Cu content (% wt.) | Theoretical max. Ag content (% wt.) | Exchange Ratio (%) | Cu(CH <sub>3</sub> COO) <sub>2</sub> Ionic Exchanges performed |
|-------------|-------|---------------------|--------------------|-------------------------------------|--------------------|--|
| HM04MFI     | 15    | Na <sup>+</sup>     | 2.3                | 3.3                                 | 72                 | 1 (0.03 M)   |
| HM05MFI     | 15    | H <sup>+</sup>      | 1.8                | 3.2                                 | 57                 | 1 (0.03 M)   |

\*(Cu content quantified by ICP-OES)

Copper zeolites have a lower theoretical maximum concentration than silver zeolites because each  $\text{Cu}^{2+}$  compensates for two negative charges produced by the Al atoms present in the zeolite framework.

When compared to silver-based zeolites, the exchange ratio (as a function of Cu/Al ratio) of copper-based zeolites follows a similar trend. As a result, copper zeolites prepared from Na-based parent zeolites had greater exchange ratios, indicating a preference for  $\text{Cu}^{2+}$  exchange with  $\text{Na}^+$  over  $\text{NH}_4^+$ .

### 3.2.1.2 Optical properties

The UV-Vis spectra of all Cu-based materials show a single wide main band at 780 nm (Figure 37). According to Martins *et al.*'s [162] findings, this wide band found in the 600-850 nm region might be attributable to  $\text{Cu}^{2+}$  cations in hexagonal coordination. The same authors attributed bands at about 890 nm to copper oxide species, although the present analysis does not include such wavelengths. TPR experiments were used to quantify and further identify the copper species.

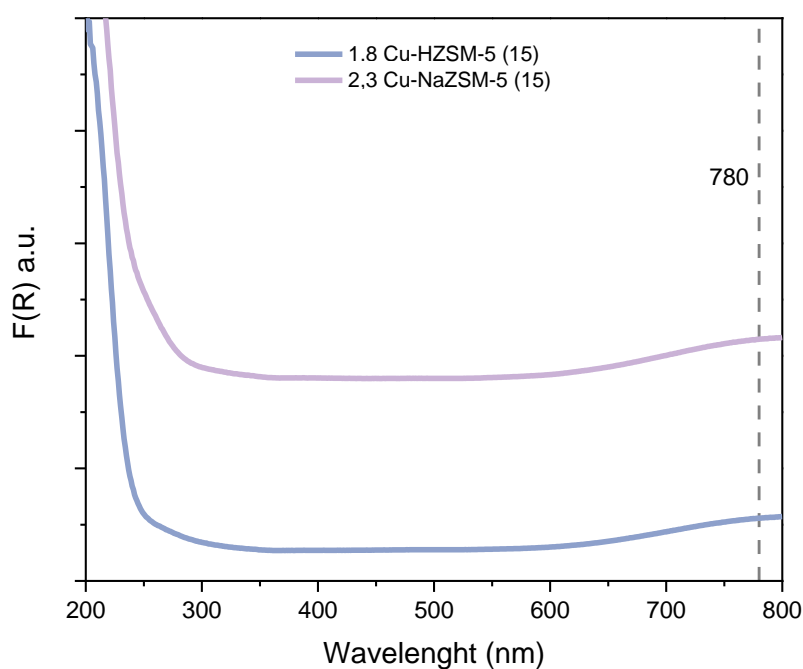


Figure 37- UV-Vis DRS spectra of Cu-based zeolites

### 3.2.1.3 $\text{H}_2$ Temperature Programmed Reduction

$\text{H}_2$  TPR's profiles reveal evidence of two distinct reduction bands in the Cu-based zeolites adsorbents. According to the literature [163], [164], the possible reactions involved in the reduction process are the reduction of CuO into metallic copper (equation 20) or the two-step reduction of  $\text{Cu}^{2+}$ , comprised by the



reduction of  $\text{Cu}^{2+}$  into  $\text{Cu}^+$  at lower temperatures (represented by equations 21) and the reduction of  $\text{Cu}^+$  into metallic copper at higher temperatures (represented by equation 20).



Before any quantitative assessment, through the analyses of the TPR profiles, the stability of certain species can be accessed. Compared to the Na form (Figure 38), the shift of the second peak to a higher temperature present in the protonic samples suggests more stability of the  $\text{Cu}^+$  species.

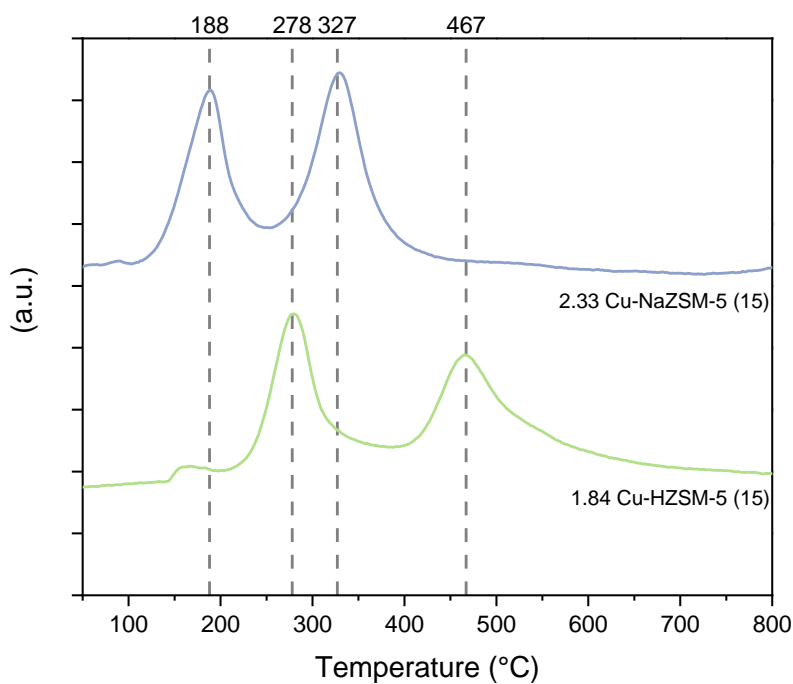


Figure 38-  $\text{H}_2$  TPR profile of Cu-based zeolites

The areas of the two peaks were analysed to further identify the specific species present in the samples. The results are summarized in Table 10.

Table 10- H2-TPR results for the Cu-based zeolites

| Sample              | Cu (μmol/g) | Cu <sup>2+</sup> (μmol/g) | Cu <sup>+</sup> (μmol/g) | Total Cu <sup>+</sup> and Cu <sup>2+</sup> (μmol/g) |
|---------------------|-------------|---------------------------|--------------------------|---|
| 2.33 Cu-NaZSM-5(15) | 367         | 287                       | 67                       | 355   |
| 1.84 Cu-HZSM-5 (15) | 290         | 294                       | 9                        | 294   |

The TPR profiles of the samples follow a similar pattern, with the second peak area being greater than the first peak area, indicating that the samples contain a minor amount of Cu<sup>+</sup> (presumably created by the pre-treatment). Furthermore, the presence of copper oxide can be ruled out because the first peak area should be greater than the second peak area in this case.[165] The copper-based samples are primarily comprised up of Cu<sup>2+</sup> species.

### 3.2.2 Adsorption breakthrough experiments under wet conditions

The performance of the copper zeolites under wet conditions was tested and compared with the silver-based zeolites. The breakthrough adsorption experiments performed under wet conditions (50 ppm C<sub>2</sub>H<sub>4</sub>, 1 °C, 50 mL/min, RH 80%) for the Cu-based zeolites are displayed in Figure 39, and the respective adsorption capacities and break-point times are summarized in Table 11.

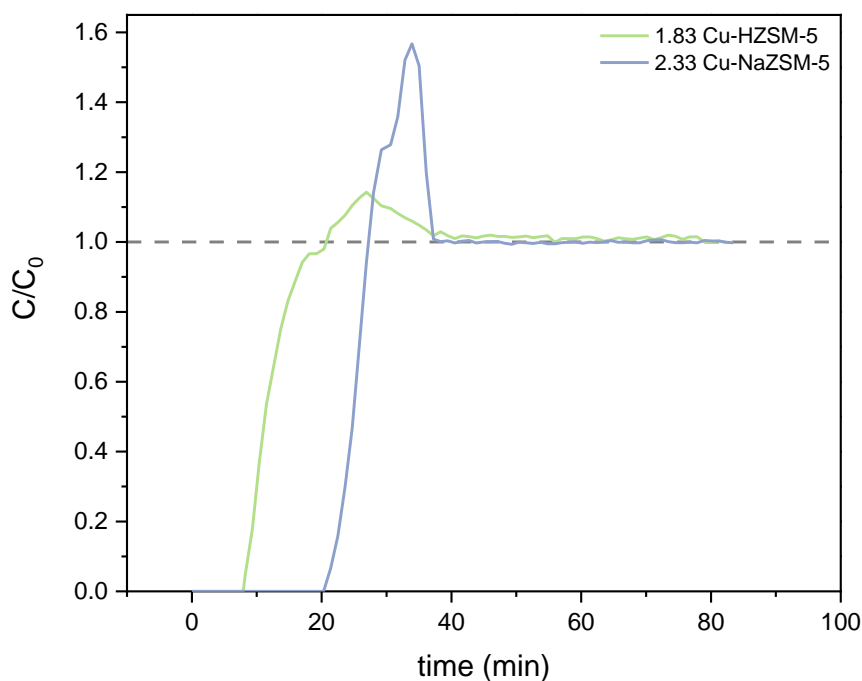


Figure 39- Breakthrough curves for Cu-based zeolites (Si/Al=15) under wet conditions

The adsorption profiles obtained from the breakthrough experiment exhibit similar behaviour to the Ag-zeolite results, implying that no significant diffusion limitations influenced the adsorption process and that water and ethylene compete for the same adsorption sites (overshoot phenomena are present).

Table 11- Summary of ethylene capacity values and break-point time for Cu-based zeolites under wet conditions

| Sample              | $t_{bp}$ (min) | q ( $\mu\text{mol/g}$ ) |
|---------------------|----------------|-------------------------|
| 2.33 Cu-NaZSM-5(15) | 21             | 26                      |
| 1.84 Cu-HZSM-5 (15) | 8              | 13                      |

As shown in Table 11, the ethylene adsorption capacity of copper-based zeolites was much lower than that of silver-based zeolites for identical metal loading. This decline can be attributed to how various copper species interact with zeolite, particularly those capable of forming  $\pi$ -complexation bonds with ethylene. Jen *et al.*'s [165] infrared spectroscopy investigation indicated that  $\text{Cu}^+$  interacts with ethylene in the same way as  $\text{Ag}^+$  does by generating  $\pi$ -complexes.  $\text{Cu}^{2+}$  interactions with ethylene, on the other hand, are mediated by van der Waals electrostatic forces that are substantially weaker. Furthermore, the bivalent nature of  $\text{Cu}^{2+}$  cations results in a higher polarization charge, which improves the interaction with water and leads to higher hydration layers. [167], [168]

The decreased adsorption capacity of the copper-based zeolites can be attributed to the prevalence of  $\text{Cu}^{2+}$  species that are unable of interacting through  $\pi$ -complexation. This is consistent with the findings of Abdi *et al.*'s [125] comparative adsorption studies (between Ag and Cu zeolites), which ascribe the decrease in performance to the presence of  $\text{Cu}^{2+}$  species. Kim *et al.*'s [169] study on copper zeolite for active cold-start hydrocarbon removal elucidates the critical role of  $\text{Cu}^+$  ions in achieving increased adsorption capacities, particularly in wet environments.

### 3.3 Ag-based extrudates

Zeolite shaping is a crucial step in the scale-up process. Powder-based adsorbents are not employed in large-scale industrial operations due to issues such as preferred pathways formation and pressure drop. Zeolite powders can be shaped into extrudates or pellets, which might have high mechanical strength. This characteristic is critical because it prevents the shaped material from deteriorating over time, resulting in the loss of active material and the accumulation of particles in outlet equipment or stored fruits. [130] With the intent to enhance the mechanical properties, extrudates of zeolite and alumina binder were prepared and loaded with the best-performing metal (silver in this case). By changing the metal amount and the zeolite to binder proportion, three distinct silver extrudates were created. Prior to testing in the pilot-scale system implemented in Rocha-Center's test chambers, breakthrough adsorption tests were carried out in the same

set-up used to test powder samples. These tests are critical for comparing the impact of shaping on adsorption performance and give useful information about diffusion issues, thermal and chemical stability. [170]

### 3.3.1 Adsorbents characterization

#### 3.3.1.1 $N_2$ Sorption measurements

The textural properties of the extrudates samples were analysed through  $N_2$  adsorption and the results are summarized on Table 12.

Table 12-  $N_2$  sorption results and microporosity loss by extrudates with different zeolite loads

| Sample references       | $V_{mic}$ | $V_{mic}$ (theoretical) | $V_{mic}$ loss (%) |
|-------------------------|-----------|-------------------------|--------------------|
| HZSM-5 40 (powder)      | 0.182     | ---                     | ---                |
| Ag-HZSM-5 (40% zeolite) | 0.041     | 0.073                   | 44                 |
| Ag-HZSM-5 (60% zeolite) | 0.09      | 0.109                   | 17                 |

As seen in Table 12, the extrudates had a significant reduction in microporosity (compared to the zeolite powder). Because  $\gamma-Al_2O_3$  is a mesoporous binder, the loss is attributed to alumina agglomeration leading to pore blockage. Adsorption is a diffusion-limited process, therefore increasing the diffusion path and decreasing the accessibility of the active site (a phenomenon known as "binder-blinding") has a significant influence on adsorbent performance.[136], [137]

Extrudates with a greater zeolite content (60 wt.%) were prepared in order to reduce this effect. As calculated by the percentage of microporous volume loss, the increase of zeolite in the extrudate (from 40 to 60 wt.%) resulted in less pore obstruction and, as a result, more accessible active sites for ethylene adsorption.

#### 3.3.1.2 Optical properties

Three prominent bands are visible in the UV-Vis spectra of the silver-based extrudates (Figure 40). The two bands at 210 and 225 nm can be assigned to the electronic transition of trigonally coordinated  $Ag^+$  species, as previously seen in silver-base zeolite powders. [154] The third band presents a maximum at 322 nm and might relate to  $Ag_n$  clusters, either neutral or slightly positively charged, which comprise a small amount of Ag atoms, according to Chaieb *et al.*'s [171] research. According to these authors, these species give the samples a fading yellow colour that becomes white after thermal treatment under oxidative conditions. This observation matches the colour change seen in the silver-based extrudates samples after an air pre-treatment prior to the

adsorption experiments. [172] The use of pre-treatment gas was made in order to maximize the number of species capable of interacting with ethylene through  $\pi$ -complexation. Following the adjustments, higher adsorption capacities were achieved, demonstrating the worse adsorption capability of  $Ag_n$  clusters (either in neutral or slightly positively charged state). The absence of  $Ag_2O$  particles should not be considered because small silver oxide particles are not detected in UV-Vis DRS spectra.[125]

For the silver loaded alumina sample (Figure 41), the lack of bands in the 210-225 nm range can imply an absence of isolated  $Ag^+$  species, and the band at 250 nm can be attributed to smaller  $Ag_n^{\delta+}$  clusters. Furthermore, the presence of  $Ag^+$  bands on zeolite extrudates could imply that these species are stabilized on zeolite active sites.

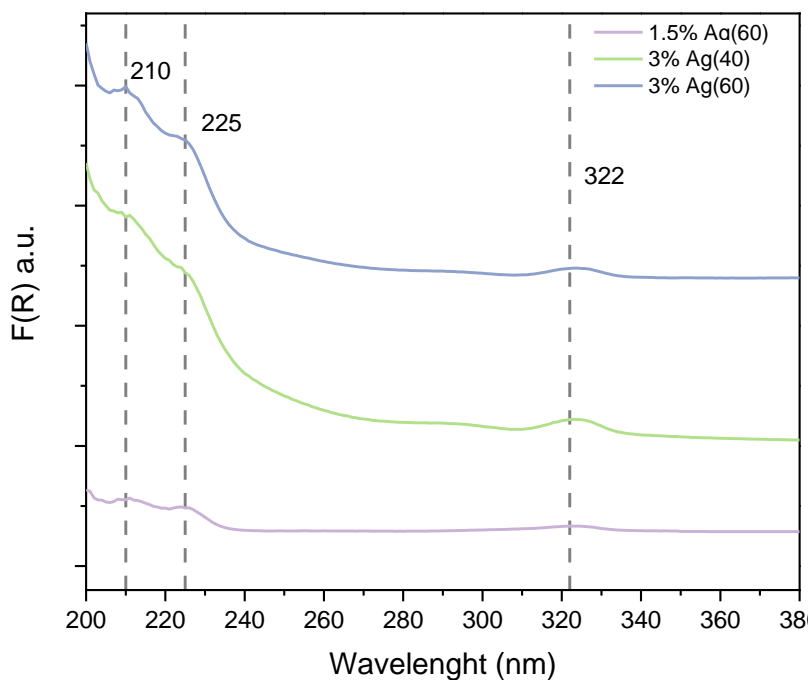


Figure 40- UV-Vis DRS spectra of Ag-based extrudates

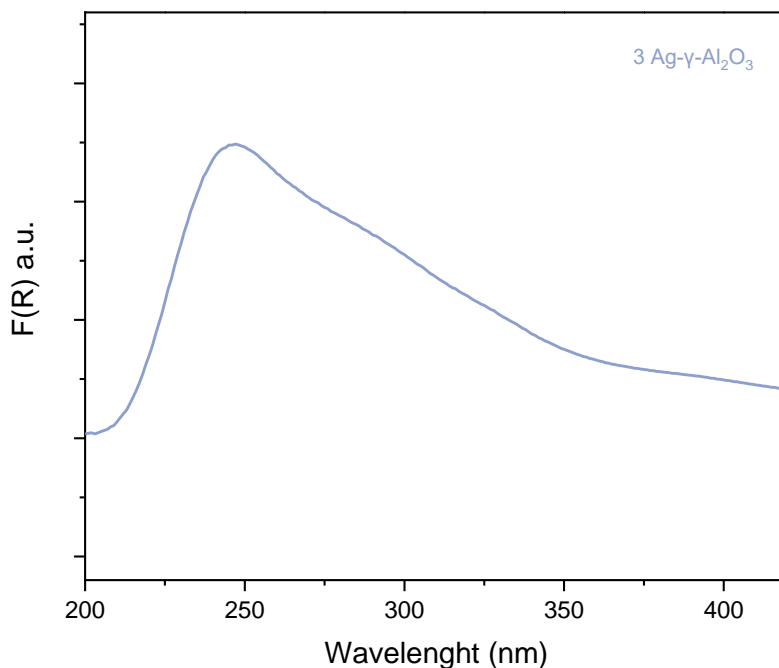


Figure 41- UV-Vis DRS spectra of Ag-based  $\gamma$ -Al<sub>2</sub>O<sub>3</sub> extrudates

### 3.3.1.3 H<sub>2</sub> Temperature Programmed Reduction

A blank test with extrudates constituted of silver-doped  $\gamma$ -Al<sub>2</sub>O<sub>3</sub> was performed to identify the type of species stabilized on this support. The pre-treatment adjustments were applied to the samples before TPR analyses in order to have a representative screening of the Ag species present on the extrudates.

The TPR profile for the silver-loaded  $\gamma$ -Al<sub>2</sub>O<sub>3</sub> extrudates (Figure 42) shows a sharp peak at 110 °C that could be associated with the reduction of Ag<sub>2</sub>O to metallic silver. Similar behaviour was evidenced by Son *et al.*[173] for similar concentrations of silver supported in  $\gamma$ -Al<sub>2</sub>O<sub>3</sub>. The attribution of two less intense peaks is quite dubious since they could be associated with the reduction of Ag<sup>+</sup> species generated by the oxidation of the clusters, as evidenced by the UV-Vis or the decomposition of more dispersed Ag<sub>2</sub>O species.[174]

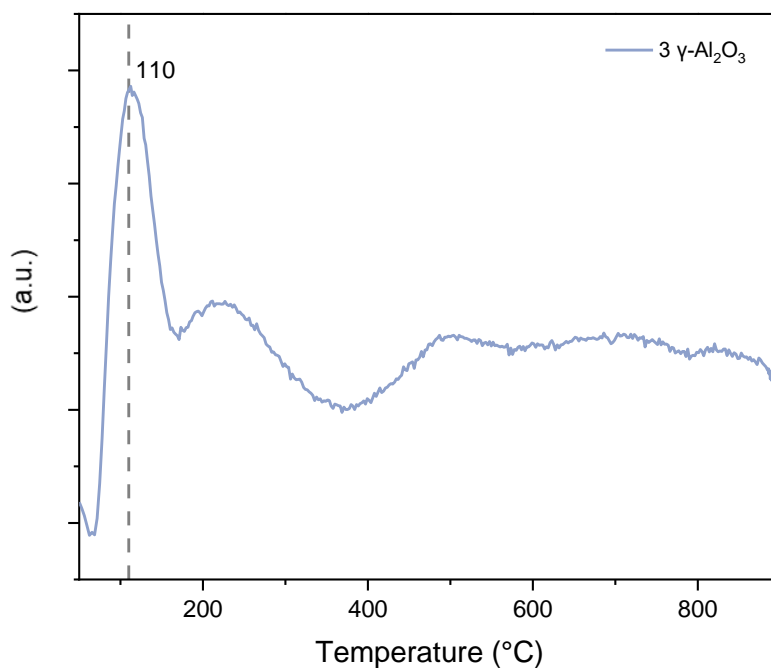


Figure 42-  $H_2$  TPR profile of silver supported in  $\gamma\text{-Al}_2\text{O}_3$  extrudates

The interpretation of the TPR profiles obtained (Figure 43) is quite complex since there is no information in the literature evidencing the selective deposition of silver in either support ( $\gamma$ -alumina or zeolite). However, the UV-Vis spectra highlighted the presence of  $\text{Ag}^+$  isolated species in the extrudates with zeolite (absent in the alumina extrudates) which could suggest the selectivity towards the deposition of silver on the zeolite active sites. These can be corroborated by the existence of two peaks in the TPR profiles, that can be associated with the partial reduction of  $\text{Ag}^+$  species to  $\text{Ag}_n^{\delta+}$  clusters, first, and then  $\text{Ag}_n^{\delta+}$  cluster into metallic silver.

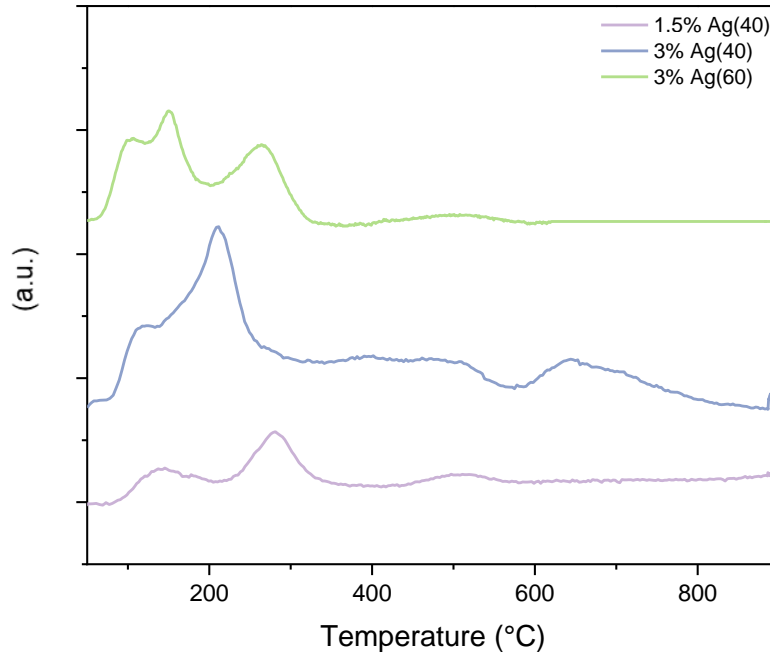


Figure 43-  $H_2$  TPR profile of silver extrudates

### 3.3.2 Adsorption breakthrough experiments under wet conditions

To determine the effect of shaping on adsorption capacity, the performance of silver-based extrudates under wet conditions was investigated and compared to the silver-based powders. Figure 44 depicts the breakthrough adsorption experiments performed under wet conditions (50 ppm  $C_2H_4$ , 1 °C, 50 mL/min, RH 80%) for the extrudates. Their breakthrough curves differ significantly from those obtained for the powder-based samples. As seen in Figure 44, the discrepancy between the saturation and the break-point times increases, resulting in s-shaped curves with lower slope. These shapes are typical of systems with diffusion problems. These diffusion challenges can be attributed to internal diffusion issues caused by binder agglomeration inside the zeolite pores, as evidenced by the  $N_2$  adsorption measurements (Table 12).



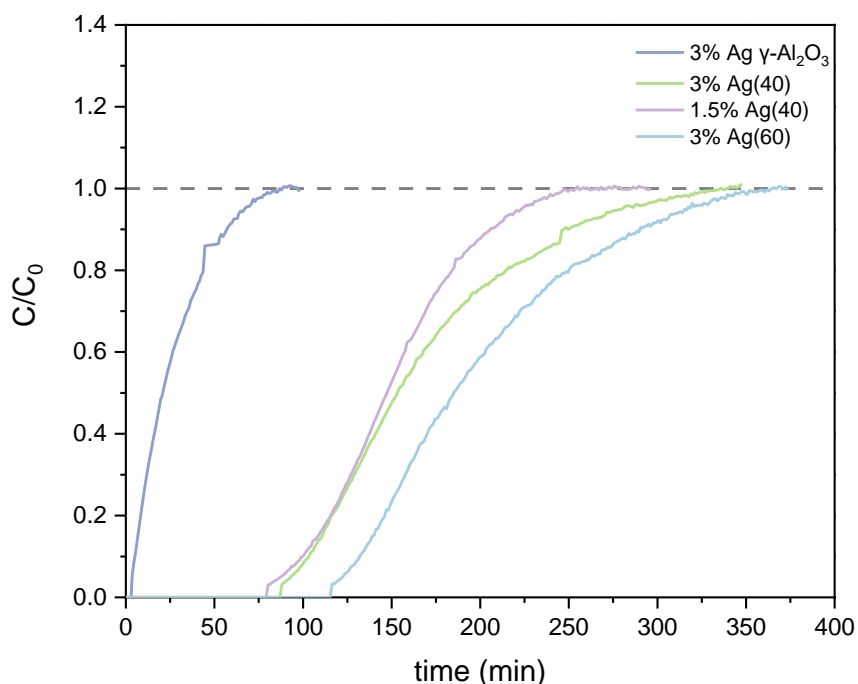


Figure 44- Breakthrough curves for silver-based extrudates (Si/Al=40) under wet conditions

Table 13- Summary of ethylene capacity values and break-point time for Ag-based extrudates under wet conditions

| Extrudates Sample                    | $t_{bp}$ (min) | q ( $\mu\text{mol/g}$ extrudates) |
|--------------------------------------|----------------|-----------------------------------|
| 3 Ag- $\gamma\text{-Al}_2\text{O}_3$ | 3              | 14                                |
| 3 Ag(40)                             | 88             | 68                                |
| 1.5 Ag(40)                           | 80             | 66                                |
| 3 Ag(60)                             | 116            | 89                                |

As previously indicated, the existing analyses cannot precisely determine the quantity and type of silver species deposited on each support material. Nonetheless, the adsorption capacities may be useful in this respect. The adsorption value of  $\gamma\text{-Al}_2\text{O}_3$  extrudates is significantly lower than that of the other samples tested, suggesting that the species stabilized in the support do not interact strongly with ethylene and are most likely undispersed silver oxide clusters. Despite the ability to form  $\pi$ -complexation bonds with ethylene, Lee *et al.*'s[121] research showed that these interactions are significantly weaker (than isolated  $\text{Ag}^+$ ) due to the Ag atom's electron deficiency. Moreover, in the scenario of  $\text{Ag}^+$  stabilized in alumina, their contribution to  $\pi$ -complexation would be significantly reduced due to electron density transfer from  $\text{Ag}^+$  to the Lewis acid sites of alumina, as demonstrated by Padin *et al.*'s[175] results. According to this hypothesis, the most active species for ethylene adsorption are found to be the active sites of the zeolite support, most likely the dispersed  $\text{Ag}^+$  species shown in the UV-Vis spectra of the extrudates.

Another conclusion is that most of the metallic clusters (neutral or slightly charged) shown in the TPR profiles are deposited in the zeolite because changing the pre-treatment gas (N<sub>2</sub> to air) resulted in an increase in adsorption capacity due to the formation of more dispersed active Ag<sup>+</sup> species (oxidation of small metallic clusters) for  $\pi$ -complexation. Jacobs *et al.* [176] identified this phenomenon during thermal treatment tests under moderate oxidative conditions, which resulted in the re-oxidation of internal neutral nanoclusters into dispersed Ag<sup>+</sup> species.

The increase in ethylene adsorption capability is strongly tied to the rise in the extrudates' zeolite percentage. These may be attributed to the decrease in binder agglomeration inside the zeolite pores, which resulted in increased accessibility for the stabilization of Ag<sup>+</sup> species. The hypothesis of active silver species being "trapped" inside the clogged micropores was rejected since the ionic exchange happened after the extrusion process. The studies with varied silver loads for the same zeolite percentage provide an unusual outcome. An explanation for the relatively lower difference in capacities could be that the active zeolite sites are fully occupied, and the extra silver is loaded as silver oxide on alumina, but further investigation is needed to validate this hypothesis.

Finally, replicability is a crucial characteristic of a technology's scalability. Multiple batches of each zeolite were made and evaluated in this regard. The experimental results for the identical extrudates demonstrated similar adsorption capabilities, ensuring replicability.

### 3.3.3 Adsorption-desorption cycles experiments under wet conditions

The recuperative nature of zeolite-based adsorption technology is one of its primary features. The extrudate samples were exposed to several adsorption-desorption cycles under wet conditions to analyse these properties, and the ethylene adsorption capacities were compared to understand the changes occurring after each cycle. The desorption temperature was deliberately kept low (60 °C) to avoid oligomerization of the adsorbed ethylene and sintering of silver ionic species [177], which might harm the extrudates' adsorption capacities.

Figure 45 and Figure 47 depicts the adsorption-desorption cycle experiments performed under wet conditions (50 ppm C<sub>2</sub>H<sub>4</sub>, 1 °C, 50 mL/min, RH 80%) for two different extrudates samples, while Figure 46 and Figure 48 summarizes the various adsorption/desorption capacities.

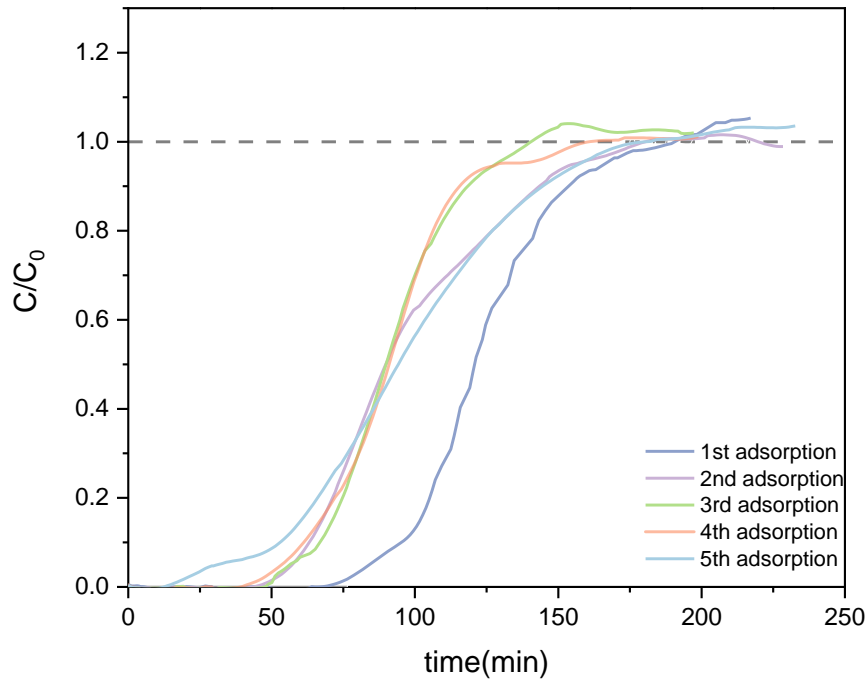


Figure 45- Breakthrough curves for the adsorption-desorption cycles for 1.5Ag(40) extrudates under wet conditions

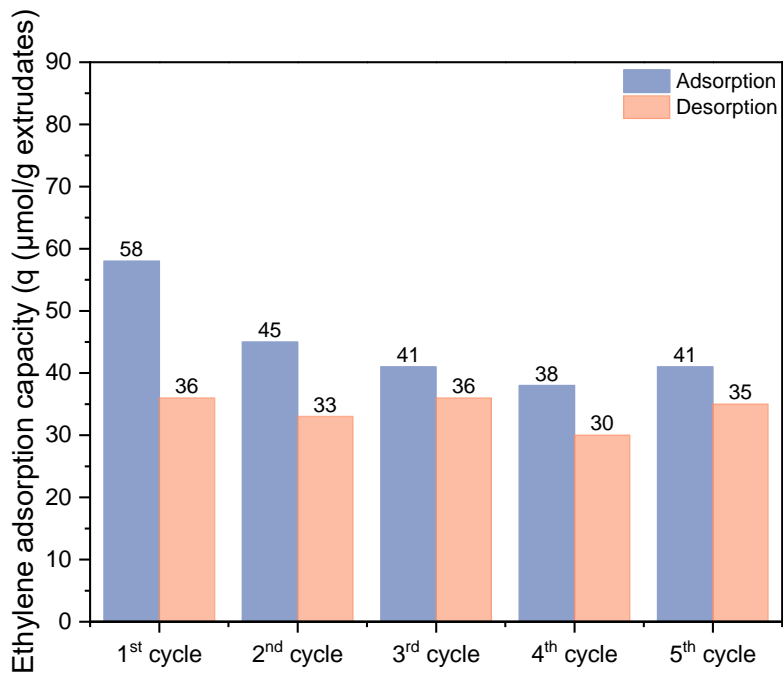


Figure 46-Summary of ethylene capacities for 1.5Ag(40) extrudates adsorption-desorption cycles tested under dry conditions

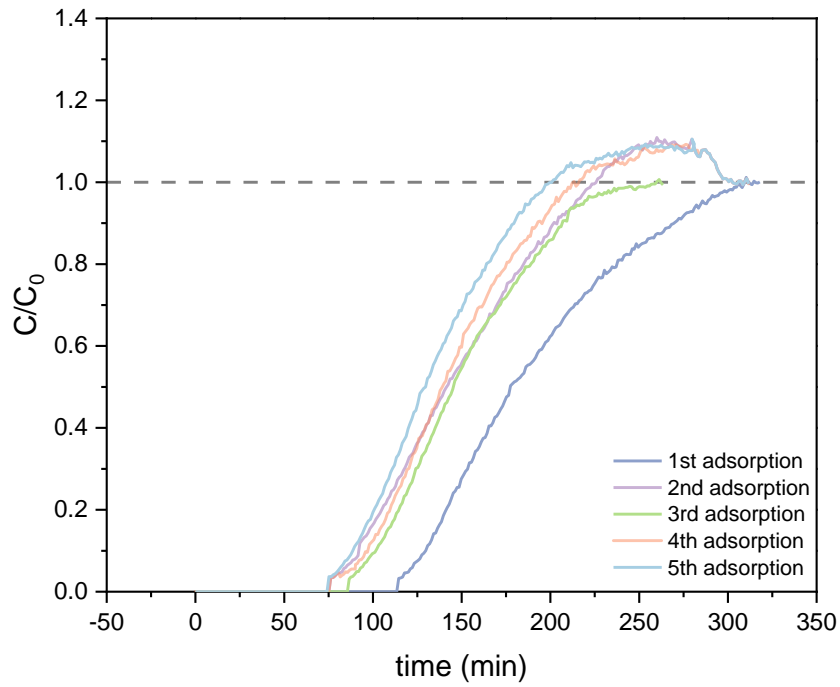


Figure 47- Breakthrough curves for the adsorption-desorption cycles for 3Ag(60) extrudates under wet conditions

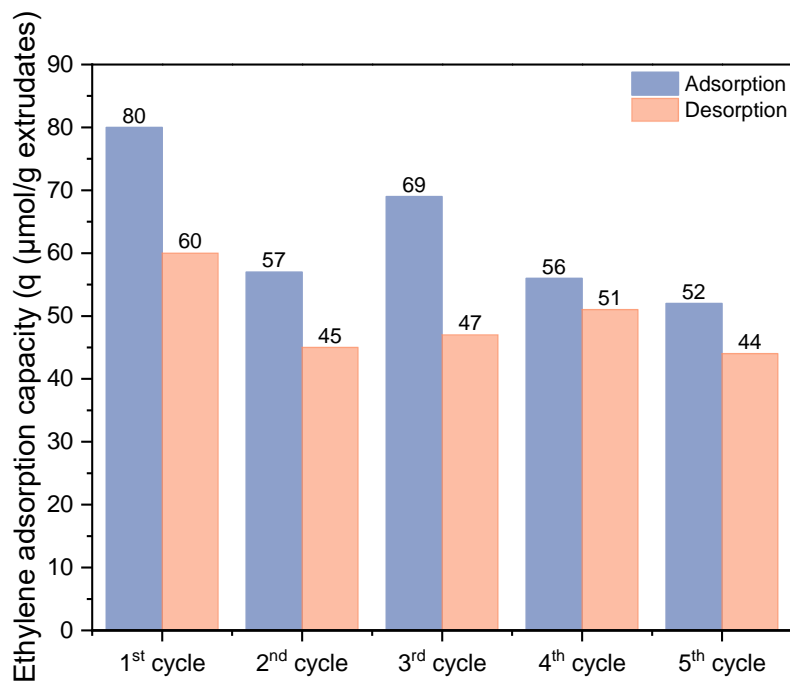


Figure 48- Summary of ethylene capacities for 3Ag(60) extrudates adsorption-desorption cycles tested under dry conditions

The adsorption-desorption cycle data for the two extrudate samples studied show comparable patterns. The first cycle has the greatest ethylene adsorption capacity, while the following cycles show a

reduction in adsorption performance that is maintained throughout the four cycles (Figure 46 and Figure 48). This decrease in performance might be attributed to incomplete ethylene or water desorption. Either compound can interact with the active species at different pore locations, with varying degrees of interaction strength. Consequently, it is extremely conceivable that a non-negligible percentage of the adsorbed compounds require higher temperatures to desorb.

There were no additional declines in adsorption capacities identified in subsequent cycles, implying that there are no large alterations in the active species present in the adsorption process, and so the oligomerization of ethylene and metal sintering are most likely discarded. The disparity in adsorption-desorption values for ethylene concentration can be attributed to data losses caused by the adjustment in experimental setup between the adsorption and desorption processes.

Despite the early decline in adsorption capacity, the subsequent cycles demonstrate the excellent extrudate's regeneration capacity, even at low temperatures. Aside from the benefits already mentioned, keeping the desorption temperature low has a significant economic influence on the technology's scalability. Reduced temperatures have a diminished heat load impact on refrigeration systems and are significantly less expensive to generate.

### 3.3.4 Adsorption-desorption cycles experiments under real conditions

The last part of the work involves testing the extrudates under "real" conditions in the Rocha-Center's test chambers. The extrudates were evaluated under real conditions and due to the continually changing nature (VOCs, O<sub>2</sub>, CO<sub>2</sub> gas composition, etc.) of the fruit storage no direct comparison of performance could be performed. However, a few conclusions may be drawn from the findings, including the recoverability of adsorption capacity following desorption and the selectivity of the adsorbents towards ethylene. All these results provide an excellent means to assess the viability of these technologies in real-life scenarios (proof of concept).

*Table 14- Summary of conditions verified during the adsorption-desorption cycle experiments performed in Rocha-Center*

| Sample    | Date       | %O <sub>2</sub> | %CO <sub>2</sub> | %RH | T (°C) | Extrudate mass (g) |
|-----------|------------|-----------------|------------------|-----|--------|--------------------|
| 3% Ag(40) | 27/10/2022 | 17.78           | 0.77             | 92  | 0.02   | 3.44               |
| 3% Ag(40) | 03/11/2022 | 16.79           | 0.53             | 92  | -0.03  | 3.24               |
| 3% Ag(60) | 22/11/2022 | 17.58           | 0.61             | 92  | -0.13  | 3.47               |
| 3% Ag(60) | 19/01/2023 | 17.76           | 0.57             | 93  | -0.1   | 3.09               |
| 3% Ag(60) | 20/01/2023 | 17.65           | 0.58             | 92  | -0.1   | 3.09               |

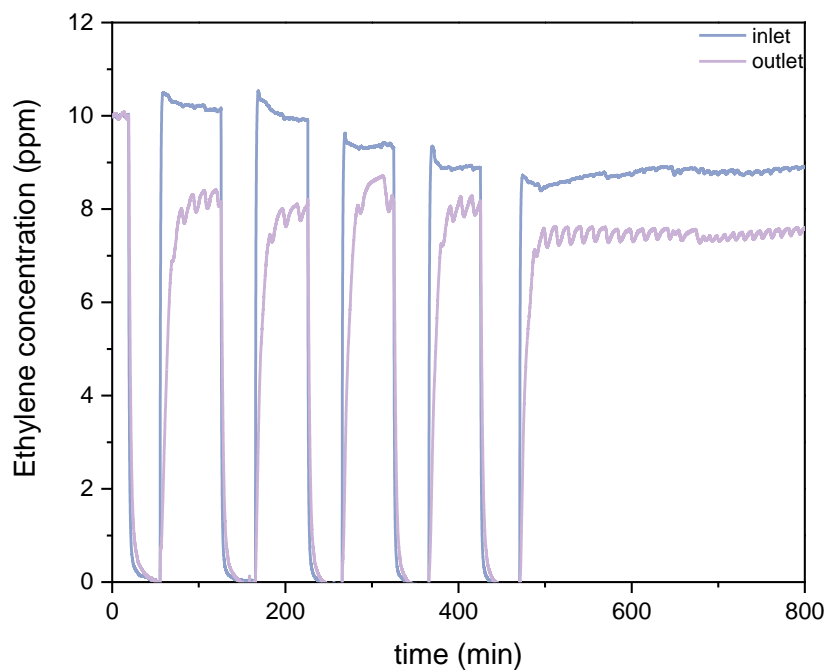


Figure 49- Ethylene concentration profile during the adsorption-desorption cycles with 3%Ag(40) on 27/10/2022

Table 15- Summary of ethylene adsorption capacity in each cycle and the overall reduction of ethylene concentration (3%Ag(40) on 27/10/2022)

| Cycle                          | Ethylene adsorbed ( $\mu\text{mol/g}$ extrudates) |
|--------------------------------|---|
| 1 <sup>st</sup>                | 19  |
| 2 <sup>nd</sup>                | 15  |
| 3 <sup>rd</sup>                | 9   |
| 4 <sup>th</sup>                | 10  |
| <b>Reduction = 2 ppm (17%)</b> |   |

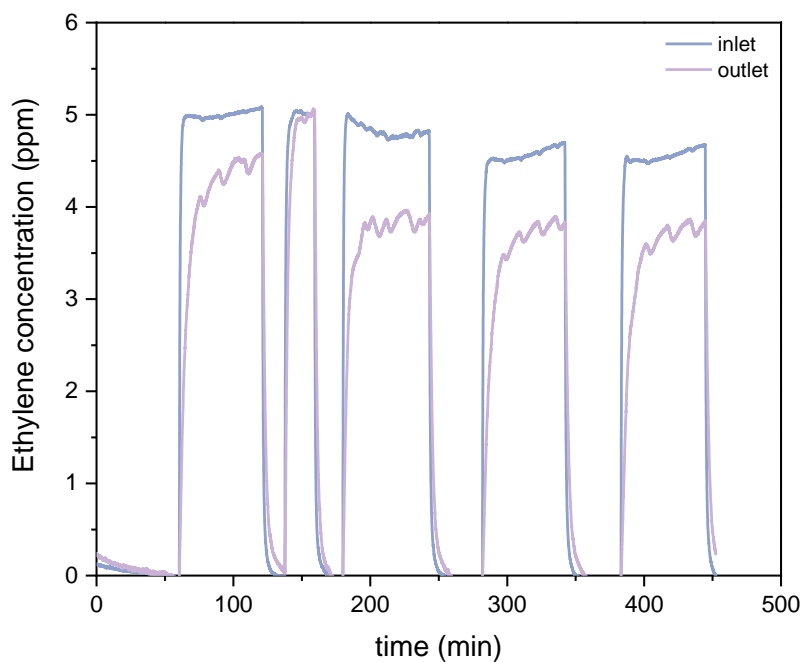


Figure 50- Ethylene concentration profile during the adsorption-desorption cycles with 3%Ag(40) on 03/11/2022

Table 16- Summary of ethylene adsorption capacity in each cycle and the overall reduction of ethylene concentration (3%Ag(40) on 03/11/2022)

| Cycle                           | Ethylene adsorbed ( $\mu\text{mol/g}$ extrudates) |
|---------------------------------|---|
| 1 <sup>st</sup>                 | 5   |
| 2 <sup>nd</sup>                 | 7   |
| 3 <sup>rd</sup>                 | 6   |
| 4 <sup>th</sup>                 | 6   |
| <b>Reduction = 0.5 ppm (8%)</b> |   |

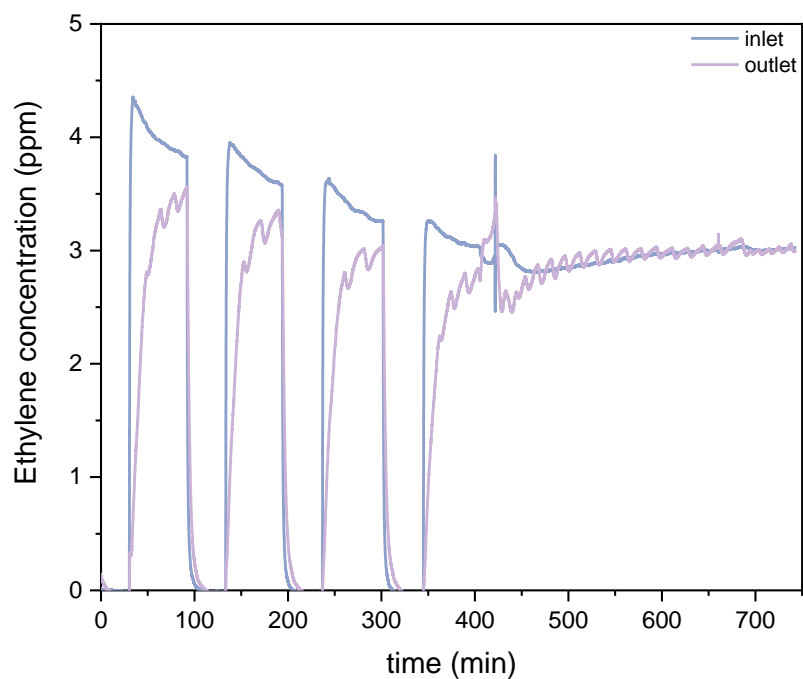


Figure 51-Ethylene concentration profile during the adsorption-desorption cycles with 3%Ag(60) on 22/11/2022

Table 17-Summary of ethylene adsorption capacity in each cycle and the overall reduction of ethylene concentration (3%Ag(60) on 22/11/2022)

| Cycle                            | Ethylene adsorbed ( $\mu\text{mol/g}$ extrudates) |
|----------------------------------|---|
| 1 <sup>st</sup>                  | 6   |
| 2 <sup>nd</sup>                  | 5   |
| 3 <sup>rd</sup>                  | 4   |
| 4 <sup>th</sup>                  | 4   |
| <b>Reduction = 1.4 ppm (31%)</b> |   |



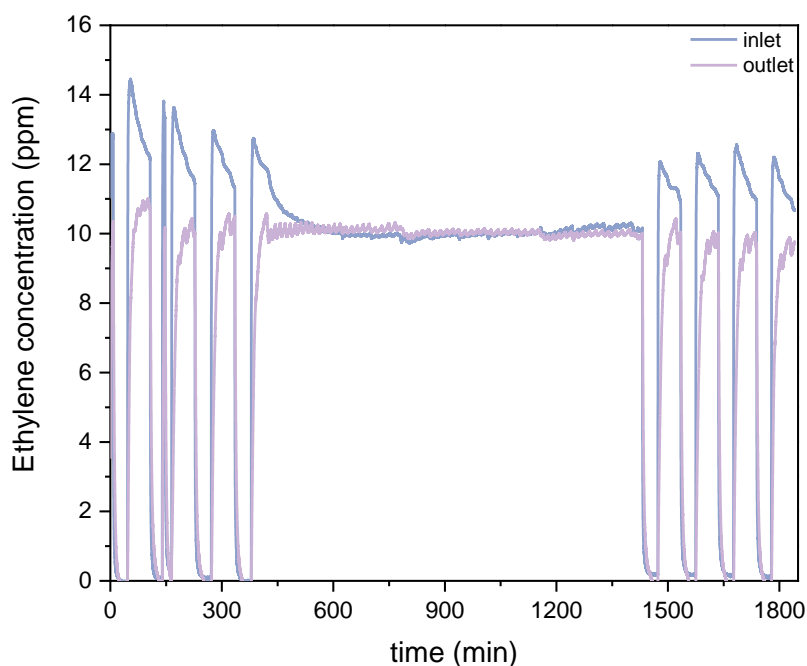


Figure 52- Ethylene profile concentration during the adsorption-desorption cycles with 3%Ag(60) on 19/01/2023 and 20/01/2023

Table 18- Summary of ethylene adsorption capacity in each cycle and the overall reduction of ethylene concentration (3%Ag(60) on 19/01/2023 and 20/01/2023)

| Cycle                          | Ethylene adsorbed ( $\mu\text{mol/g}$ extrudates) |
|--------------------------------|---|
| 1 <sup>st</sup>                | 18  |
| 2 <sup>nd</sup>                | 19  |
| 3 <sup>rd</sup>                | 16  |
| 4 <sup>th</sup>                | 17  |
| 5 <sup>th</sup>                | 13  |
| 6 <sup>th</sup>                | 17  |
| 7 <sup>th</sup>                | 15  |
| 8 <sup>th</sup>                | 15  |
| <b>Reduction = 4 ppm (26%)</b> |   |

Each adsorption-desorption experiment shows a significant decrease in ethylene concentration (Figure 49-52 and Table 15-18). In general, the extrudates restore their adsorption capacities over the cycles after regeneration. The most recent test (Table 18), which was conducted on two distinct days and kept the zeolite active over the night, underlined this characteristic. The large changes in ethylene adsorbed between the same sample trials are primarily due to the starting ethylene concentration in the chamber (10-5 ppm). This affects the adsorption process because the difference in concentration is a driving force behind the adsorption process. For comparable baseline ethylene concentrations, increasing the zeolite fraction in the extrudates increases ethylene removal from 8 to 31%.

Preliminarily, it can be noted that the developed adsorbents demonstrated high selectivity for ethylene in an environment including various VOCs and CO<sub>2</sub>. The regeneration ability of extrudates is one of the most essential properties since it considerably influences the amount of active medium required for ethylene removal. Despite the various gas compositions, an average ethylene concentration decrease of 16.4% after 8 hours was verified for rather small cartridge loadings of active extrudates (3.5 g). The extrudates showed great mechanical strength, mainly because no significant deterioration was verified even at a substantially higher desorption gas flow rate.

Despite the absence of information on gas composition, this comparison further corroborates the importance of an increase in active Ag<sup>+</sup> species in selective ethylene adsorption. The revealed regenerative capacity, together with the low temperature required for desorption, shows the concept's promise as a less expensive and more dependable method of extending fruit shelf-life during storage and transport.

## Conclusion and future perspectives

The current study aimed to create a novel adsorbent based on metal-loaded zeolites that ensures effective ethylene adsorption, with the goal of controlling the ethylene concentration in industrial fruit storage chambers. To that end, silver zeolite samples with varied properties (Si/Al, compensating cation) and metal loadings were studied to determine the effect of water on ethylene adsorption capacity. This effect was investigated by comparing the adsorption capabilities under dry and wet conditions (typical of the high RH observed in industrial storage chambers). As a more economic-friendly alternative, Copper-based zeolites were synthesised and evaluated under wet conditions, and their ethylene adsorption characteristics were compared to those of their silver-based counterparts.

The best-performing metal supported zeolites were shaped by mixing-extrusion, and their performance for adsorption under wet conditions was compared to powder samples, as well as the impact of different zeolite percentages and metal loadings. Wet adsorption-desorption cycle tests were also carried out to investigate the regeneration capabilities and their impact on adsorption performance. Finally, the shaped samples were subjected to real-world adsorption-desorption cycles in a pilot scale adsorption system installed in the Rocha-Center's test storage chambers (filled with Rocha Pear fruits) to evaluate the performance capabilities under practical storage conditions.

Multiple characterization techniques were employed to identify the most active species in ethylene adsorption and, in the case of extrudates, to investigate the influence of shaping on textural properties.

Comparatively, the silver-based zeolite demonstrated superior adsorption performance. This is supported by the highly dispersed  $\text{Ag}^+$  species capable of interacting with ethylene via a chemisorption process known as  $\pi$ -complexation. Copper-based zeolites were characterized by the stability of  $\text{Cu}^{2+}$  species, which interact with ethylene via lower-strength Van der Waals electrostatic interactions, resulting in lower ethylene adsorption performances.

The addition of water to the studies resulted in a considerable decrease in performance (about 75%). This was attributable to competing ethylene and water adsorption in the zeolite, as indicated by a shift in the number of molecules of ethylene adsorbed per  $\text{Ag}^+$  active site. In dry conditions, the  $\text{C}_2\text{H}_4/\text{Ag}^+$  ratio was 1, whereas, in wet conditions, the  $\text{C}_2\text{H}_4/\text{Ag}^+$  ratio was 0.23 (Si/Al=15) and 0.32 (Si/Al=40). Concerning the change in properties, higher silver loading was verified for Na-based parent zeolites, and a rise in Si/Al ratio resulted in an improvement in adsorption performance under wet conditions, indicating lower water affinity (more hydrophobic). Overall, an increase in silver loading enhanced ethylene adsorption due to an increased amount of active  $\pi$ -complexation species ( $\text{Ag}^+$ ).

Shaping had a considerable influence on textural properties, which was confirmed by characterization. The decrease of microporosity caused by binder agglomeration has a significant impact on the availability of zeolite sites for stabilizing active  $\text{Ag}^+$  species. Silver species were most likely stabilized as  $\text{Ag}_2\text{O}$  species in the

alumina support, resulting in a reduced interaction with ethylene. When compared to powder zeolites, a significant drop in performance was observed. The synthesis of extrudates with greater zeolite percentages reduced the loss of microporosity owing to binder agglomeration, resulting in improved ethylene adsorption capabilities. This improvement is due to an increase in zeolite pore space, which is capable of stabilizing Ag<sup>+</sup> species and reducing internal diffusional problems.

The extrudate adsorption-desorption cycles demonstrated the regeneration capability of zeolite adsorption technologies under low-temperature desorption (60 °C). Following an initial decrease in adsorption capacity, performance was maintained during the next four cycles. The first performance decline was attributed to a tiny amount of ethylene that was not desorbed.

Adsorption-desorption investigations using the pilot scale equipment installed in the Rocha-Center's fruit test chambers confirmed the regeneration qualities and efficient adsorption of ethylene under real conditions. After 8 hours, an ethylene concentration drop of 16.4% was observed for relatively tiny cartridge loads of active extrudates (3.5 g). The prepared extrudates have high mechanical strength since no significant degradation was observed even at high desorption gas flow rates.

The current study reveals the potential of zeolite-based adsorption systems in industrial storage systems. Nevertheless, there is still more work to be done. Carbon dioxide is an important gas in CA storage systems; hence its adsorption influence should be examined in the laboratory. Longer adsorption-desorption cycles (either in the laboratory or at the Rocha-Center) might be beneficial when studying the influence on performance in longer studies. Some ideas were formed in the lab scale studies regarding the early decrease in performance throughout the adsorption-desorption cycles, therefore GC-MS analysis would be valuable to understand the desorption process. Because temperature has a significant influence on the economic landscape of cooling, greater temperatures during transportation might be employed to lessen the economic impact. Understanding the effect of temperature on ethylene adsorption might have a significant impact on the process in this line of thinking. In terms of shaped zeolites, efforts should be directed at mitigating binder agglomeration and determining the selective load of silver on zeolite and alumina using characterization techniques such as scanning transmission electron microscopy. Further studies on the stabilized species in the alumina binder would be necessary to validate the assumptions suggested during the current work.

## References

- [1] Rossi R, "The EU fruit and vegetable sector: Main features, challenges and prospects," *Think Tank, European Parliament*, 2019.
- [2] Cicco Antonella, "The fruit and vegetable sector in the EU - a statistical overview," *eurostat Statistics Explained*, 2019.
- [3] "The Mediterranean Region."  
[https://ec.europa.eu/environment/nature/natura2000/biogeog\\_regions/mediterranean/index\\_en.htm](https://ec.europa.eu/environment/nature/natura2000/biogeog_regions/mediterranean/index_en.htm)  
(accessed Apr. 12, 2023).
- [4] "Almería, líder nacional en exportación de legumbres y hortalizas en 2019."  
[https://www.diariodealmeria.es/finanzasyagricultura/Almeria-nacional-exportacion-legumbres-hortalizas\\_0\\_1491751056.html](https://www.diariodealmeria.es/finanzasyagricultura/Almeria-nacional-exportacion-legumbres-hortalizas_0_1491751056.html) (accessed Apr. 12, 2023).
- [5] "Solar greenhouses in southern Europe are major generators of stable employment," Sep. 28, 2021.  
<https://www.freshplaza.com/europe/article/9358611/solar-greenhouses-in-southern-europe-are-major-generators-of-stable-employment/> (accessed May 28, 2023).
- [6] A. J. Castro *et al.*, "Six Collective Challenges for Sustainability of Almería Greenhouse Horticulture," *International Journal of Environmental Research and Public Health* 2019, Vol. 16, Page 4097, vol. 16, no. 21, p. 4097, Oct. 2019, doi: 10.3390/IJERPH16214097.
- [7] E. El País, "Por qué el Mar de Plástico se llama así," Sep. 23, 2015.  
[https://verne.elpais.com/verne/2015/09/23/articulo/1443003299\\_631218.html](https://verne.elpais.com/verne/2015/09/23/articulo/1443003299_631218.html) (accessed Apr. 12, 2023).
- [8] "Los plásticos de la agricultura inundan Almería | Clima y Medio Ambiente | EL PAÍS."  
<https://elpais.com/america/sociedad/2020-11-06/los-plasticos-de-la-agricultura-inundan-almeria.html>  
(accessed Apr. 12, 2023).
- [9] D. Zhou, H. Meinke, M. Wilson, L. F. M. Marcelis, and E. Heuvelink, "Towards delivering on the sustainable development goals in greenhouse production systems," *Resour Conserv Recycl*, vol. 169, p. 105379, Jun. 2021, doi: 10.1016/J.RESCONREC.2020.105379.
- [10] P. Garcia-Caparros, J. I. Contreras, R. Baeza, M. L. Segura, and M. T. Lao, "Integral Management of Irrigation Water in Intensive Horticultural Systems of Almería," *Sustainability* 2017, Vol. 9, Page 2271, vol. 9, no. 12, p. 2271, Dec. 2017, doi: 10.3390/SU9122271.
- [11] Alonso Inés, "The Environmental Impacts of Greenhouse Agriculture in Almería, Spain," Sep. 23, 2021.  
<https://www.foodunfolded.com/article/the-environmental-impacts-of-greenhouse-agriculture-in-almeria-spain> (accessed May 28, 2023).

- [12] “Contribuciones económicas, sociales y mediambientales de la agricultura intensiva de Almería”.
- [13] P. Garcia-Caparros, J. I. Contreras, R. Baeza, M. L. Segura, and M. T. Lao, “Integral Management of Irrigation Water in Intensive Horticultural Systems of Almería,” *Sustainability* 2017, Vol. 9, Page 2271, vol. 9, no. 12, p. 2271, Dec. 2017, doi: 10.3390/SU9122271.
- [14] “En el ‘mar de plástico’ en España, los insectos reemplazan a los insecticidas.” <https://www.lavanguardia.com/vida/20190726/463701741615/mar-plastico-espana-insectos-reemplazan-insecticidas.html> (accessed Apr. 12, 2023).
- [15] “Spain: Cooling trend in Almería by its greenhouses surface | Nieuwsbericht | Agroberichten Buitenland.” <https://www.agroberichtenbuitenland.nl/actueel/nieuws/2019/08/13/spain-cooling-trend-in-almeria-by-its-greenhouses-surface> (accessed Apr. 12, 2023).
- [16] “Portugal’s agriculture sector: still dual, but promising.” <https://www.caixabankresearch.com/en/sector-analysis/agrifood/portugals-agriculture-sector-still-dual-promising> (accessed Apr. 12, 2023).
- [17] A. Informations-Gesellschaft mbH, “European Statistics Handbook – FRUIT LOGISTICA 2022”, Accessed: Apr. 12, 2023. [Online]. Available: [www.AMI-informiert.de](http://www.AMI-informiert.de)
- [18] “PDO and PGI products represent the excellence of European agricultural food production,” <https://www.pdopgi.eu/european-certification-system/> (accessed Apr. 12, 2023).
- [19] “The pear market in the EU Production, yields and areas,” *European Commission*, 2022.
- [20] “Produção e Comercialização de Pera.” <https://www.rootnews.net/post/produ%C3%A7%C3%A3o-e-comercializa%C3%A7%C3%A3o-de-pera> (accessed Apr. 12, 2023).
- [21] “Top 10 Pear producing countries in the world - production and area under cultivation [2019].” <https://numerical.co.in/numerons/collection/61214ddd1785141f7892d563> (accessed Apr. 12, 2023).
- [22] “Producing pears in Portugal | Good Fruit Grower.” <https://www.goodfruit.com/producing-pears-in-portugal/> (accessed Apr. 12, 2023).
- [23] “Jornal de Leiria - Exportação de pêra rocha cresce 16% e vale 90 milhões de euros.” <https://www.jornaldeleiria.pt/noticia/exportacao-de-pera-rocha-cresce-16percent-e-vale-90-milhoes-de-euros> (accessed Apr. 12, 2023).
- [24] “Exportações de pera rocha sobem para os 90 milhões de euros em 2019 – Observador.” <https://observador.pt/2020/01/31/exportacoes-de-pera-rocha-sobem-para-os-90-milhoes-de-euros-em-2019/> (accessed Apr. 12, 2023).
- [25] “ANP – Pêra Rocha.” <https://perarocha.pt/anp/> (accessed Apr. 12, 2023).

- [26] “Pera Rocha – Pêra Rocha.” <http://perarocha.pt/pera-rocha/#historia> (accessed Apr. 12, 2023).
- [27] M. A. A. Mariah *et al.*, “The Emergence and Impact of Ethylene Scavengers Techniques in Delaying the Ripening of Fruits and Vegetables,” *Membranes* 2022, Vol. 12, Page 117, vol. 12, no. 2, p. 117, Jan. 2022, doi: 10.3390/MEMBRANES12020117.
- [28] “Your vegetables are alive — and they change in response to light and dark.” <https://www.elsevier.com/connect/your-vegetables-are-alive-and-they-change-in-response-to-light-and-dark> (accessed Apr. 12, 2023).
- [29] R. Wills and J. Golding, *Postharvest: An Introduction to the Physiology and Handling of Fruit and Vegetables*, 6th ed. CABI, 2016.
- [30] J. Valente, R. Almeida, and L. Kooistra, “A Comprehensive Study of the Potential Application of Flying Ethylene-Sensitive Sensors for Ripeness Detection in Apple Orchards,” *Sensors (Basel)*, vol. 19, no. 2, Jan. 2019, doi: 10.3390/S19020372.
- [31] C. S. Barry and J. J. Giovannoni, “Ethylene and Fruit Ripening,” *J Plant Growth Regul*, pp. 143–157, 2007, doi: 10.1007/s00344-007-9002-y.
- [32] A. A. Saquet, “Storage of pears,” *Sci Horti*, vol. 246, pp. 1009–1016, Feb. 2019, doi: 10.1016/J.SCIENTA.2018.11.091.
- [33] Jorge. Soares, Amado. Silva, and J. Alexandre, *O Livro da pera rocha*, 1st ed. Cadaval: ANP- Associação Nacional de Produtores de Pera, 2011.
- [34] A. C. Galvis-Sánchez, S. C. Fonseca, A. M. M. B. Morais, and F. X. Malcata, “Physicochemical and Sensory Evaluation of ‘Rocha’ Pear Following Controlled Atmosphere Storage,” *J Food Sci*, vol. 68, no. 1, pp. 318–327, Jan. 2003, doi: 10.1111/J.1365-2621.2003.TB14159.X.
- [35] R. Lufu, A. Ambaw, and U. L. Opara, “Water loss of fresh fruit: Influencing pre-harvest, harvest and postharvest factors,” *Sci Horti*, vol. 272, p. 109519, Oct. 2020, doi: 10.1016/J.SCIENTA.2020.109519.
- [36] N. Keller, M. N. Ducamp, D. Robert, and V. Keller, “Ethylene removal and fresh product storage: A challenge at the frontiers of chemistry. Toward an approach by photocatalytic oxidation,” *Chem Rev*, vol. 113, no. 7, pp. 5029–5070, Jul. 2013, doi: 10.1021/CR900398V/ASSET/IMAGES/LARGE/CR-2009-00398V\_0026.JPEG.
- [37] U. Opara and A. Mahdoury, “Physiological responses and changes in postharvest quality attributes of ‘Hellow’ pomegranate variety (*Punica granatum* L.) during refrigerated storage,” *International Commission of Agricultural Engineering (CIGR)*, 2008.

- [38] S. Ben-Yehoshua and V. Rodov, "Transpiration and water stress," in *Postharvest Physiology and Pathology*, J. A. Bartz and J. K. Brecht, Eds., 2003.
- [39] T. A. Nguyen, P. Verboven, N. Scheerlinck, S. Vandewalle, and B. M. Nicolai, "Estimation of effective diffusivity of pear tissue and cuticle by means of a numerical water diffusion model," *J Food Eng*, vol. 72, no. 1, pp. 63–72, Jan. 2006, doi: 10.1016/J.JFOODENG.2004.11.019.
- [40] M. E. K. Ngcobo, M. A. Delele, U. L. Opara, and C. J. Meyer, "Performance of multi-packaging for table grapes based on airflow, cooling rates and fruit quality," *J Food Eng*, vol. 116, no. 2, pp. 613–621, May 2013, doi: 10.1016/J.JFOODENG.2012.12.044.
- [41] D. Almeida, M. Correia De Barros, and M. Dias, *Manuseamento de produtos hortofrutícolas*, 1st ed. Principia, Publicações Universitárias e Científicas, 2005.
- [42] B. M. Popkin, K. E. D'Anci, and I. H. Rosenberg, "Water, Hydration and Health," *Nutr Rev*, vol. 68, no. 8, p. 439, 2010, doi: 10.1111/J.1753-4887.2010.00304.X.
- [43] S. Bodbodak and M. Moshfeghifar, "Advances in controlled atmosphere storage of fruits and vegetables," *Eco-Friendly Technology for Postharvest Produce Quality*, pp. 39–76, Jan. 2016, doi: 10.1016/B978-0-12-804313-4.00002-5.
- [44] E. Hoehn, R. K. Prange, and C. Vigneault, "Storage Technology and Applications," in *Modified and Controlled Atmospheres for the Storage, Transportation, and Packaging of Horticultural Commodities*, 1st Edition. CRC Press, 2009, pp. 35–68. doi: 10.1201/9781420069587-6.
- [45] G. L. Malcolm, "Advancements in the implementation of CA technology for storage of perishable commodities," *Acta Horti*, vol. 682, pp. 1593–1598, 2005, doi: 10.17660/ACTAHORTIC.2005.682.212.
- [46] M. S. Martin, C. A. A. C. V. T. Steffens, A. Brackmann, M. F. Rodrigues, and C. Soethe, "'Rocha' pears stored under controlled atmosphere with Ultra-Low and Low O<sub>2</sub> associated with different Co<sub>2</sub> levels," *Rev Bras Frutic*, vol. 39, no. 5, p. 143, Dec. 2017, doi: 10.1590/0100-29452017143.
- [47] A. A. Saquet, J. Streif, and F. Bangerth, "Reducing internal browning disorders in 'braeburn' apples by delayed controlled atmosphere storage and some related physiological and biochemical changes," *Acta Horti*, vol. 628, pp. 453–458, Dec. 2003, doi: 10.17660/ACTAHORTIC.2003.628.57.
- [48] D. R. Dilley, "Development of controlled atmosphere storage technologies," *Stewart Postharvest Review*, vol. 2, no. 6, pp. 1–8, 2006, doi: 10.2212/spr.2006.6.5.
- [49] D. Bishop, "Controlled atmosphere storage," in *Cold and chilled storage technology*, C. V. J. Dellino, Ed., 2nd ed. Blackie Academic & Professional, 1996, pp. 53–92.



- [50] A. Thompson, R. Prange, R. Bancroft, and T. Puttongsiri, *Controlled atmosphere storage of fruit and vegetables*. CAB International, 2018. doi: 10.1079/9781786393739.0000.
- [51] N. Lallu *et al.*, "Effect of Carbon Dioxide Removal Systems on Volatile Profiles and Quality of 'Hayward' Kiwifruit Stored in Controlled Atmosphere Rooms," *Horttechnology*, vol. 15, no. 2, pp. 253–260, Jan. 2005, doi: 10.21273/HORTTECH.15.2.0253.
- [52] K. Olsen, "Views on CA storage of apples.," *Postharvest pomology newsletter*, vol. 4, no. 2, pp. 3–8, 1986, doi: 10.3/JQUERY-UI.JS.
- [53] H. G. Blank, "The possibility of simple CO<sub>2</sub> absorption in CA storage.," *Mitteilungen des Obstbauversuchsringes des Alten Landes*, pp. 202–208, 1973.
- [54] J.-F. Chapon and Pascale Westercamp, "Entreposage frigorifique des pommes et des poires. Tome 2 : Conduite de la conservation," *Centre Technique Interprofessionnel des Fruits et Légumes*, p. 205, 1996.
- [55] N. R. Markarian, C. Vigneault, Y. Gariépy, and T. J. Rennie, "Computerized monitoring and control for a research controlled-atmosphere storage facility," *Comput Electron Agric*, vol. 39, no. 1, pp. 23–37, Apr. 2003, doi: 10.1016/S0168-1699(03)00005-X.
- [56] A. L. Ryall, "Effects of modified atmospheres from liquefied gases on fresh produce," in *Seventeenth National Conference on Handling Perishable Agricultural Commodities (Purdue University)*, Mar. 1963, pp. 21–24.
- [57] J. M. DeLong, R. K. Prange, J. C. Leyte, and P. A. Harrison, "A New Technology That Determines Low-oxygen Thresholds in Controlled-atmosphere-stored Apples," *Horttechnology*, vol. 14, no. 2, pp. 262–266, Jan. 2004, doi: 10.21273/HORTTECH.14.2.0262.
- [58] F. Gasser, T. Eppler, W. Naunheim, S. Gabioud, and E. Hoehn, "Control of the critical oxygen level during dynamic CA storage of apples by monitoring respiration as well as chlorophyll fluorescence," *Acta Horti*, vol. 796, pp. 69–76.
- [59] Y. Qi, C. Li, H. Li, H. Yang, and J. Guan, "Elimination or Removal of Ethylene for Fruit and Vegetable Storage via Low-Temperature Catalytic Oxidation," *J Agric Food Chem*, vol. 69, no. 36, pp. 10419–10439, Sep. 2021, doi: 10.1021/ACS.JAFC.1C02868/ASSET/IMAGES/MEDIUM/JF1C02868\_0012.GIF.
- [60] D. A. Brummell, "Regulation and genetic manipulation of ripening in climacteric fruit," *Stewart Postharvest Review*, vol. 1, no. 3, pp. 1–19, Jan. 2008, doi: 10.2212/SPC.2005.3.1.
- [61] E. C. Sisler, "The discovery and development of compounds counteracting ethylene at the receptor level," *Biotechnol Adv*, vol. 24, no. 4, pp. 357–367, Jul. 2006, doi: 10.1016/j.biotechadv.2006.01.002.

- [62] C. B. Watkins, "The use of 1-methylcyclopropene (1-MCP) on fruits and vegetables," *Biotechnol Adv*, vol. 24, no. 4, pp. 389–409, Jul. 2006, doi: 10.1016/J.BIOTECHADV.2006.01.005.
- [63] T. L. Ohashi, S. Foukaraki, D. S. Corrêa, M. D. Ferreira, and L. Terry, "INFLUENCE OF 1-METHYLCYCLOPROPENE ON THE BIOCHEMICAL RESPONSE AND RIPENING OF 'SOLO' PAPAYAS," *Rev Bras Frutic*, vol. 38, no. 2, p. 791, Jun. 2016, doi: 10.1590/0100-29452016791.
- [64] X. Yang *et al.*, "Ethylene and 1-MCP regulate major volatile biosynthetic pathways in apple fruit," *Food Chem*, vol. 194, pp. 325–336, Aug. 2016, doi: 10.1016/J.FOODCHEM.2015.08.018.
- [65] M. H. Álvarez-Hernández *et al.*, "Current Scenario of Adsorbent Materials Used in Ethylene Scavenging Systems to Extend Fruit and Vegetable Postharvest Life," *Food Bioproc Tech*, vol. 11, no. 3, pp. 511–525, Mar. 2018, doi: 10.1007/S11947-018-2076-7/TABLES/2.
- [66] R. B. H. Wills and M. A. Warton, "Efficacy of Potassium Permanganate Impregnated into Alumina Beads to Reduce Atmospheric Ethylene," *Journal of the American Society for Horticultural Science*, vol. 129, no. 3, pp. 433–438, 2004, doi: 10.21273/JASHS.129.3.0433.
- [67] N. Pathak, O. J. Caleb, M. Geyer, W. B. Herppich, C. Rauh, and P. V. Mahajan, "Photocatalytic and Photochemical Oxidation of Ethylene: Potential for Storage of Fresh Produce—a Review," *Food Bioproc Tech*, vol. 10, no. 6, pp. 982–1001, Jun. 2017, doi: 10.1007/S11947-017-1889-0.
- [68] S. Mallakpour and E. Khadem, "Recent development in the synthesis of polymer nanocomposites based on nano-alumina," *Prog Polym Sci*, vol. Complete, no. 51, pp. 74–93, Oct. 2015, doi: 10.1016/J.PROGPOLYMSCI.2015.07.004.
- [69] E. Kavanagh and N. Wade, "Role of the carrier in the removal of ethylene by permanganate from storage atmospheres," *ASEAN Food Journal*, pp. 128–134, 1987.
- [70] G. D. Blanpied, J. A. Bartsch, and J. R. Turc, "A commercial development programme for low ethylene controlled-atmosphere storage of apples," in *Ethylene and Plant Development*, J. A. Roberts and G. A. Tucker, Eds., London: Butterworths, 1985, p. 393.
- [71] R. B. H. Wills and M. A. Warton, "Efficacy of potassium permanganate impregnated into alumina beads to reduce atmospheric ethylene," *Journal of the American Society for Horticultural Science*, vol. 129, no. 3, pp. 433–438, 2004, doi: 10.21273/JASHS.129.3.0433.
- [72] D. F. P. Silva, L. C. C. Salomão, D. L. De Siqueira, P. R. Cecon, and A. Rocha, "Potassium permanganate effects in postharvest conservation of the papaya cultivar Sunrise Golden," *Pesqui Agropecu Bras*, vol. 44, no. 7, pp. 669–675, Jul. 2009, doi: 10.1590/S0100-204X2009000700003.

- [73] R. Dobrucka, A. Leonowicz, and R. Cierpiszewski, "Preparation of Ethylene Scavenger Based on KMNO<sub>4</sub> to the Extension of the Storage Time of Tomatoes," *Studia Oeconomica Posnaniensia*, vol. 5, no. 7, pp. 7–18, 2017, doi: 10.18559/SOEP.2017.7.1.
- [74] A. A. Kader, R. Cavalieri, and I. Ferguson, "A Perspective on Postharvest Horticulture (1978-2003)," *HortScience*, vol. 38, no. 5, pp. 1004–1008, Aug. 2003, doi: 10.21273/HORTSCI.38.5.1004.
- [75] C. F. Forney, "Postharvest Response of Horticultural Products to Ozone," in *Postharvest Oxidative Stress in Horticultural Crops*, D. M. Hodges, Ed., New York: Food Products Press, 2003, pp. 13–54.
- [76] C. H. Crisosto, D. Garner, J. Smilanick, and J. P. Zoffoli, "Central Valley Postharvest News ," 2000.
- [77] "EU air quality standards." [https://environment.ec.europa.eu/topics/air/air-quality/eu-air-quality-standards\\_en](https://environment.ec.europa.eu/topics/air/air-quality/eu-air-quality-standards_en) (accessed May 17, 2023).
- [78] T. V Suslow, "Ozone Applications for Postharvest Disinfection of Edible Horticultural Crops," *Ozone Applications for Postharvest Disinfection of Edible Horticultural Crops*, 2004.
- [79] "Ozone generator air purifier." <https://www.okayenergy.com/ozone-generator/> (accessed May 15, 2023).
- [80] J. A. M. de Bont, "Oxidation of ethylene by soil bacteria," *Antonie Van Leeuwenhoek*, vol. 42, no. 1–2, pp. 59–71, Mar. 1976, doi: 10.1007/BF00399449/METRICS.
- [81] J. S. Devanny, M. A. Deshusses, and T. S. Webster, "Biofiltration for air pollution control," *Biofiltration for Air Pollution Control*, pp. 1–299, Jan. 2017, doi: 10.1201/9781315138275/BIOFILTRATION-AIR-POLLUTION-CONTROL-JOSEPH-DEVINNY-TODD-STEPHEN-WEBSTER-MARC-DESHUSSES.
- [82] L. Elsgaard, "Ethylene removal at low temperatures under biofilter and batch conditions," *Appl Environ Microbiol*, vol. 66, no. 9, pp. 3878–3882, 2000, doi: 10.1128/AEM.66.9.3878-3882.2000.
- [83] W. H. Prokop and H. L. Bohn, "Soil bed system for control of rendering plant odors," *Journal of the Air Pollution*, vol. 35, no. 12, pp. 1332–1338, 1985, doi: 10.1080/00022470.1985.10466036.
- [84] C. van Lith, G. Leson, and R. F. Michelsen, "Evaluating design options for biofilters," *J Air Waste Manage Assoc*, vol. 47, no. 1, pp. 37–48, Jan. 1997, doi: 10.1080/10473289.1997.10464410.
- [85] J. Kim, "Assessment of ethylene removal with Pseudomonas strains," *J Hazard Mater*, vol. 131, no. 1–3, pp. 131–136, Apr. 2006, doi: 10.1016/J.JHAZMAT.2005.09.019.
- [86] N. Pathak and P. V. Mahajan, "Ethylene Removal From Fresh Produce Storage: Current Methods and Emerging Technologies," *Reference Module in Food Science*, Jan. 2017, doi: 10.1016/B978-0-08-100596-5.22330-5.

- [87] W. J. Xue, Y. F. Wang, P. Li, Z. T. Liu, Z. P. Hao, and C. Y. Ma, "Morphology effects of Co<sub>3</sub>O<sub>4</sub> on the catalytic activity of Au/Co<sub>3</sub>O<sub>4</sub> catalysts for complete oxidation of trace ethylene," *Catal Commun*, vol. 12, no. 13, pp. 1265–1268, Jul. 2011, doi: 10.1016/J.CATCOM.2011.04.003.
- [88] H. Yang *et al.*, "Synthesis, characterization and evaluations of the Ag/ZSM-5 for ethylene oxidation at room temperature: Investigating the effect of water and deactivation," *Chemical Engineering Journal*, vol. 347, pp. 808–818, Sep. 2018, doi: 10.1016/J.CEJ.2018.04.095.
- [89] Q. H. Trinh and Y. S. Mok, "Effect of the adsorbent/catalyst preparation method and plasma reactor configuration on the removal of dilute ethylene from air stream," *Catal Today*, vol. 256, no. P1, pp. 170–177, Nov. 2015, doi: 10.1016/J.CATTOD.2015.01.027.
- [90] M. G. Nielsen, P. C. K. Vesborg, O. Hansen, and I. Chorkendorff, "Removal of low concentration contaminant species using photocatalysis: Elimination of ethene to sub-ppm levels with and without water vapor present," *Chemical Engineering Journal*, vol. 262, pp. 648–657, Feb. 2015, doi: 10.1016/J.CEJ.2014.10.008.
- [91] R. López and R. Gómez, "Band-gap energy estimation from diffuse reflectance measurements on sol-gel and commercial TiO<sub>2</sub>: A comparative study," *J Solgel Sci Technol*, vol. 61, no. 1, pp. 1–7, Jan. 2012, doi: 10.1007/S10971-011-2582-9/TABLES/2.
- [92] I. N. Reddy *et al.*, "Effect of seed layers (Al, Ti) on optical and morphology of Fe-doped ZnO thin film nanowires grown on Si substrate via electron beam evaporation," *Mater Sci Semicond Process*, vol. 71, pp. 296–303, Nov. 2017, doi: 10.1016/J.MSSP.2017.08.015.
- [93] S. Kumar, A. G. Fedorov, and J. L. Gole, "Photodegradation of ethylene using visible light responsive surfaces prepared from titania nanoparticle slurries," *Appl Catal B*, vol. 57, no. 2, pp. 93–107, Apr. 2005, doi: 10.1016/J.APCATB.2004.10.012.
- [94] Y. T. Lin, C. H. Weng, H. J. Hsu, J. W. Huang, A. L. Srivastav, and C. C. Shiesh, "Effect of oxygen, moisture, and temperature on the photo oxidation of ethylene on N-doped TiO<sub>2</sub> catalyst," *Sep Purif Technol*, vol. 134, pp. 117–125, Sep. 2014, doi: 10.1016/J.SEPPUR.2014.07.039.
- [95] C. Young, T. M. Lim, K. Chiang, J. Scott, and R. Amal, "Photocatalytic oxidation of toluene and trichloroethylene in the gas-phase by metallised (Pt, Ag) titanium dioxide," *Appl Catal B*, vol. 78, no. 1–2, pp. 1–10, Jan. 2008, doi: 10.1016/J.APCATB.2007.08.011.
- [96] S. Yamazaki, S. Tanaka, and H. Tsukamoto, "Kinetic studies of oxidation of ethylene over a TiO<sub>2</sub> photocatalyst," *J Photochem Photobiol A Chem*, vol. 121, no. 1, pp. 55–61, Feb. 1999, doi: 10.1016/S1010-6030(98)00448-1.

- [97] Z. Zhu, Y. Zhang, Y. Shang, and Y. Wen, "Electrospun Nanofibers Containing TiO<sub>2</sub> for the Photocatalytic Degradation of Ethylene and Delaying Postharvest Ripening of Bananas," *Food Bioproc Tech*, vol. 12, no. 2, pp. 281–287, Feb. 2019, doi: 10.1007/S11947-018-2207-1/FIGURES/6.
- [98] K. J. Scott, R. B. H. Wills, and B. D. Patterson, "Removal by ultra-violet lamp of ethylene and other hydrocarbons produced by bananas," *J Sci Food Agric*, vol. 22, no. 9, pp. 496–497, Sep. 1971, doi: 10.1002/JSFA.2740220916.
- [99] Z. B. Jozwiak, J. A. Bartsch, and D. J. Aneshansley, "Experimental verification of a model describing UV initiated decomposition of ethylene in CA storage of apples," *Acta Horti*, vol. 600, pp. 707–710, Mar. 2003, doi: 10.17660/ACTAHORTIC.2003.600.107.
- [100] A. R. Lawton, "Measurement of Ethylene Gas Prior to and During Transport," in *New Challenges in Refrigeration*, Montreal, Quebec: IIR, Aug. 1991, p. 2068.
- [101] D. Vargas-Hernández, M. A. Pérez-Cruz, and R. Hernández-Huesca, "Selective adsorption of ethylene over ethane on natural mordenite and on K<sup>+</sup>-exchanged mordenite," *Adsorption*, vol. 21, no. 1–2, pp. 153–163, Feb. 2015, doi: 10.1007/S10450-015-9658-8/TABLES/6.
- [102] E. Pérez-Botella, S. Valencia, and F. Rey, "Zeolites in Adsorption Processes: State of the Art and Future Prospects," *Chem Rev*, vol. 122, no. 24, p. 17647, Dec. 2022, doi: 10.1021/ACS.CHEMREV.2C00140.
- [103] P. Wright, *Microporous framework solids*, 1st ed., vol. 4. Royal Society of Chemistry Publishing, 2007.
- [104] C. Yang *et al.*, "Abatement of various types of VOCs by adsorption/catalytic oxidation: A review," *Chemical Engineering Journal*, vol. 370, pp. 1128–1153, Aug. 2019, doi: 10.1016/J.CEJ.2019.03.232.
- [105] "Welcome to It's Fresh! - It's Fresh!" <https://itsfresh.com/> (accessed May 24, 2023).
- [106] C. Martínez and A. Corma, "Zeolites," *Comprehensive Inorganic Chemistry II (Second Edition): From Elements to Applications*, vol. 5, pp. 103–131, Jan. 2013, doi: 10.1016/B978-0-08-097774-4.00506-4.
- [107] A. H. Yonli, I. Gener, and S. Mignard, "Comparative study of the hydrophobicity of BEA, HZSM-5 and HY zeolites determined by competitive adsorption," *Microporous and Mesoporous Materials*, vol. 132, no. 1–2, pp. 37–42, Jul. 2010, doi: 10.1016/J.MICROMESO.2009.08.007.
- [108] G. Calleja, J. Pau, and J. A. Calles, "Pure and Multicomponent Adsorption Equilibrium of Carbon Dioxide, Ethylene, and Propane on ZSM-5 Zeolites with Different Si/Al Ratios," *J Chem Eng Data*, vol. 43, no. 6, pp. 994–1003, 1998, doi: 10.1021/JE9702100.
- [109] Z. Tahraoui, H. Nouali, C. Marichal, P. Forler, J. Klein, and T. J. Daou, "Influence of the Compensating Cation Nature on the Water Adsorption Properties of Zeolites," *Molecules* 2020, Vol. 25, Page 944, vol. 25, no. 4, p. 944, Feb. 2020, doi: 10.3390/MOLECULES25040944.

- [110] A. Dyer, "Ion-Exchange Properties of Zeolites and Related Materials," in *Introduction to Zeolite Science and Practice*, J. Čejka, H. Van Bekkum, A. Coma, and F. Schüth, Eds., 3rd ed. Amsterdam: Elsevier B.V., 2007, pp. 525–553.
- [111] B. Erdoğan, M. Sakizci, and E. Yörükoğullari, "Characterization and ethylene adsorption of natural and modified clinoptilolites," *Appl Surf Sci*, vol. 254, no. 8, pp. 2450–2457, Feb. 2008, doi: 10.1016/J.APSUSC.2007.09.058.
- [112] C. G. P. M. Bernardo and J. A. N. F. Gomes, "The adsorption of ethylene on the (110) surfaces of copper, silver and platinum: a DFT study," *Journal of Molecular Structure: THEOCHEM*, vol. 582, no. 1–3, pp. 159–169, Apr. 2002, doi: 10.1016/S0166-1280(01)00771-0.
- [113] C. G. P. M. Bernardo and J. A. N. F. Gomes, "The adsorption of ethylene on the (100) surfaces of platinum, palladium and nickel: a DFT study," *Journal of Molecular Structure: THEOCHEM*, vol. 542, no. 1–3, pp. 263–271, Jun. 2001, doi: 10.1016/S0166-1280(00)00846-0.
- [114] D. Saha, M. B. Kim, A. J. Robinson, R. Babarao, and P. K. Thallapally, "Elucidating the mechanisms of Paraffin-Olefin separations using nanoporous adsorbents: An overview," *iScience*, vol. 24, no. 9, Sep. 2021, doi: 10.1016/J.ISCI.2021.103042.
- [115] L. A. Terry, T. Ilkenhans, S. Poulston, L. Rowsell, and A. W. J. Smith, "Development of new palladium-promoted ethylene scavenger," *Postharvest Biol Technol*, vol. 45, no. 2, pp. 214–220, Aug. 2007, doi: 10.1016/J.POSTHARVBIO.2006.11.020.
- [116] "Palladium Price in Euro (EUR) - Live Price and Historical Chart | GoldBroker.com." <https://goldbroker.com/charts/palladium-price/eur> (accessed Apr. 20, 2023).
- [117] "Live Silver Spot Prices and Historical Charts | GoldBroker.com." <https://goldbroker.com/charts/silver-price> (accessed Apr. 20, 2023).
- [118] J. D. Monzón *et al.*, "Ethylene adsorption onto thermally treated AgA-Zeolite," *Appl Surf Sci*, vol. 542, p. 148748, Mar. 2021, doi: 10.1016/J.APSUSC.2020.148748.
- [119] L. Cisneros, F. Gao, and A. Corma, "Silver nanocluster in zeolites. ADSORPTION of ETHYLENE traces for fruit preservation," *Microporous and Mesoporous Materials*, vol. 283, pp. 25–30, Jul. 2019, doi: 10.1016/J.MICROMESO.2019.03.032.
- [120] C. Horvatits, D. Li, M. Dupuis, E. A. Kyriakidou, and E. A. Walker, "Ethylene and Water Co-Adsorption on Ag/SSZ-13 Zeolites: A Theoretical Study," *Journal of Physical Chemistry C*, vol. 124, no. 13, pp. 7295–7306, Apr. 2020, doi: 10.1021/ACS.JPCC.0C00849/ASSET/IMAGES/LARGE/JP0C00849\_0007.JPEG.

- [121] J. Lee, K. Giewont, J. Chen, C. H. Liu, E. A. Walker, and E. A. Kyriakidou, "Ag/ZSM-5 traps for C<sub>2</sub>H<sub>4</sub> and C<sub>7</sub>H<sub>8</sub> adsorption under cold-start conditions," *Microporous and Mesoporous Materials*, vol. 327, p. 111428, Nov. 2021, doi: 10.1016/J.MICROMESO.2021.111428.
- [122] J. G. Min, K. C. Kemp, and S. B. Hong, "Silver ZK-5 zeolites for selective ethylene/ethane separation," *Sep Purif Technol*, vol. 250, p. 117146, Nov. 2020, doi: 10.1016/J.SEPPUR.2020.117146.
- [123] Y. S. Mok, S. G. Kim, D. Ba Nguyen, Q. H. Trinh, H. W. Lee, and S. B. Kim, "Plasma-catalytic oxidation of ethylene over zeolite-supported catalysts to improve the storage stability of agricultural products," *Catal Today*, vol. 337, pp. 208–215, Oct. 2019, doi: 10.1016/J.CATTOD.2019.02.059.
- [124] "Copper PRICE Today | Copper Spot Price Chart | Live Price of Copper per Ounce | Markets Insider." <https://markets.businessinsider.com/commodities/copper-price/euro> (accessed Jul. 06, 2023).
- [125] H. Abdi, H. Maghsoudi, and V. Akhoundi, "Adsorption properties of ion-exchanged SSZ-13 zeolite for ethylene/ethane separation," *Fluid Phase Equilib*, vol. 546, Oct. 2021, doi: 10.1016/J.FLUID.2021.113171.
- [126] S. Mitchell, N. L. Michels, and J. Pérez-Ramírez, "From powder to technical body: the undervalued science of catalyst scale up," *Chem Soc Rev*, vol. 42, no. 14, pp. 6094–6112, Jun. 2013, doi: 10.1039/C3CS60076A.
- [127] M. P. Dudukovic, "Frontiers in reactor engineering," *Science (1979)*, vol. 325, no. 5941, pp. 698–701, 2009, doi: 10.1126/SCIENCE.1174274.
- [128] C. Perego and P. Villa, "Catalyst preparation methods," *Catal Today*, vol. 34, no. 3–4, pp. 281–305, Feb. 1997, doi: 10.1016/S0920-5861(96)00055-7.
- [129] S. Kulprathipanja, "Zeolites in Industrial Separation and Catalysis," *Zeolites in Industrial Separation and Catalysis*, Mar. 2010, doi: 10.1002/9783527629565.
- [130] R. Bingre, B. Louis, and P. Nguyen, "An Overview on Zeolite Shaping Technology and Solutions to Overcome Diffusion Limitations," *Catalysts 2018, Vol. 8, Page 163*, vol. 8, no. 4, p. 163, Apr. 2018, doi: 10.3390/CATAL8040163.
- [131] C. Perego, G. Bassi, 642,172 G Girotti - US Patent 6, and undefined 2003, "Extruded catalyst based on silica/alumina gel," *Google Patents*, 1991.
- [132] W. M. Sigmund, N. S. Bell, and L. Bergström, "Novel Powder-Processing Methods for Advanced Ceramics," *Journal of the American Ceramic Society*, vol. 83, no. 7, pp. 1557–1574, Jul. 2000, doi: 10.1111/J.1151-2916.2000.TB01432.X.

- [133] A. Martin, H. Berndt, U. Lohse, and U. Wolf, "Effect of Si: Al ratio and type of binder on the catalytic properties of HZSM-5 catalysts," *Journal of the Chemical Society, Faraday Transactions*, vol. 89, no. 8, pp. 1277–1282, 1993, doi: 10.1039/FT9938901277.
- [134] A. Lucas, P. Sánchez, A. Fúnez, M. Jesús Ramos, and J. Luis Valverde, "Liquid-Phase Hydroisomerization of n-Octane over Platinum-Containing Zeolite-Based Catalysts with and without Binder," *ACS Publications*, vol. 45, no. 26, pp. 8852–8859, Dec. 2006, doi: 10.1021/ie060388s.
- [135] A. De Lucas, P. Sánchez, F. Dorado, M. J. Ramos, and J. L. Valverde, "Effect of the metal loading in the hydroisomerization of n-octane over beta agglomerated zeolite based catalysts," *Appl Catal A Gen*, vol. 294, no. 2, pp. 215–225, Oct. 2005, doi: 10.1016/J.APCATA.2005.07.035.
- [136] N. Wakao and J. M. Smith, "Diffusion in catalyst pellets," *Chem Eng Sci*, vol. 17, no. 11, pp. 825–834, Nov. 1962, doi: 10.1016/0009-2509(62)87015-8.
- [137] S. Schwarz, M. Kojima, and C. T. O'Connor, "Effect of stirring, extrusion and pelletisation on high pressure propene oligomerisation and xylene isomerisation over ZSM-5," *Appl Catal*, vol. 68, no. 1, pp. 81–96, Jan. 1991, doi: 10.1016/S0166-9834(00)84095-6.
- [138] H. Sun, B. Shen, and J. Liu, "N-Paraffins adsorption with 5A zeolites: The effect of binder on adsorption equilibria," *Sep Purif Technol*, vol. 64, no. 1, pp. 135–139, Nov. 2008, doi: 10.1016/J.SEPPUR.2008.08.013.
- [139] F. Ferreira *et al.*, "Ethylene removal by Ag-based ZSM-5 adsorbents for the preservation of climacteric fruits," Lisbon, Unpublished manuscript, 2023.
- [140] P. S. F. Mendes, "Hydroconversion catalysts based on zeolite mixtures, from ideality to reality," Doctoral dissertation, Instituto Superior Técnico, 2017.
- [141] A. Hydrates, "PURAL CATAPAL".
- [142] "ICP-OES principle, ICP-OES Analysis, ICP-OES FAQ's | Agilent." <https://www.agilent.com/en/support/atomic-spectroscopy/inductively-coupled-plasma-optical-emission-spectroscopy-icp-oes/icp-oes-faq> (accessed Apr. 13, 2023).
- [143] S. Landi, I. Rocha Segundo, E. Freitas, M. Vasilevskiy, J. Carneiro, and C. J. Tavares, "Use and misuse of the Kubelka-Munk function to obtain the band gap energy from diffuse reflectance measurements," *Solid State Commun*, vol. 341, pp. 38–1098, 2022, doi: 10.1016/j.ssc.2021.114573.
- [144] P. Sudhakar, P. Latha, and P. V. Reddy, "Analytical techniques," *Phenotyping Crop Plants for Physiological and Biochemical Traits*, pp. 137–149, Jan. 2016, doi: 10.1016/B978-0-12-804073-7.00017-X.



- [145] "How Does an FID Work?" <https://www.peakscientific.com/discover/news/how-does-an-fid-work/> (accessed Apr. 18, 2023).
- [146] X. Zhang, C. W. Yang, H. Q. Yu, and G. P. Sheng, "Light-induced reduction of silver ions to silver nanoparticles in aquatic environments by microbial extracellular polymeric substances (EPS)," *Water Res*, vol. 106, pp. 242–248, Dec. 2016, doi: 10.1016/J.WATRES.2016.10.004.
- [147] "Overshooting in single component breakthrough curve? | ResearchGate." [https://www.researchgate.net/post/Reg\\_overshooting\\_in\\_single\\_component\\_breakthrough\\_curve](https://www.researchgate.net/post/Reg_overshooting_in_single_component_breakthrough_curve) (accessed May 24, 2023).
- [148] H. Marsh and F. Rodríguez-Reinoso, "Characterization of Activated Carbon," *Activated Carbon*, pp. 143–242, Jan. 2006, doi: 10.1016/B978-008044463-5/50018-2.
- [149] A. I. Prilipko, V. G. Il'in, N. V. Turutina, V. A. Nazarenko, and G. N. Mel'nichenko, "Thermographic and mass spectrometric study on zeolite dehydration and deammoniation," *Theoretical and Experimental Chemistry*, vol. 25, no. 4, pp. 467–470, Jul. 1990, doi: 10.1007/BF00530445/METRICS.
- [150] "ZSM-5 - Zeolite Socony Mobil-5." <https://www.acsmaterial.com/blog-detail/zsm-5-molecular-seive.html> (accessed May 24, 2023).
- [151] M. Chebbi, B. Azambre, L. Cantrel, M. Huve, and T. Albiol, "Influence of structural, textural and chemical parameters of silver zeolites on the retention of methyl iodide," *Microporous and Mesoporous Materials*, vol. 244, pp. 137–150, May 2017, doi: 10.1016/J.MICROMESO.2017.02.056.
- [152] C. Spiegel, "Kinetics of Ion Exchange Materials," Jan. 02, 2022. <https://www.fuelcellstore.com/blog-section/kinetics-of-ion-exchange-materials> (accessed Apr. 21, 2023).
- [153] R. Bartolomeu, A. N. Mendes, A. Fernandes, C. Henriques, P. Da Costa, and M. F. Ribeiro, "NO<sub>x</sub> SCR with decane using Ag–MFI catalysts: on the effect of silver content and co-cation presence," *Catal Sci Technol*, vol. 6, no. 9, pp. 3038–3048, May 2016, doi: 10.1039/C5CY01460C.
- [154] L. Cisneros, F. Gao, and A. Corma, "Silver nanocluster in zeolites. ADSORPTION of ETHYLENE traces for fruit preservation," *Microporous and Mesoporous Materials*, vol. 283, pp. 25–30, Jul. 2019, doi: 10.1016/J.MICROMESO.2019.03.032.
- [155] R. Seifert, A. Kunzmann, and G. Calzaferri, "The Yellow Color of Silver-Containing Zeolite A\*\*," *Angew. Chem. Int. Ed*, vol. 37, no. 11, 1998, doi: 10.1002/(SICI)1521-3773(19980619)37:11.
- [156] J. Michalik, J. Sadlo, T. Kodaira, and Shimomura S, "ESR and optical studies of cationic silver clusters in zeolite rho," *Springer*, vol. 232, no. 2, p. 137, 1998.

- [157] J. Shibata, Y. Takada, A. Shichi, S. Satokawa, A. Satsuma, and T. Hattori, "Ag cluster as active species for SCR of NO by propane in the presence of hydrogen over Ag-MFI," *J Catal*, vol. 222, no. 2, pp. 368–376, Mar. 2004, doi: 10.1016/J.JCAT.2003.11.007.
- [158] A. Satsuma, J. Shibata, A. Wada, and Shinozaki Y, "In-situ UV-visible spectroscopic study for dynamic analysis of silver catalyst," *Elsevier*.
- [159] T. Nanba, S. Masukawa, J. Uchisawa, and A. Obuchi, "Effect of support materials on Ag catalysts used for acrylonitrile decomposition," *J Catal*, vol. 259, no. 2, pp. 250–259, Oct. 2008, doi: 10.1016/J.JCAT.2008.08.013.
- [160] J. Shibata *et al.*, "Structure of active Ag clusters in Ag zeolites for SCR of NO by propane in the presence of hydrogen," *J Catal*, vol. 227, no. 2, pp. 367–374, Oct. 2004, doi: 10.1016/J.JCAT.2004.08.007.
- [161] S. B. Kang, C. Kalamaras, Vemuri Balakotaiah, and W. Epling, "Hydrocarbon Trapping over Ag-Beta Zeolite for Cold-Start Emission Control," *Catal Letters*, vol. 147, pp. 1355–1362, 2044, doi: 10.1007/s10562-017-2044-2.
- [162] L. Martins, R. P. S. Peguin, and E. A. Urquieta-González, "Cu and Co exchanged ZSM-5 zeolites: activity towards no reduction and hydrocarbon oxidation," *Quim Nova*, vol. 29, no. 2, pp. 223–229, 2006, doi: 10.1590/S0100-40422006000200009.
- [163] S. J. Gentry, N. W. Hurst, and A. Jones, "Temperature programmed reduction of copper ions in zeolites," *Journal of the Chemical Society, Faraday Transactions 1: Physical Chemistry in Condensed Phases*, vol. 75, pp. 1688–1699, 1979, doi: 10.1039/F19797501688.
- [164] J. Sárkány, J. L. d'Itri, and W. M. H. Sachtler, "Redox chemistry in excessively ion-exchanged Cu/Na-ZSM-5," *Catal Letters*, vol. 16, no. 3, pp. 241–249, Sep. 1992, doi: 10.1007/BF00764336.
- [165] C. Torre-Abreu, C. Henriques, F. R. Ribeiro, G. Delahay, and M. F. Ribeiro, "Selective catalytic reduction of NO on copper-exchanged zeolites: the role of the structure of the zeolite in the nature of copper-active sites," *Catal Today*, vol. 54, no. 4, pp. 407–418, Dec. 1999, doi: 10.1016/S0920-5861(99)00204-7.
- [166] H. W. Jen and K. Otto, "Chemisorption of alkenes on copper-exchanged ZSM-5 zeolite," *Catal Letters*, vol. 26, no. 1–2, pp. 217–225, Mar. 1994, doi: 10.1007/BF00824047/METRICS.
- [167] Y. Marcus, "A simple empirical model describing the thermodynamics of hydration of ions of widely varying charges, sizes, and shapes," *Biophys Chem*, vol. 51, no. 2–3, pp. 111–127, Aug. 1994, doi: 10.1016/0301-4622(94)00051-4.
- [168] B. Hribar, N. T. Southall, V. Vlachy, and K. A. Dill, "How ions affect the structure of water," *J Am Chem Soc*, vol. 124, no. 41, pp. 12302–12311, Oct. 2002, doi: 10.1021/JA026014H/ASSET/IMAGES/LARGE/JA026014HF00012.JPEG.

- [169] J. Kim *et al.*, "A Cu-impregnated ZSM-5 zeolite for active cold start hydrocarbon removal: Cation-type-dependent Cu species and their synergetic HC adsorption/oxidation functions," *Chemical Engineering Journal*, vol. 430, p. 132552, Feb. 2022, doi: 10.1016/J.CEJ.2021.132552.
- [170] S. Mitchell, N. L. Michels, and J. Pérez-Ramírez, "From powder to technical body: the undervalued science of catalyst scale up," *Chem Soc Rev*, vol. 42, no. 14, pp. 6094–6112, Jun. 2013, doi: 10.1039/C3CS60076A.
- [171] T. Chaieb *et al.*, "On the origin of the changes in color of Ag/Al<sub>2</sub>O<sub>3</sub> catalysts during storage," *Research on Chemical Intermediates*, vol. 45, no. 12, pp. 5877–5905, Dec. 2019, doi: 10.1007/s11164-019-04007-8.
- [172] S. Pal, G. D.-M. R. Bulletin, and undefined 2009, "Reversible transformations of silver oxide and metallic silver nanoparticles inside SiO<sub>2</sub> films," *Elsevier*.
- [173] I. H. Son, M. C. Kim, H. L. Koh, and K. L. Kim, "On the promotion of Ag/ $\gamma$ -Al<sub>2</sub>O<sub>3</sub> by Cs for the SCR of NO by C<sub>3</sub>H<sub>6</sub>," *Catal Letters*, vol. 75, no. 3–4, pp. 191–197, Sep. 2001, doi: 10.1023/A:1016796022644/METRICS.
- [174] M. C. Kung and H. H. Kung, "Lean NOx catalysis over alumina-supported catalysts," *Top Catal*, vol. 10, no. 1–2, pp. 21–26, 2000, doi: 10.1023/A:1019147630269/METRICS.
- [175] J. Padin and R. T. Yang, "New sorbents for olefin/paraffin separations by adsorption via  $\pi$ -complexation: synthesis and effects of substrates," *Chem Eng Sci*, vol. 55, no. 14, pp. 2607–2616, Apr. 2000, doi: 10.1016/S0009-2509(99)00537-0.
- [176] P. A. Jacobs, "Chapter 8 Metal Clusters and Zeolites," *Stud Surf Sci Catal*, vol. 29, no. C, pp. 357–414, Jan. 1986, doi: 10.1016/S0167-2991(08)65379-3.
- [177] H. O. Mohamed *et al.*, "Stable and reusable hierarchical ZSM-5 zeolite with superior performance for olefin oligomerization when partially coked," *Appl Catal B*, vol. 316, p. 121582, Nov. 2022, doi: 10.1016/J.APCATB.2022.121582.

